Cosmology

Scale shows temperature. Not much structure at the time, just tiny differences in the temperature of ten parts per million.

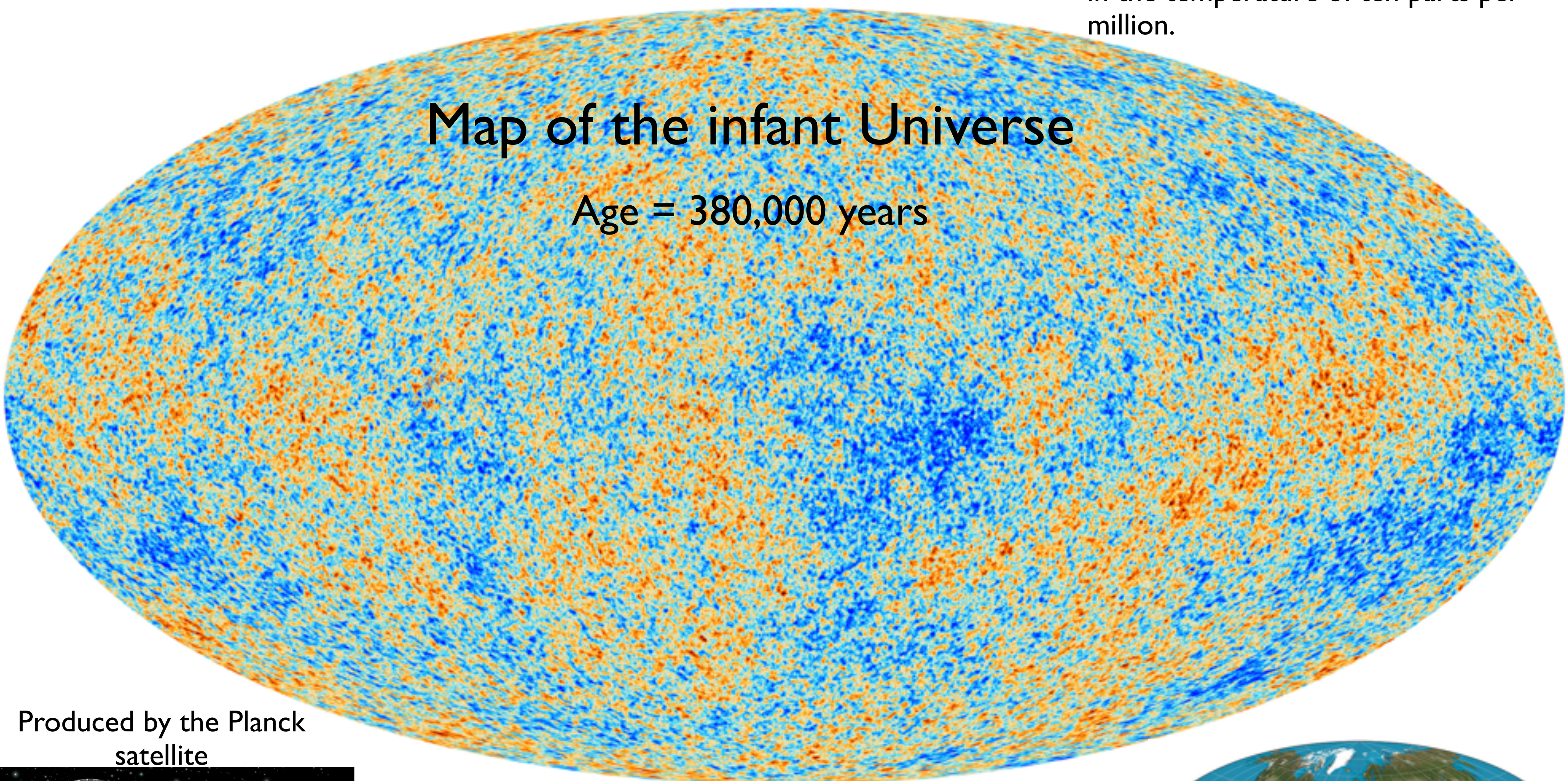

Produced by the Planck satellite

Current Age = 13, 800, 000, 000 years

Introduction

Questions in Cosmology

- What is the Universe made off?
- How did it start?
- What physical laws govern the dynamics?
- What objects/structures form as the Universe evolves?
- How and when did they form?
- What will happen in the future?

These question connect to fundamental physics, astronomy and astrophysics. Many have broad appeal.

The Expansion of the Universe

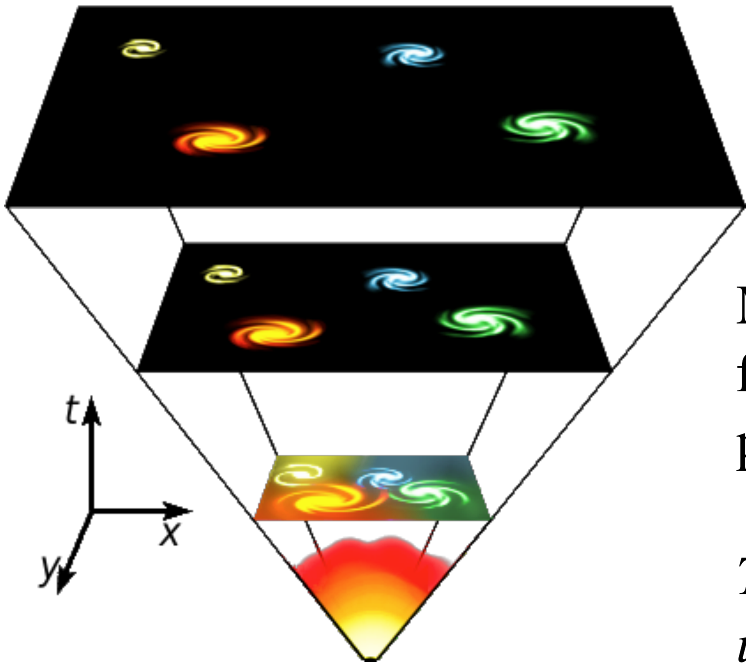

Edwin Hubble

More distant objects are moving away from us faster, with a velocity proportional to their distance.

This is what we call the expansion of the universe.

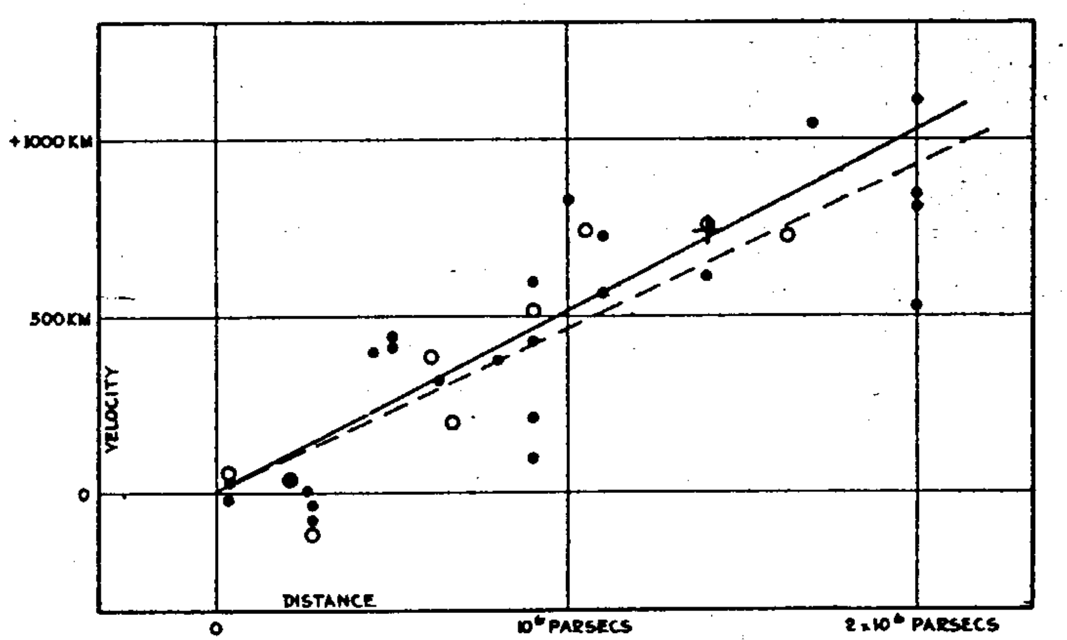

FIGURE 1

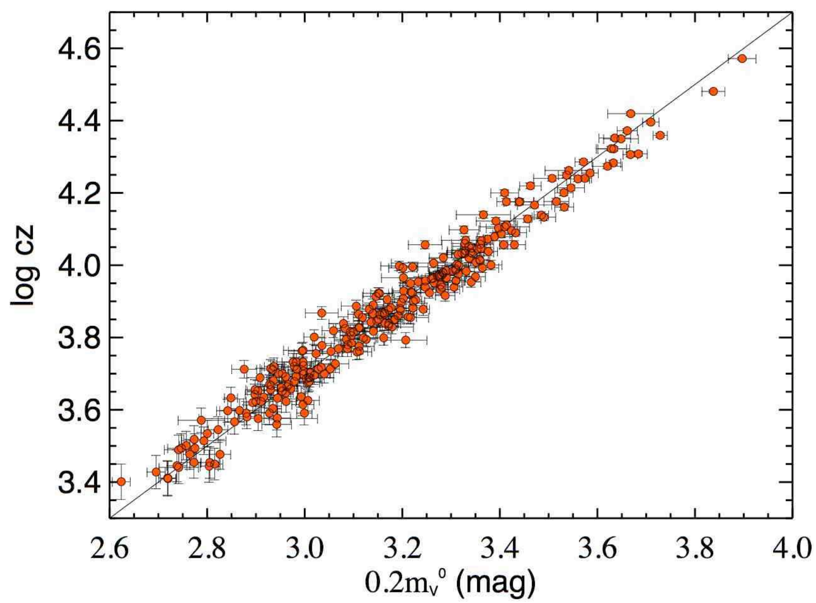

????

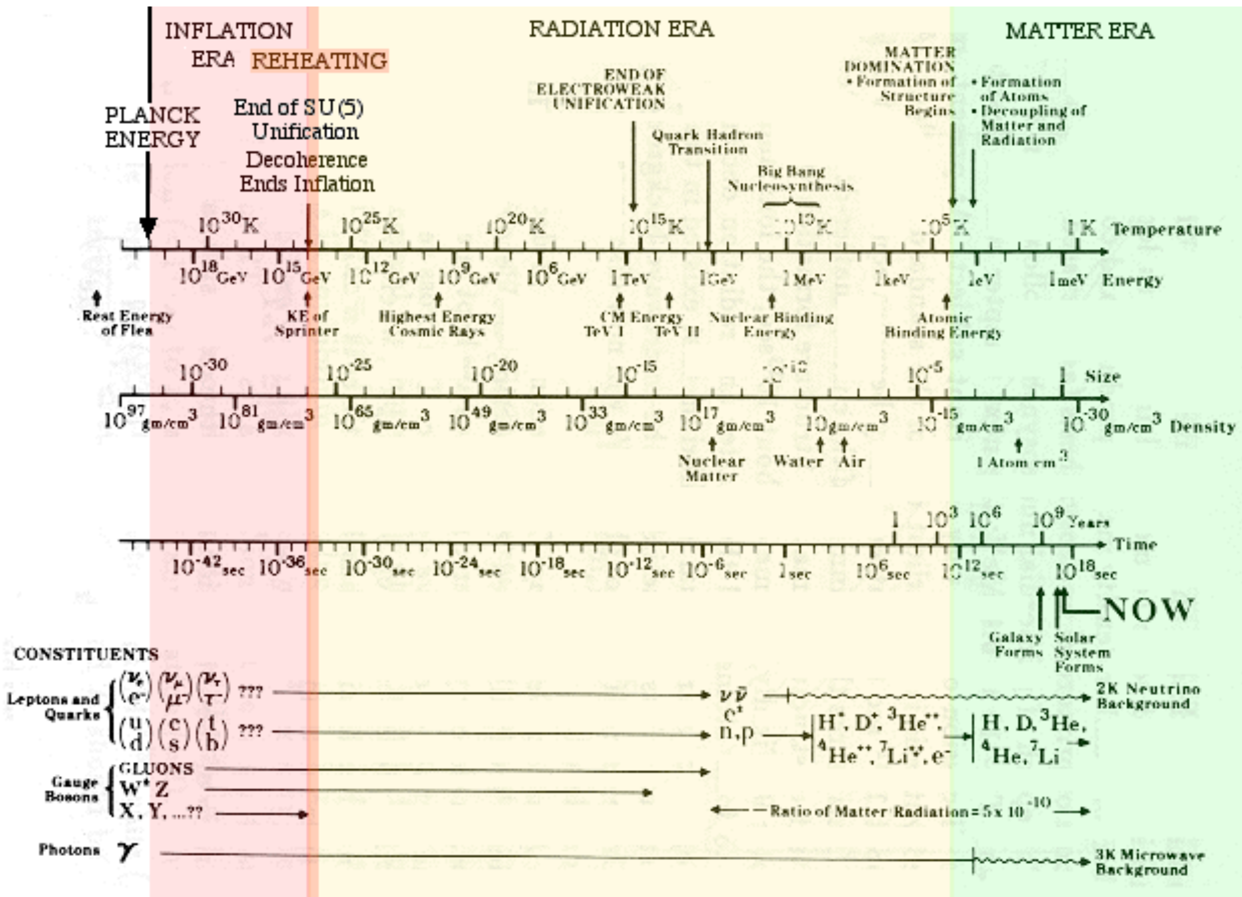

INFLATION ERA
REHEATING
RADIATION ERA
MATTER ERA
PLANCK ENERGY
End of SU(5) Unification
Decoherence Ends Inflation
END OF ELECTROWEAK UNIFICATION
Quark Hadron Transition
Big Bang Nucleosynthesis
MATTER DOMINATION
• Formation of Structure Begins
• Formation of Atoms
• Decoupling of Matter and Radiation
Temperature
Energy
Rest Energy of Flea
KE of Sprinter
Highest Energy Cosmic Rays
CM Energy TeV I TeV II
Nuclear Binding Energy
Atomic Binding Energy
Size
Density
Nuclear Matter
Water
Air
1 Atom cm⁻³
Years
Time
NOW
Galaxy Forms
Solar System Forms
CONSTITUENTS
Leptons and Quarks
Gauge Bosons
GLUONS
Photons
2K Neutrino Background
Ratio of Matter Radiation
3K Microwave Background

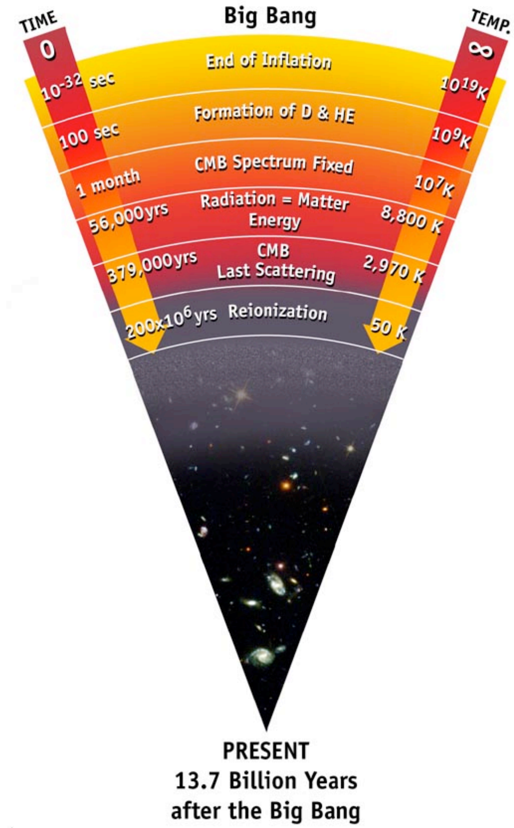

TIME
Big Bang
TEMP.
End of Inflation
Formation of D & HE
CMB Spectrum Fixed
Radiation = Matter Energy
CMB Last Scattering
Reionization
100 sec
1 month
56,000yrs
379,000yrs
8,800 K
2,970 K
50 K
PRESENT
13.7 Billion Years after the Big Bang

The History of our Universe

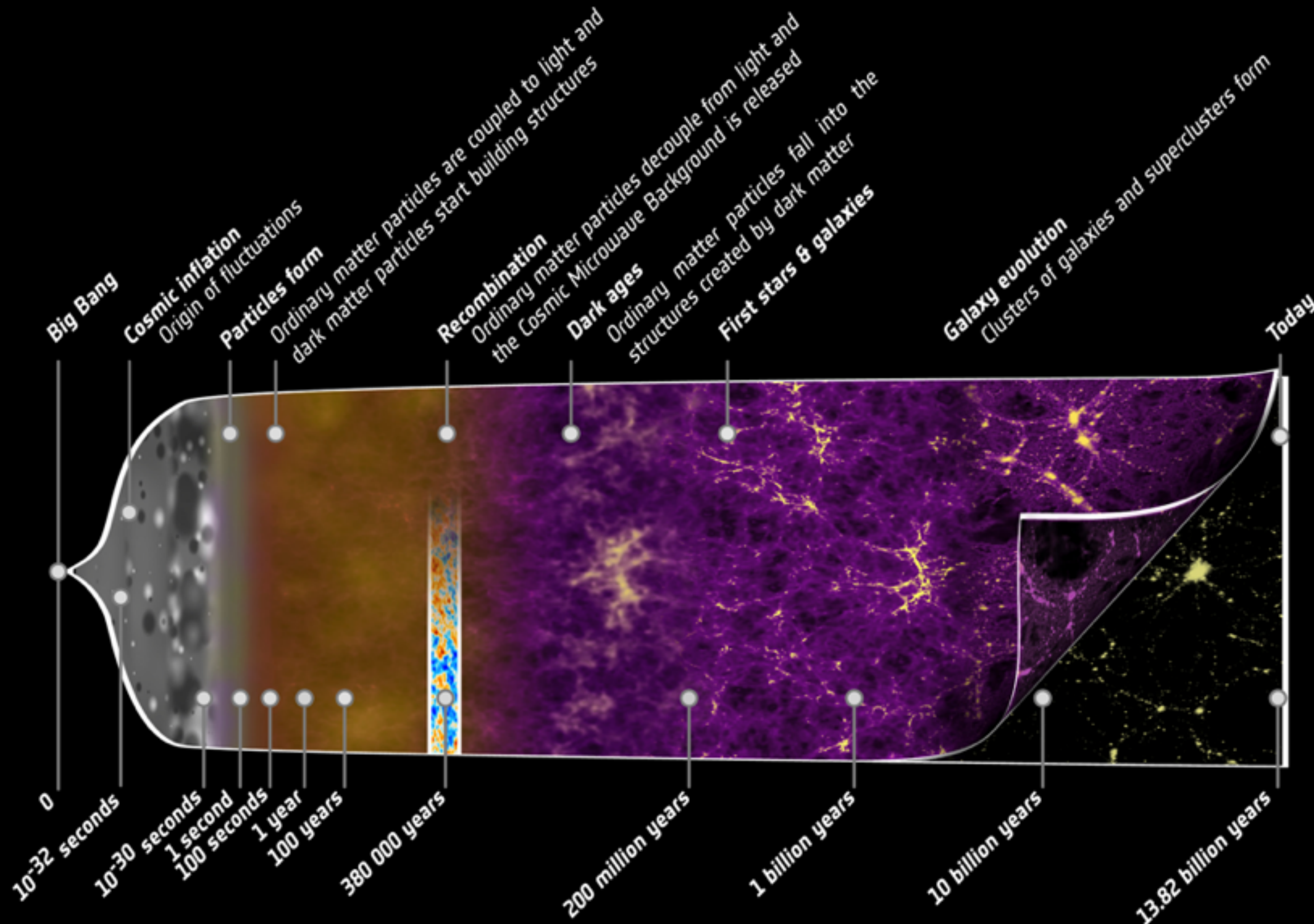

Evolution of the density

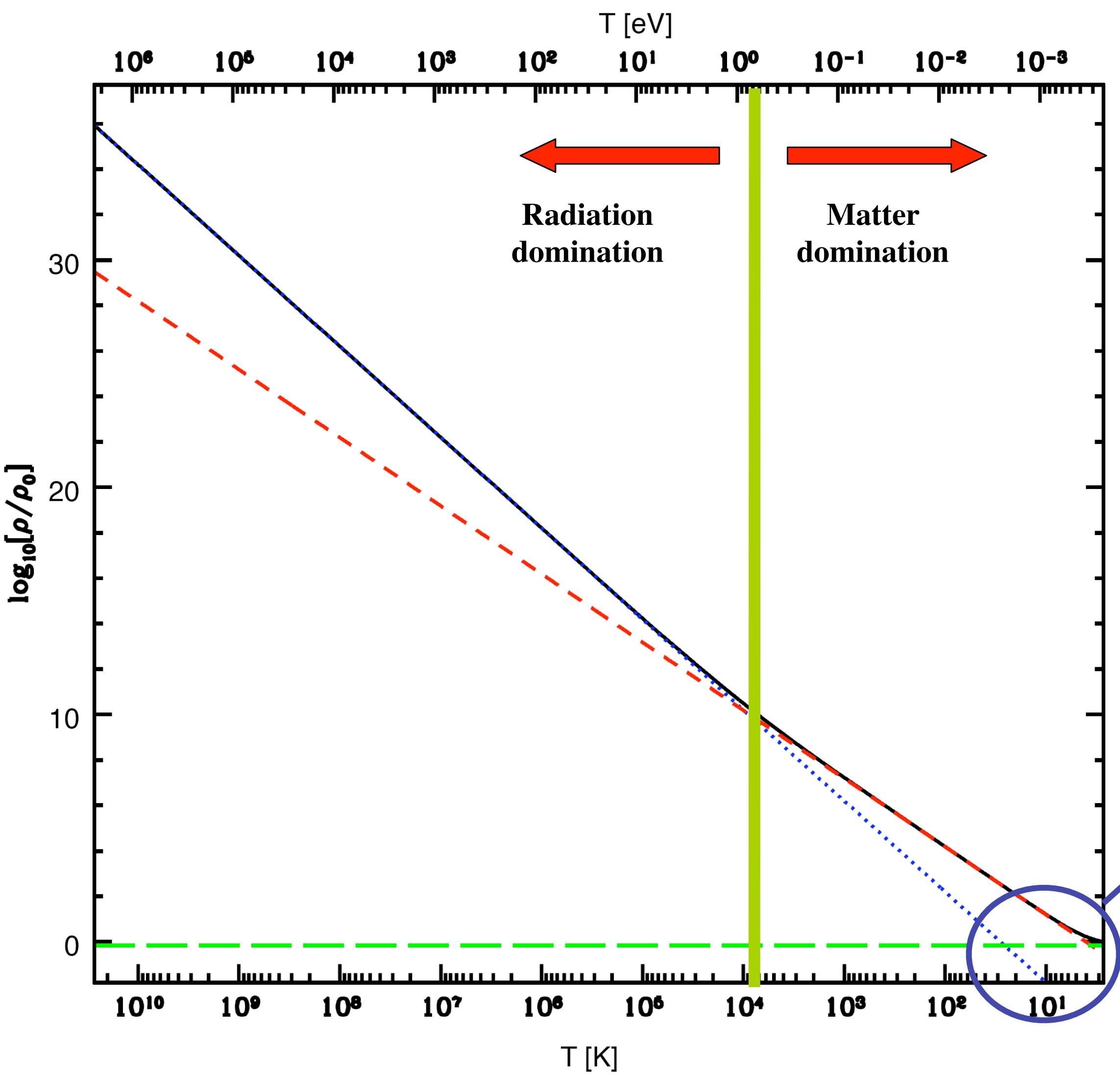

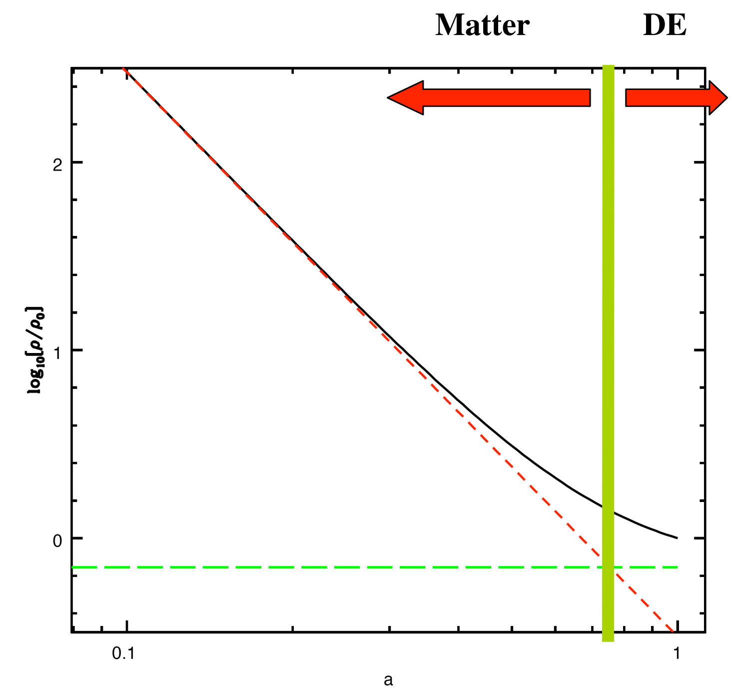

$$1 + z_{eq} = 1/a_{eq} \approx 3600$$

$$\Omega_m = 0.3\ ;\ \Omega_v = 0.7$$

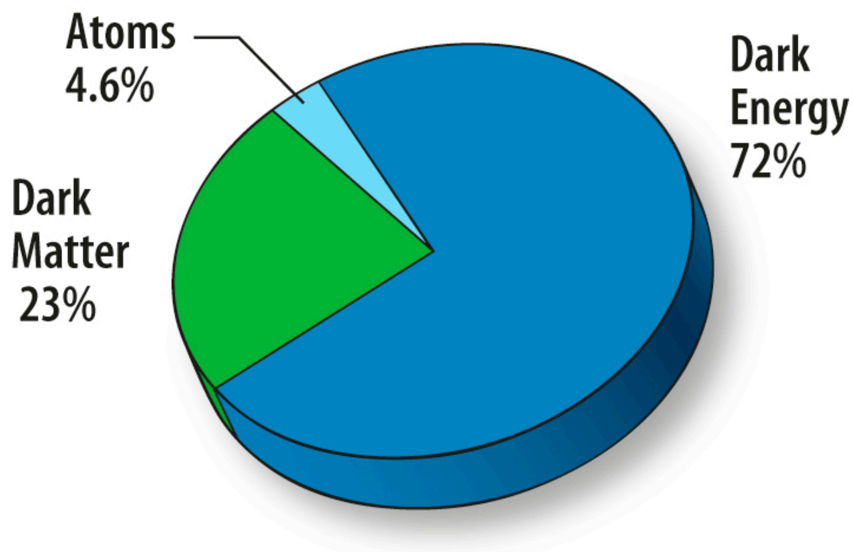

TODAY

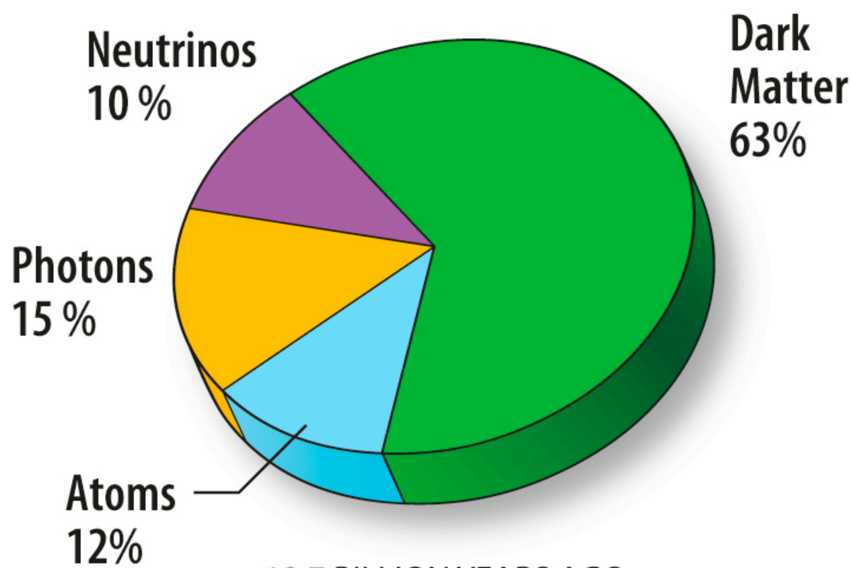

13.7 BILLION YEARS AGO
(Universe 380,000 years old)

Thermal History

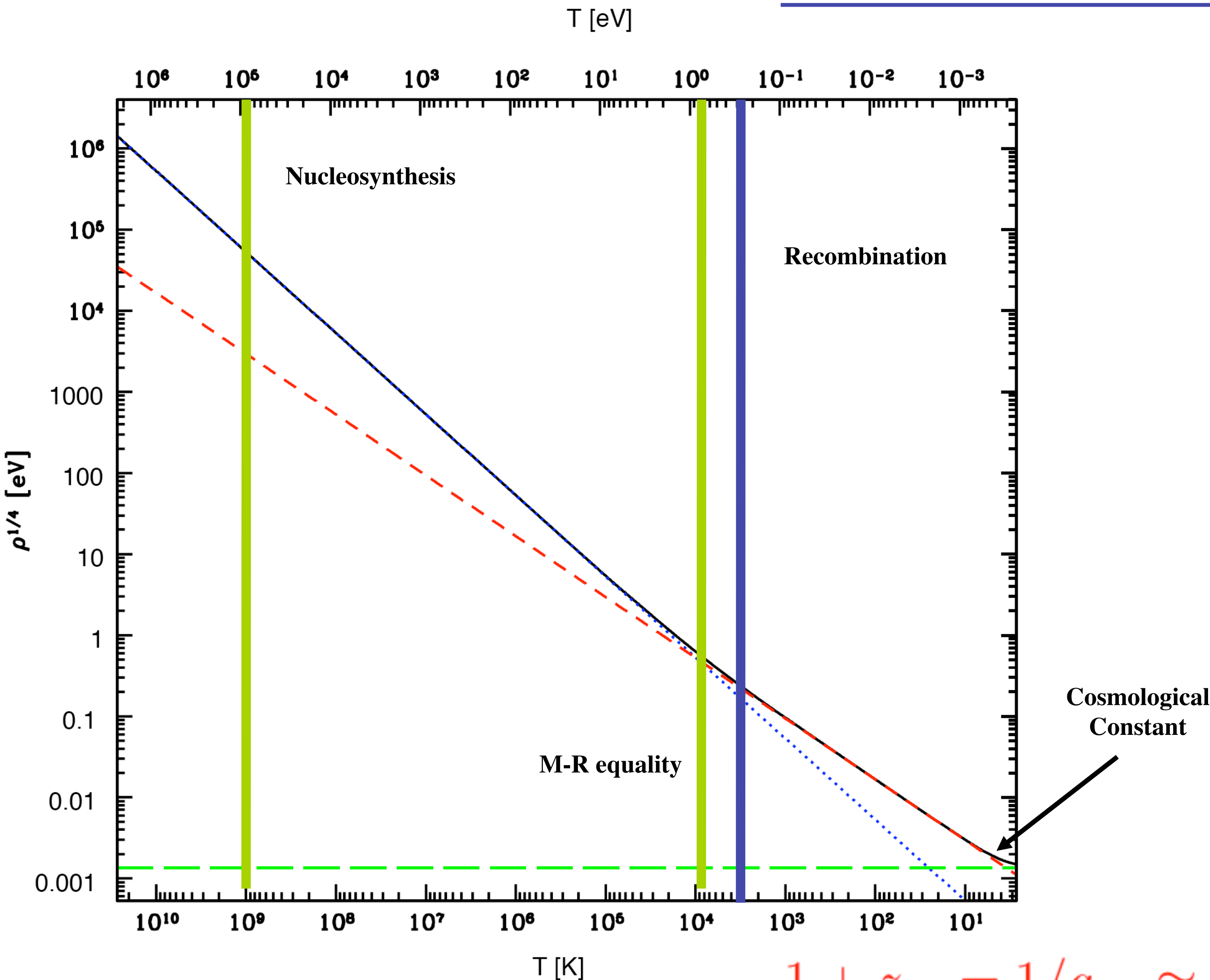

$$1 + z_{eq} = 1/a_{eq} \approx 3600$$

$$\Omega_m = 0.3 \; ; \; \Omega_v = 0.7$$

The changing Universe

Conditions in the Universe changed dramatically with time.

The history of the Universe can be used to probe physics in many different regimes including ones that have not been probed in the laboratory.

Sometimes we can do this by directly looking at different regions with our telescopes.
Sometimes we can do this by analyzing fossils.
Sometimes we cannot do it.

Fossils

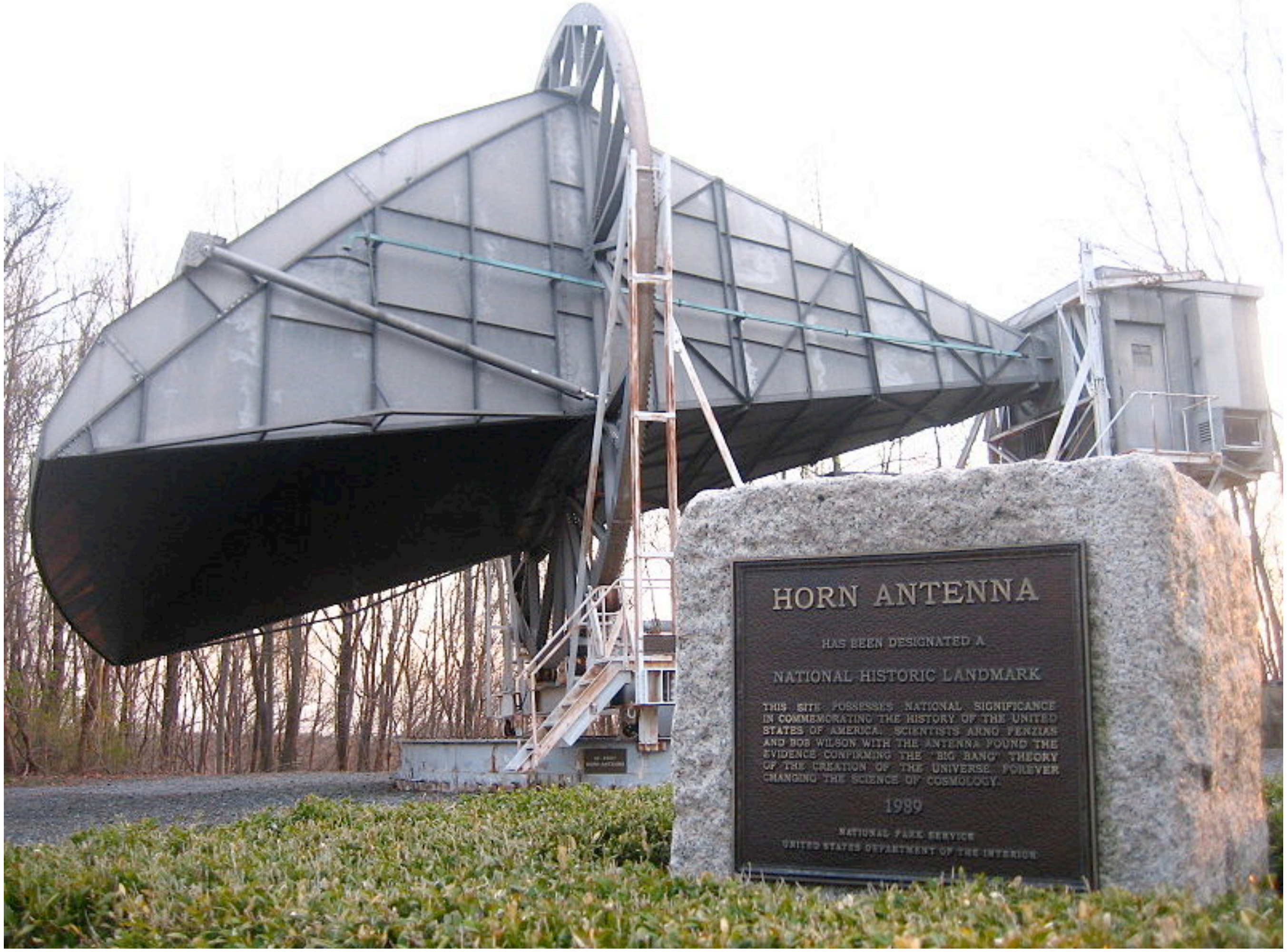

Penzias & Wilson

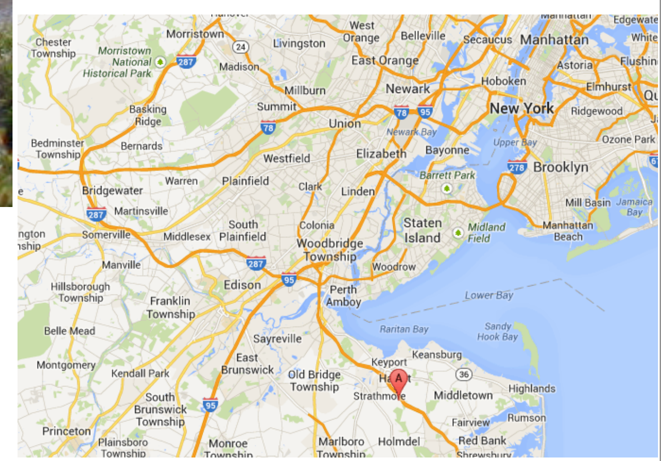

The Spectrum of the CMB

$n_\gamma \approx 422\ \mathrm{cm}^{-3}$

$\Omega_\gamma \approx 5\ 10^{-5}$

$T_\gamma \approx 2.7\ \mathrm{cm}^{-3}$

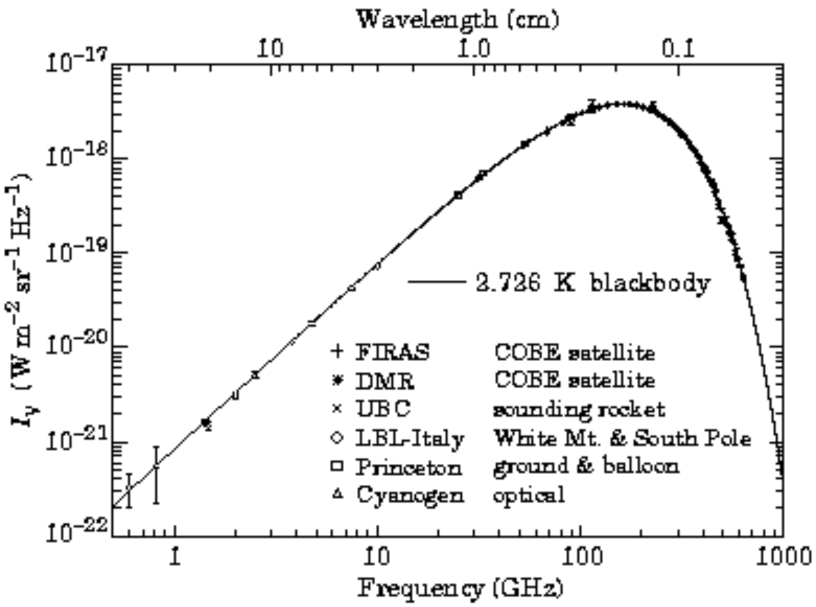

Figure 1. Precise measurements of the CMB spectrum. The line represents a 2.73 K blackbody, which describes the spectrum very well, especially around the peak of intensity. The spectrum is less well constrained at frequencies of 3 GHz and below (10 cm and longer wavelengths). (References for this figure are at the end of this section under "CMB Spectrum References.")

Fossil from the first month.

Smoot & Scott '98

There is also a background of neutrinos with $T_\nu \approx 2$ K and $n_\nu \approx 115\ \mathrm{cm}^{-3}$.

They are detected indirectly through their effect in the expansion history.

<u>BBN</u>: Nuclear physics applied in an expanding universe

Fossil from the first minutes.

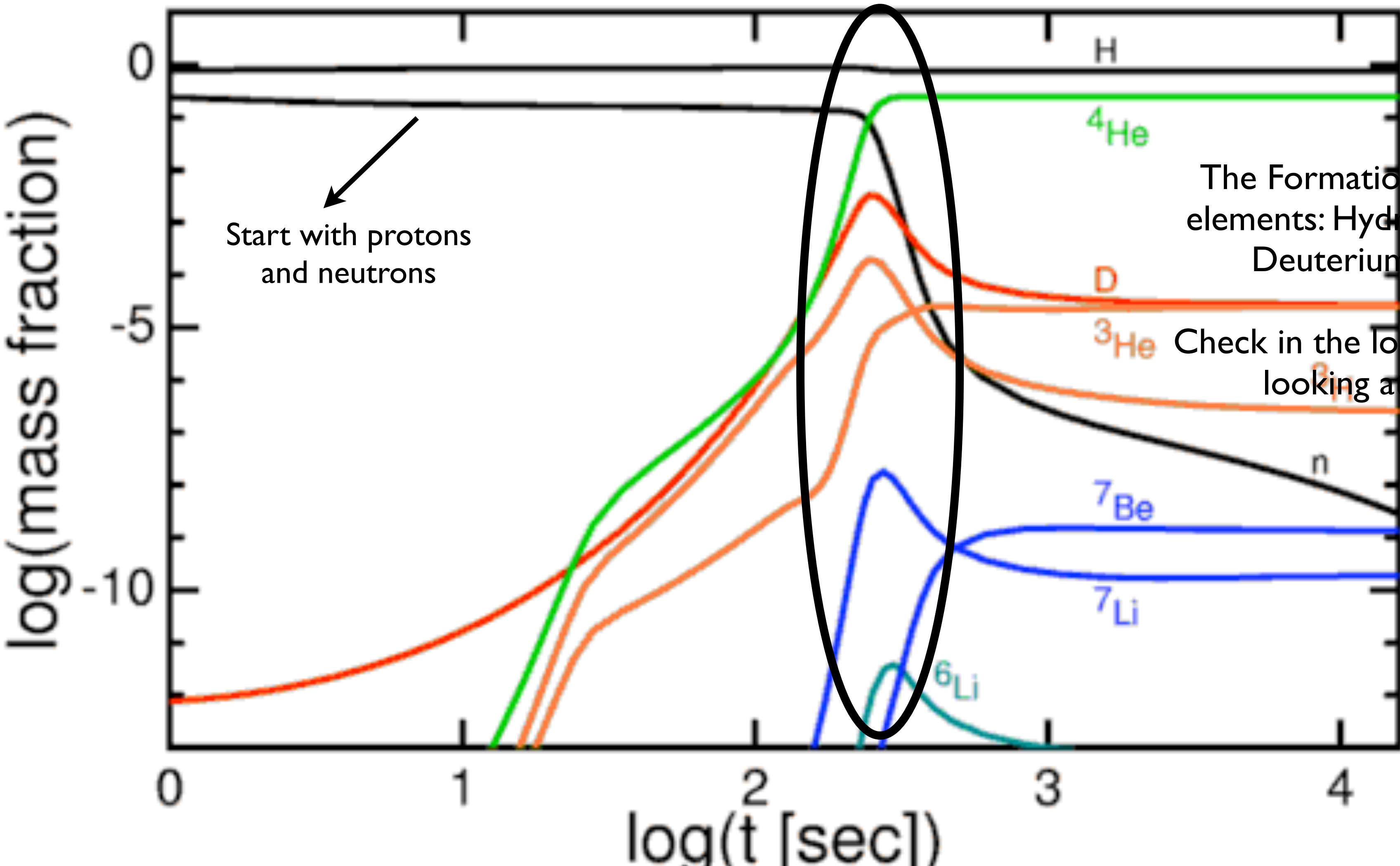

The Formation of the light elements: Hydrogen, Helium, Deuterium, Lithium

Check in the local universe by looking at spectra

Direct imaging

Scale shows temperature. Not much structure at the time, just tiny differences in the temperature of ten parts per million.

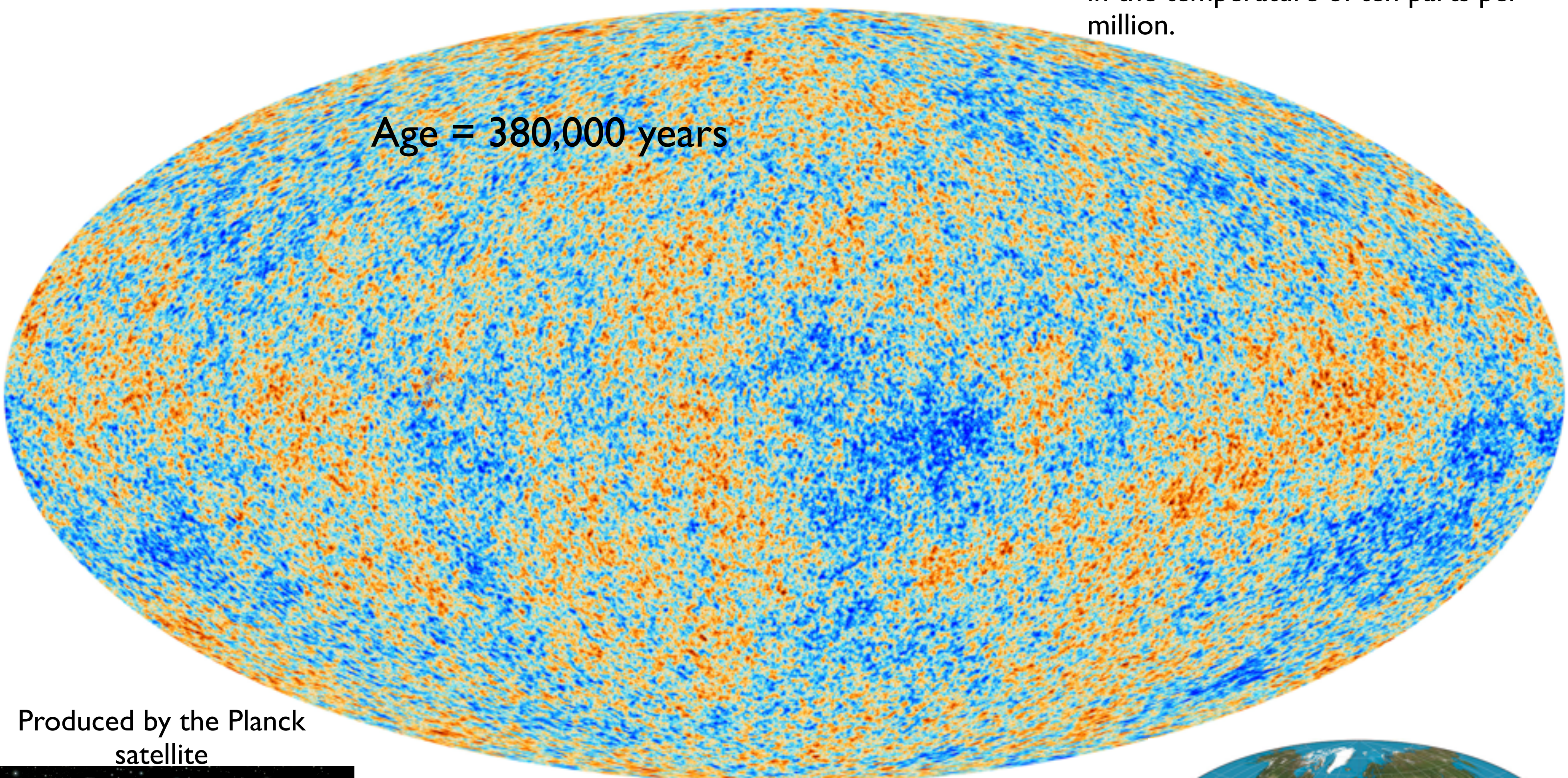

Produced by the Planck satellite

Current Age = 13, 800, 000, 000 years

1965 Penzias and Wilson

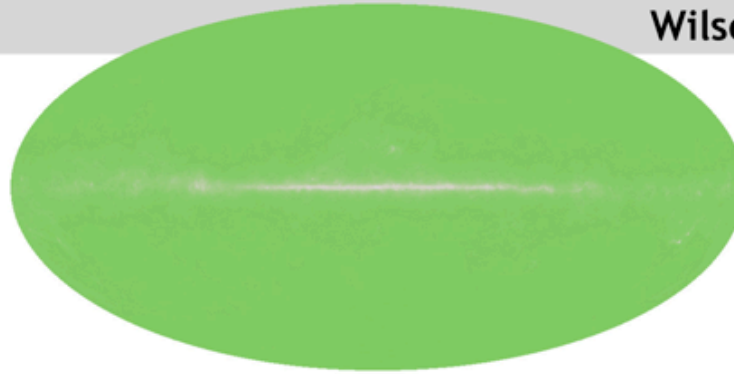

1992 COBE

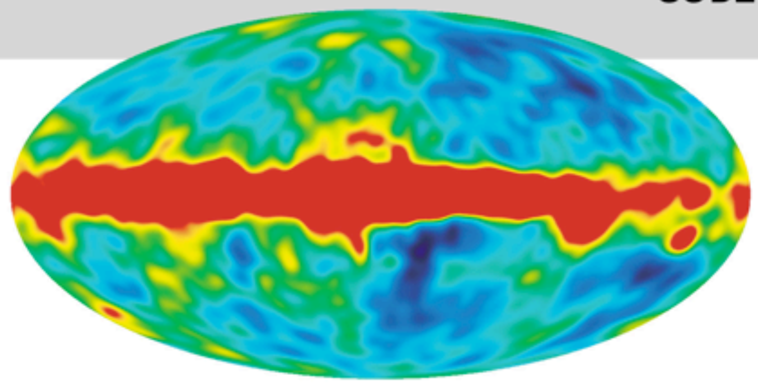

2003 WMAP

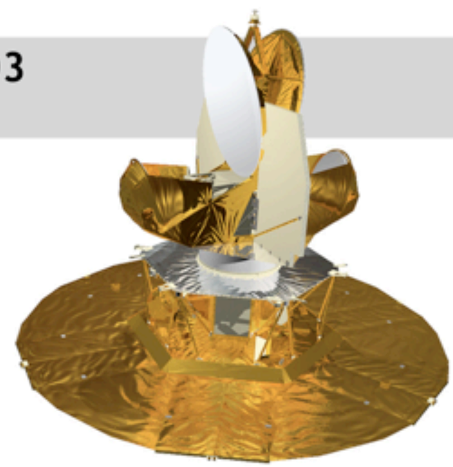

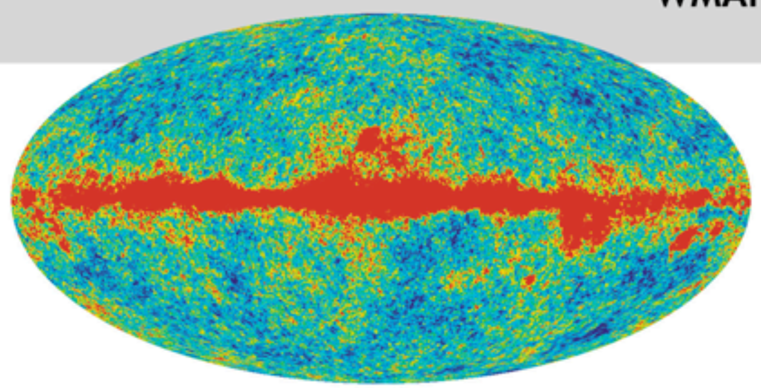

The Cosmic Microwave Background as seen by Planck and WMAP

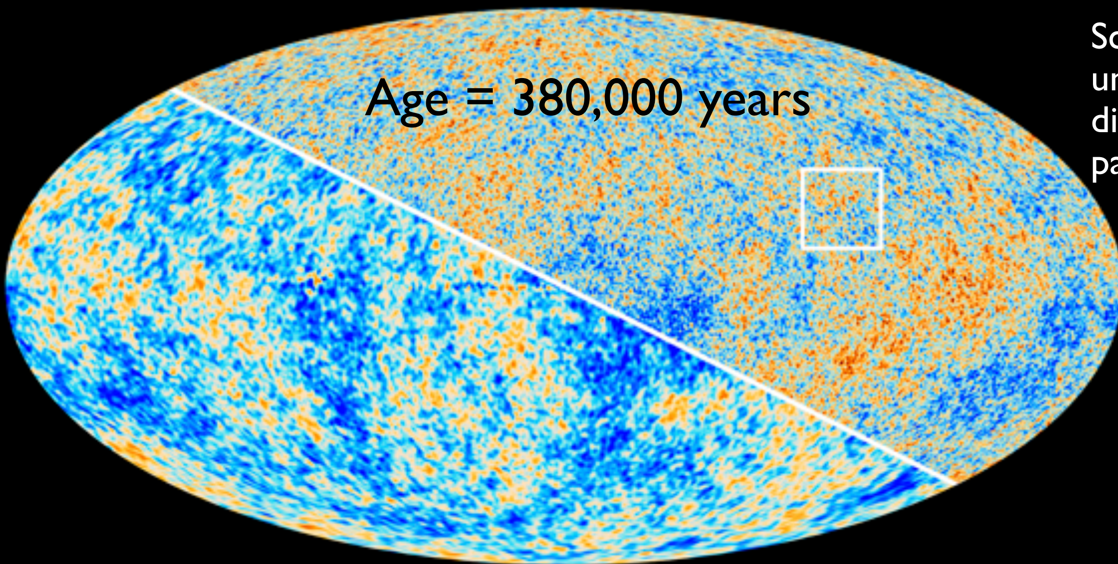

Scale shows the temperature of the universe. No real structure, just tiny differences in the temperature of ten parts per million.

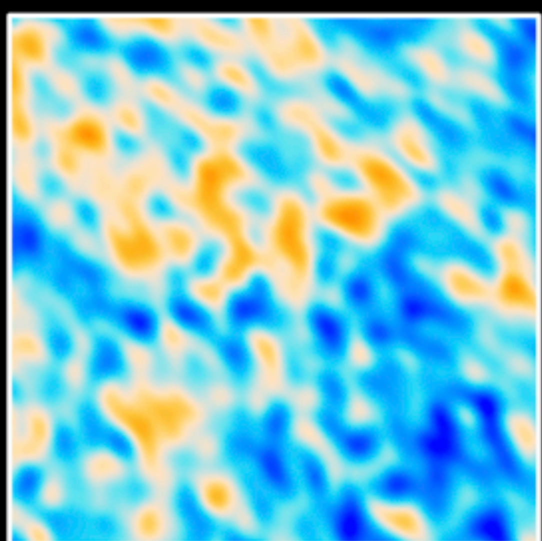

WMAP

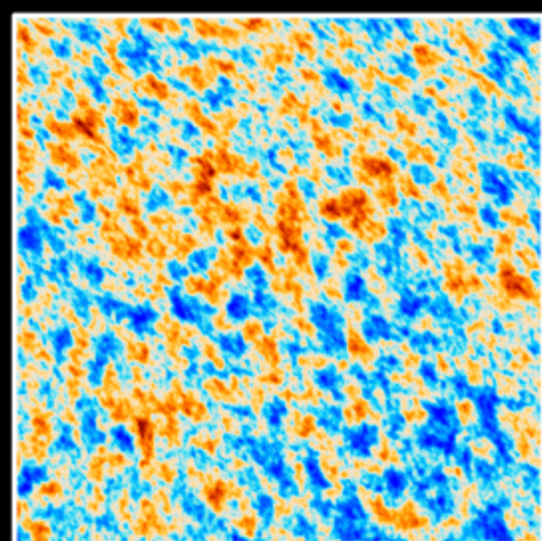

Planck

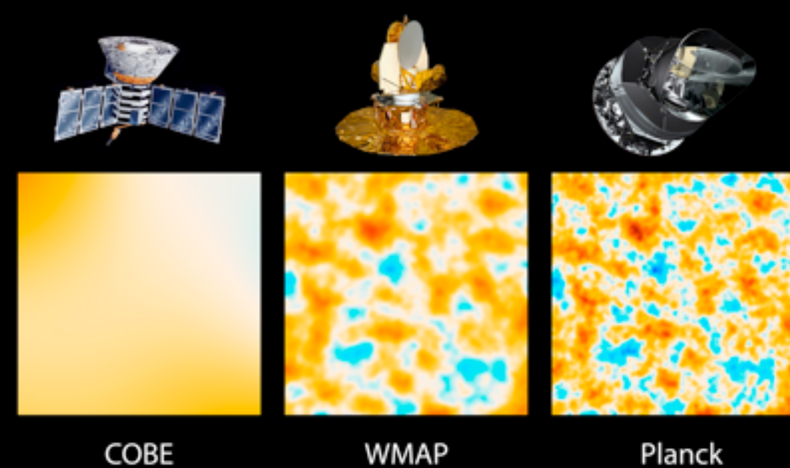

Current Age = 13, 800, 000, 000 years

Anisotropies and gravitational instability

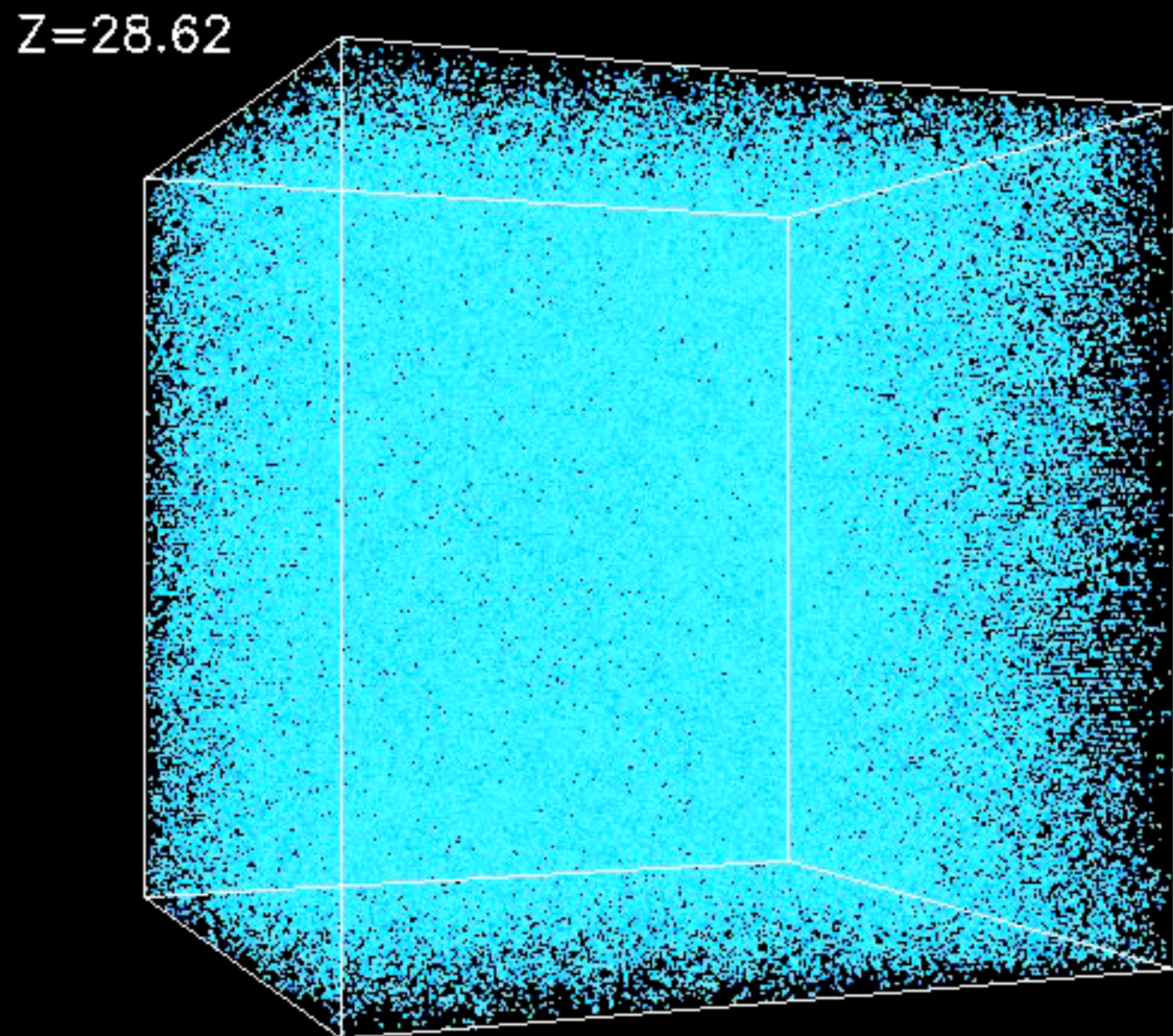

Large Scale Structure of the Universe

Map of a region of the Universe around us. Each point shows the location of a galaxy.

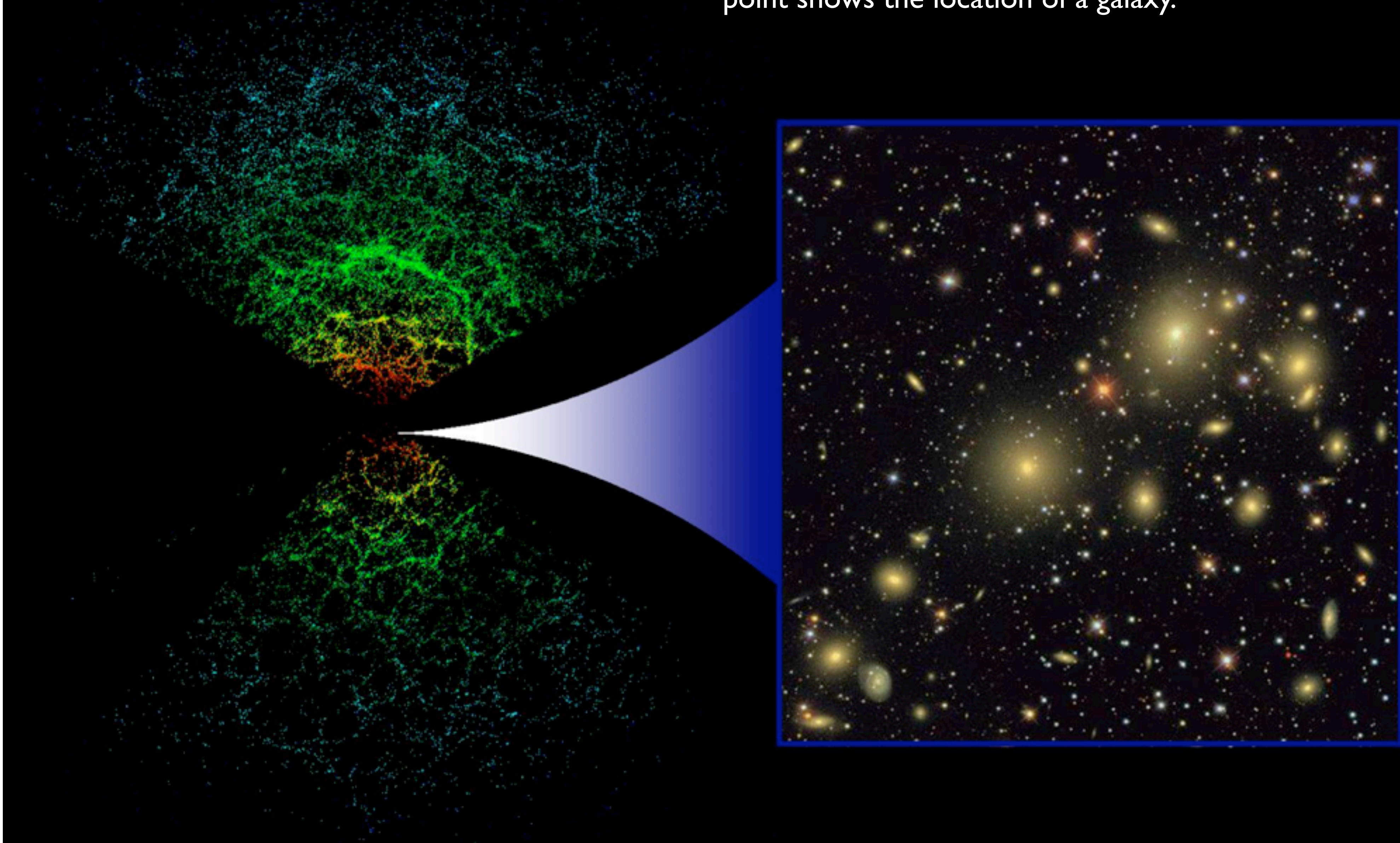

Sloan Digital Sky Survey

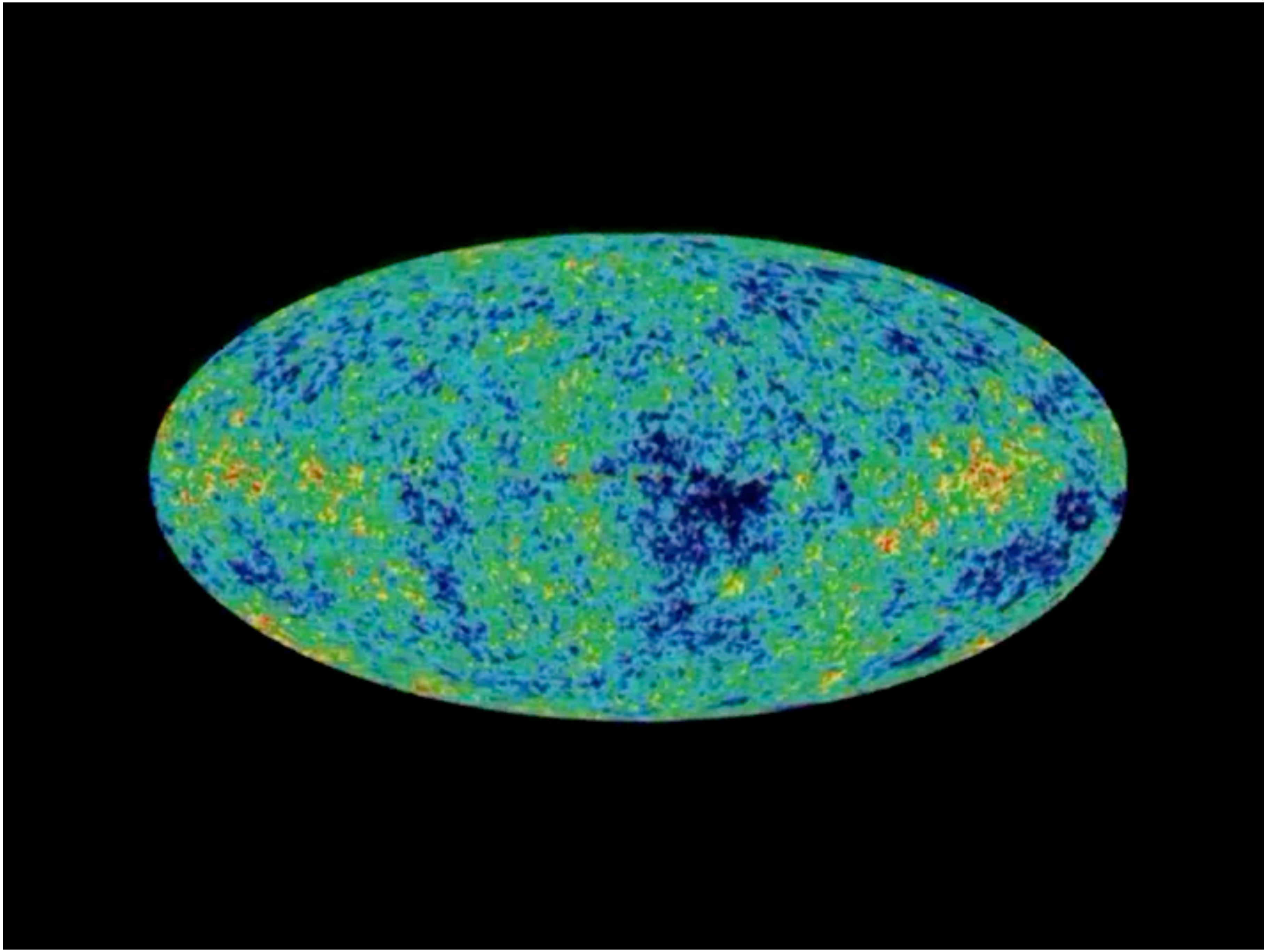

http://lambda.gsfc.nasa.gov/

Anisotropies and gravitational instability

If we know the composition we know the relevant dynamical equations but we still need to initial conditions. Initial conditions are not forgotten.

Predictions are statistical in nature.

We typically compute the amplitude of fluctuations as a function of scale or power spectrum.

Fluctuations are fossils from before the big bang itself.

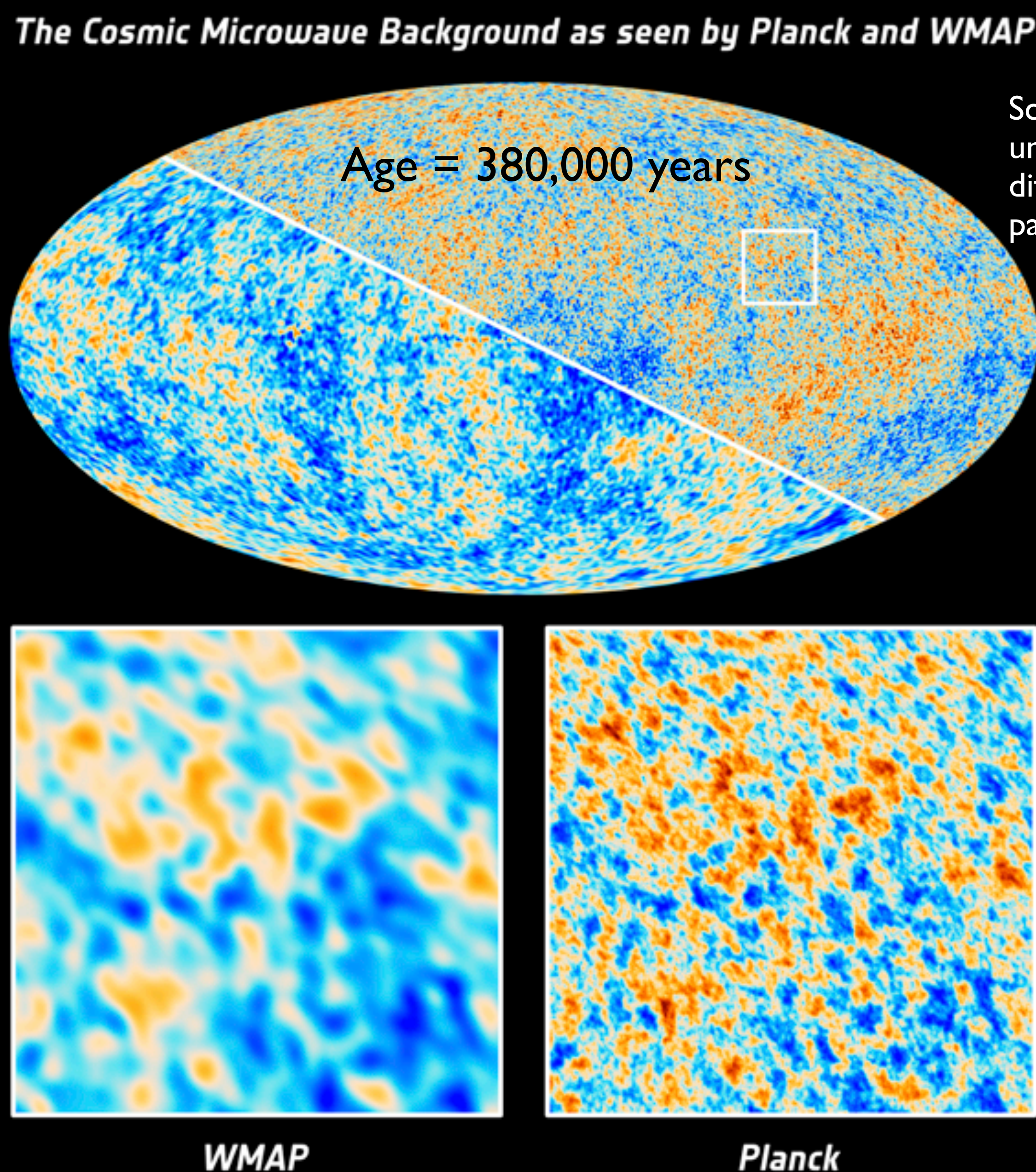

Scale shows the temperature of the universe. No real structure, just tiny differences in the temperature of ten parts per million.

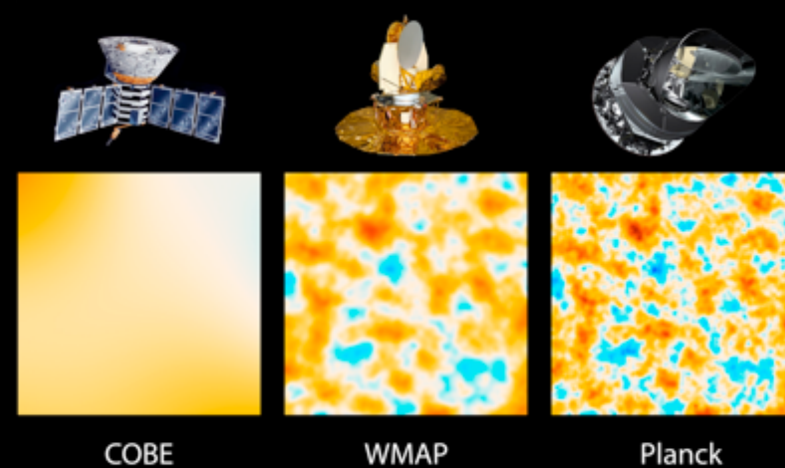

Current Age = 13, 800, 000, 000 years

CMB Spectra

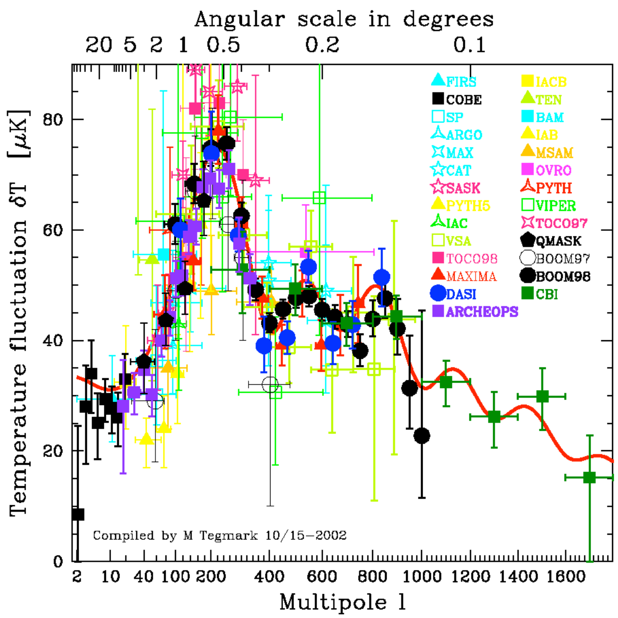

Angular scale in degrees
20 5 2 1 0.5 0.2 0.1
Temperature fluctuation δT [μK]
0 20 40 60 80
FIRS
COBE
SP
ARGO
MAX
CAT
SASK
PYTH5
IAC
VSA
TOCO98
MAXIMA
DASI
ARCHEOPS
IACB
TEN
BAM
IAB
MSAM
OVRO
PYTH
VIPER
TOCO97
QMASK
BOOM97
BOOM98
CBI
Compiled by M Tegmark 10/15–2002
2 10 40 100 200 400 600 800 1000 1200 1400 1600
Multipole l

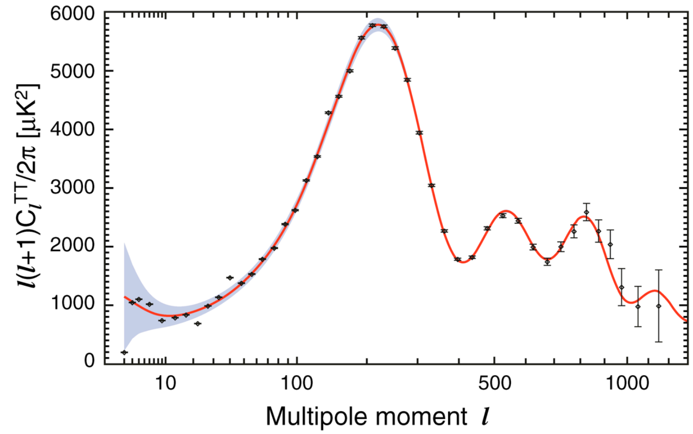

$l(l+1)C_l^{TT}/2\pi$ [μK²]
0 1000 2000 3000 4000 5000 6000
10 100 500 1000
Multipole moment l

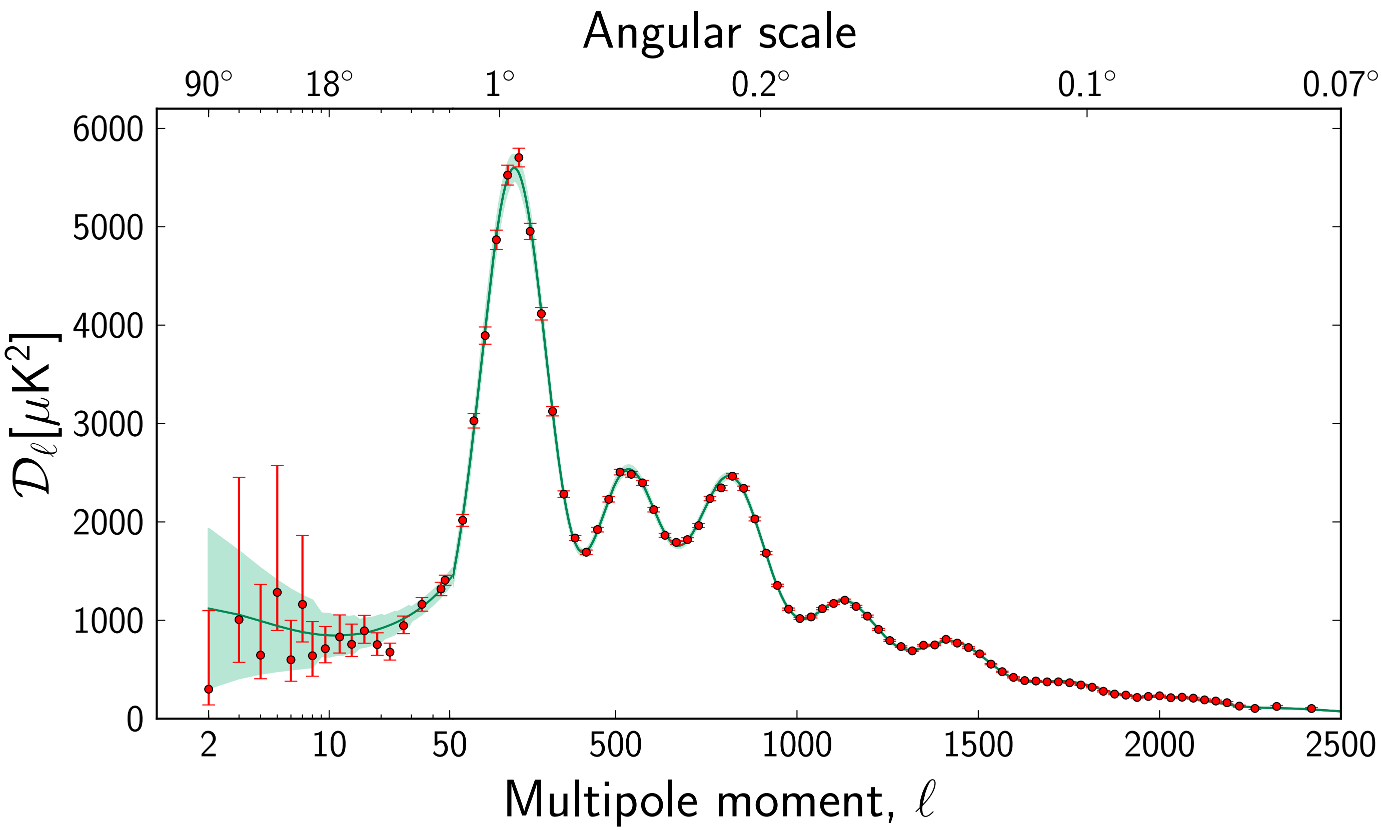

Angular scale
90° 18° 1° 0.2° 0.1° 0.07°
$\mathcal{D}_\ell [\mu K^2]$
0 1000 2000 3000 4000 5000 6000
2 10 50 500 1000 1500 2000 2500
Multipole moment, ℓ

Temperature differences on different angular scales

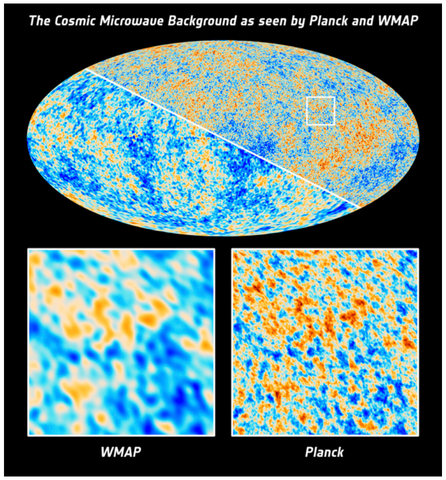

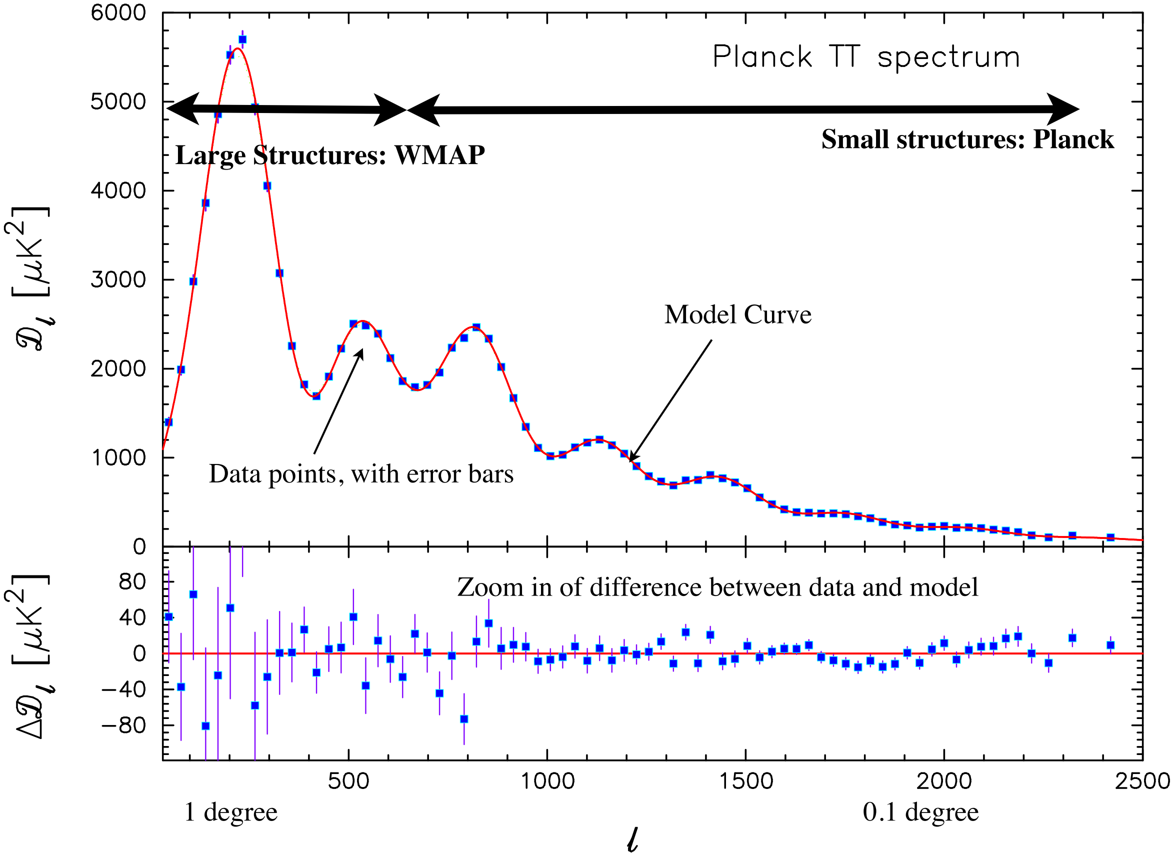

CMB in the year 2000

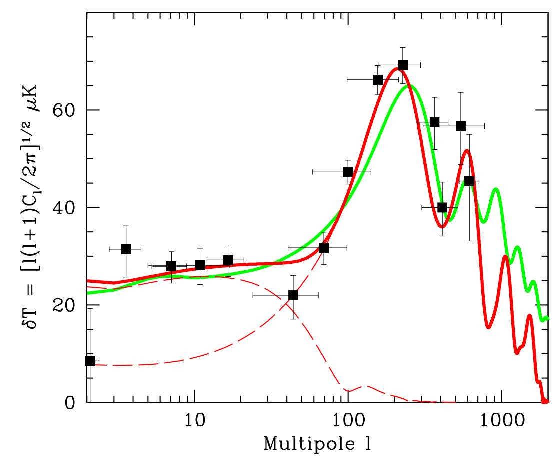

Observational Results

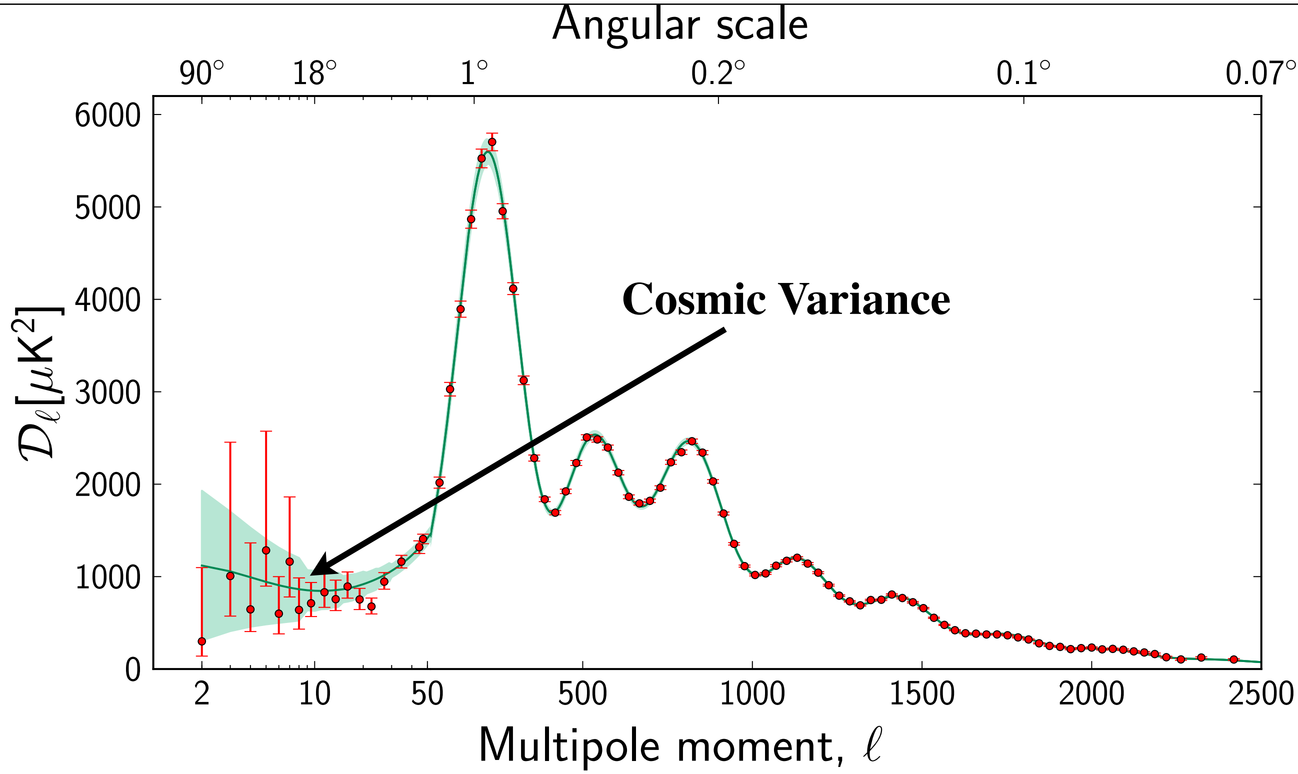

	Parameter	*Planck* Best fit	*Planck* 68% limits	*Planck*+WP Best fit	*Planck*+WP 68% limits
Recombination/Composition	$\Omega_b h^2$	0.022068	0.02207 ± 0.00033	0.022032	0.02205 ± 0.00028
	$\Omega_c h^2$	0.12029	0.1196 ± 0.0031	0.12038	0.1199 ± 0.0027
	$100\theta_{MC}$	1.04122	1.04132 ± 0.00068	1.04119	1.04131 ± 0.00063
Late times	τ	0.0925	0.097 ± 0.038	0.0925	$0.089^{+0.012}_{-0.014}$
Initial Conditions	n_s	0.9624	0.9616 ± 0.0094	0.9619	0.9603 ± 0.0073
	$\ln(10^{10} A_s)$	3.098	3.103 ± 0.072	3.0980	$3.089^{+0.024}_{-0.027}$
Derived parameters	Ω_Λ	0.6825	0.686 ± 0.020	0.6817	$0.685^{+0.018}_{-0.016}$
	Ω_m	0.3175	0.314 ± 0.020	0.3183	$0.315^{+0.016}_{-0.018}$
	σ_8	0.8344	0.834 ± 0.027	0.8347	0.829 ± 0.012
	z_{re}	11.35	$11.4^{+4.0}_{-2.8}$	11.37	11.1 ± 1.1
	H_0	67.11	67.4 ± 1.4	67.04	67.3 ± 1.2
	$10^9 A_s$	2.215	2.23 ± 0.16	2.215	$2.196^{+0.051}_{-0.060}$
	$\Omega_m h^2$	0.14300	0.1423 ± 0.0029	0.14305	0.1426 ± 0.0025
	Age/Gyr	13.819	13.813 ± 0.058	13.8242	13.817 ± 0.048
	z_*	1090.43	1090.37 ± 0.65	1090.48	1090.43 ± 0.54
	$100\theta_*$	1.04139	1.04148 ± 0.00066	1.04136	1.04147 ± 0.00062
	z_{eq}	3402	3386 ± 69	3403	3391 ± 60

FRW Background

$$t_{dyn} = \frac{a}{\dot{a}} = \frac{1}{H} = \frac{1}{a\mathcal{H}}$$

$$ds^2 = a^2(\tau)[-d\tau^2 + dx^2]$$

$$\mathcal{H}^2 = (\frac{\dot{a}}{a})^2 = \frac{8\pi G a^2}{3}\rho$$

$$a d\tau = dt$$

$$\dot{\rho} = 3\mathcal{H}(\rho + p)$$

$$\Omega = \frac{8\pi G}{3H^2}\rho \equiv \frac{\rho}{\rho_{\rm crit}}$$

$$\rho \propto \Omega h^2 \equiv \omega \propto \frac{\rho}{\rho_\gamma}$$

$$(1+z) = \frac{a_{obs}}{a_{em}}$$

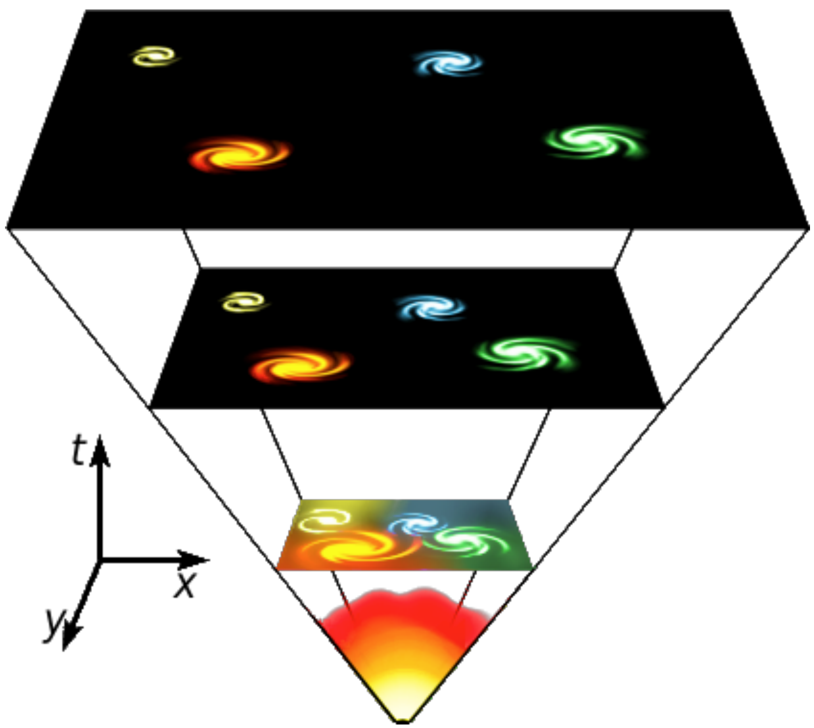

Take to test particles separated by 10 million light years and trace their position back in time.

light year = distance light can travel in one year = 10 000 000 000 000 km = 6 000 000 000 000 miles

Age of the Universe	Distance
14 Billion years	10 Million light years
1/3 second	1/2 light day

This happens because of gravity is an attractive force so the expansion of the universe has been decelerating. This implies that as you trace the atom back in time it was both closer but also moving away from us faster.

Conformal diagram

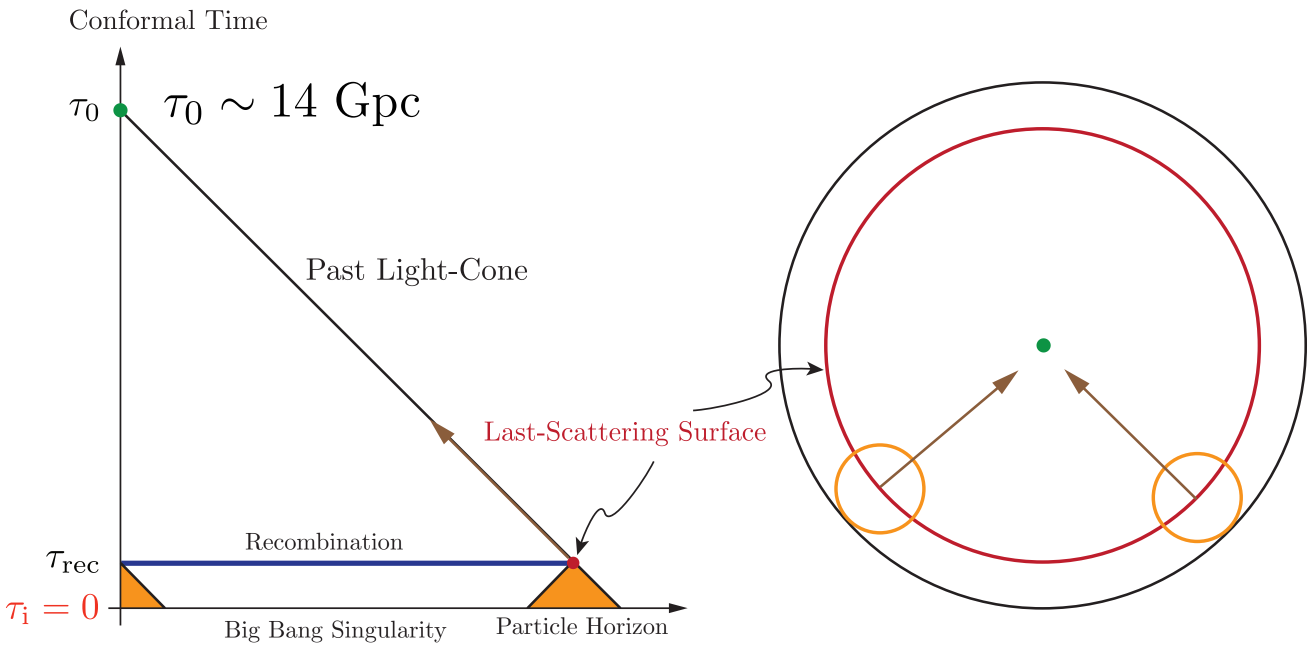

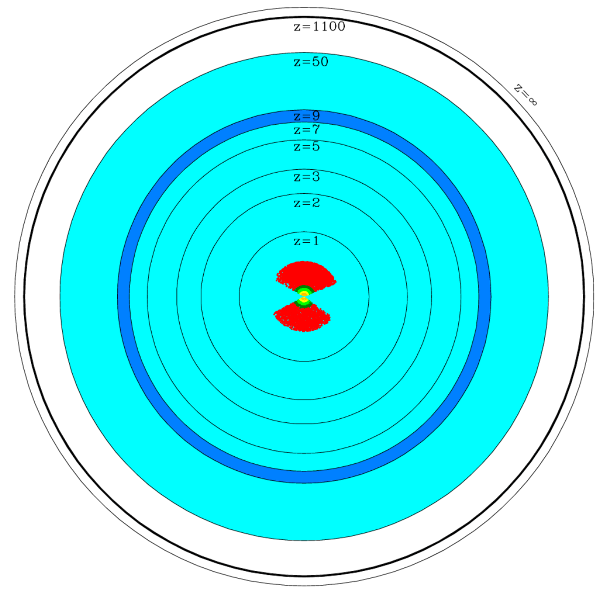

Figure 8: Conformal diagram of Big Bang cosmology. The CMB at last-scattering (recombination) consists of 10^5 causally disconnected regions!

$$\tau_{rec} \sim 300 \text{ Mpc}$$

$$a(\tau) \propto \tau \quad \text{(Radiation era)}$$

$$a(\tau) \propto \tau^2 \quad \text{(Matter era)}$$

$$ds^2 = a^2(\tau)[-d\tau^2 + dx^2]$$

Horizon Scale

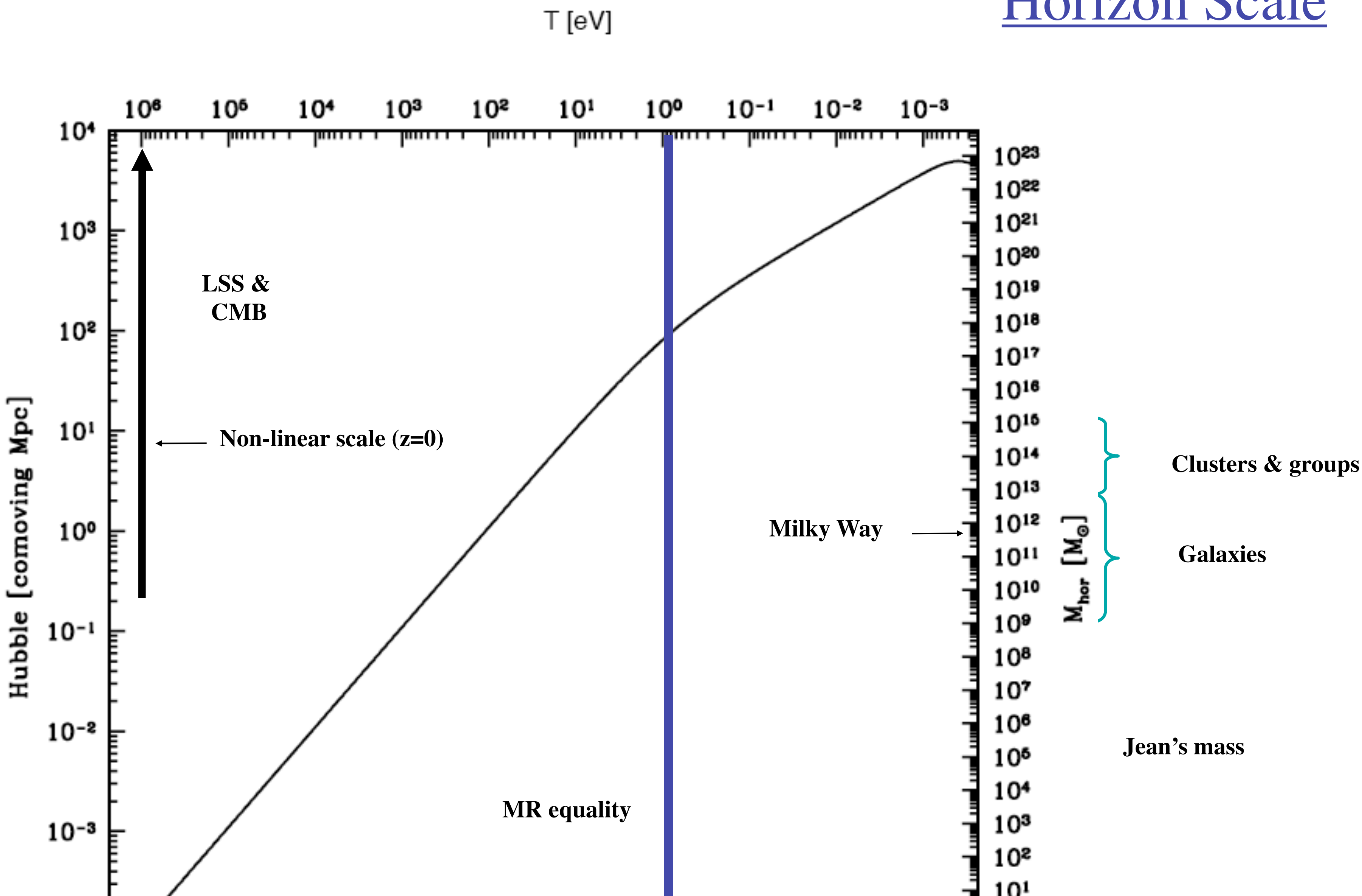

$$\frac{1}{Ha} = \frac{1}{\mathcal{H}}$$

Anisotropies in the CMB Temperature

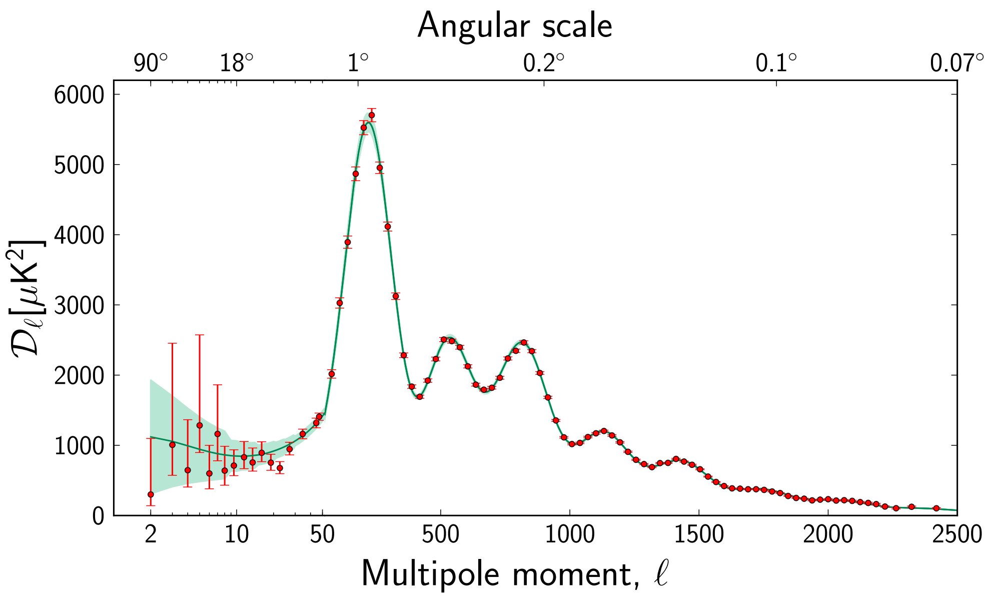

Outline

- Basic equations
- Solution under some simplifying assumption
- Basic parameter dependences

References:

Bashinky & Seljak astro-ph/0310198
Bashinky astro-ph/0405157
Seljak ApJ 435 L87 (1994)
Ma & Bertschinger ApJ 455 7 (1995)

Recombination

T = 0.3 eV << $m_e c^2$

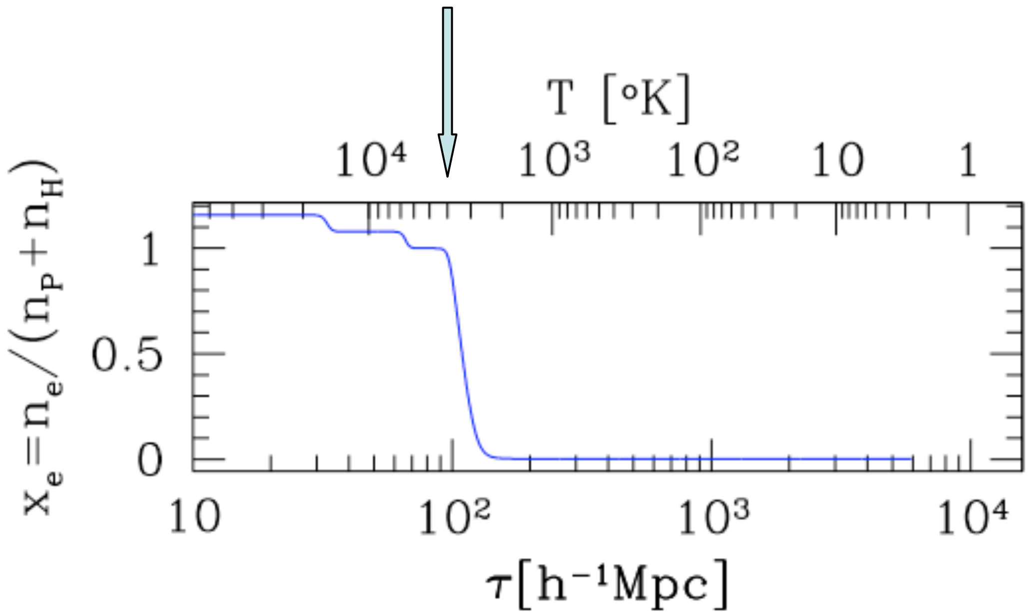

Hydrogen is ionized **Hydrogen is neutral**

Thomson Scattering

$$\tau_c = \frac{1}{a n_e \sigma_T}$$

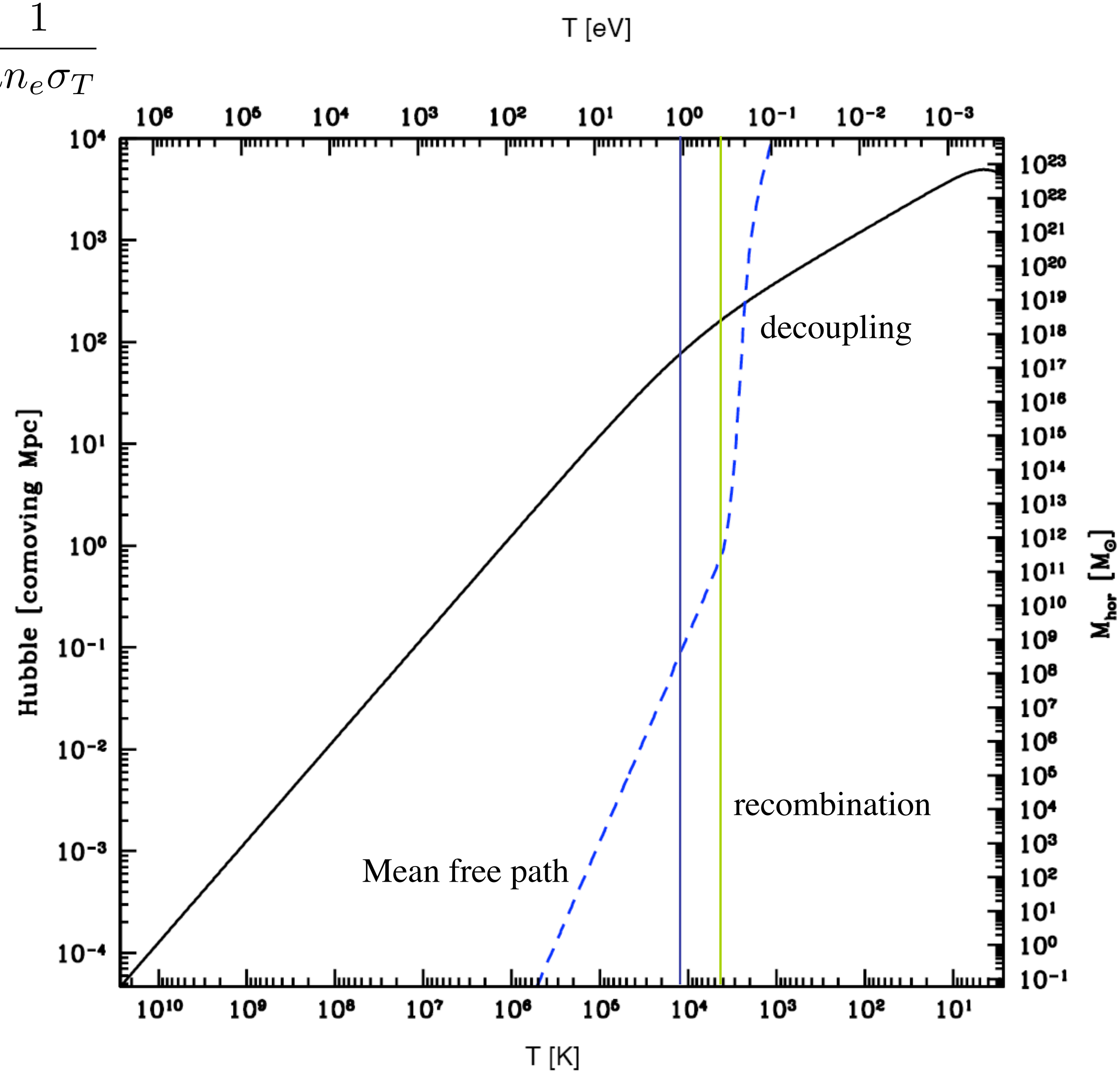

Perturbations

Relativistic perturbation theory

$$ds^2 = a^2(\tau)[-(1+2\Phi)d\tau^2 + (1-2\Psi)dx^2]$$

Conformal-Newtonian

$$T^{\mu\nu}_{a;\nu} = 0$$

$$\begin{aligned}
T^0_{a0} &= -(\rho_a + \delta\rho_a) \\
T^0_{ai} &= (\rho_a + p_a)v_{ia} \\
T^i_{aj} &= \delta^i_j(p_a + \delta p_a) + (\rho_a + p_a)\Pi^i_{aj} \\
v_{ia} &= -\nabla_i u_a \\
\Pi^i_{aj} &= \frac{3}{2}(\nabla^i\nabla^j - \frac{1}{3}\delta^i_j\nabla^2)\pi_a
\end{aligned}$$

$$\begin{aligned}
\delta\rho_a &= (\rho_a + p_a)\delta_a \\
\delta p_a &= c_a^2\delta\rho_a
\end{aligned}$$

$$\begin{aligned}
w_a &= \frac{p_a}{\rho_a} \\
c_a^2 &= \frac{\dot{p}_a}{\dot{\rho}_a}
\end{aligned}$$

δ_a Fluctuation in the number density

$$\begin{aligned}
\dot{\delta}_a &= \nabla^2 u_a + 3\dot{\Psi} \\
\dot{u}_a &= c_a^2\delta_a - \mathcal{H}(1-3c_a^2)u_a + \nabla^2\pi_a + \Phi
\end{aligned}$$

Perturbations

$$ds^2 = a^2(\tau)[-(1+2\Phi)d\tau^2 + (1-2\Psi)dx^2]$$

$$\dot{\delta}_a = \nabla^2 u_a + 3\dot{\Psi}$$

$$d_a = \delta_a - 3\Psi$$

$$\begin{aligned} \dot{d}_a &= \nabla^2 u_a \\ \dot{u}_a &= c_a^2 d_a - \mathcal{H}(1-3c_a^2)u_a + \nabla^2\pi_a + \Phi + 3c_a^2\Psi \end{aligned}$$

$$\ddot{d}_a + \mathcal{H}(1-3c_a^2)\dot{d}_a - c_a^2\nabla^2 d_a - \nabla^4\pi_a = \nabla^2(\Phi + 3c_a^2\Psi)$$

$$\begin{aligned} \nabla^2\Psi - 3\gamma\Psi &= \gamma(d + 3\mathcal{H}u) \\ \Psi - \Phi &= 3\gamma\pi \\ \gamma &= 4\pi G a^2(\rho + p) \\ d &= \sum_a x_a d_a \quad u = \sum_a x_a u_a \quad \pi = \sum_a x_a \pi_a \\ x_a &= (\rho_a + p_a)/(\rho + p) \end{aligned}$$

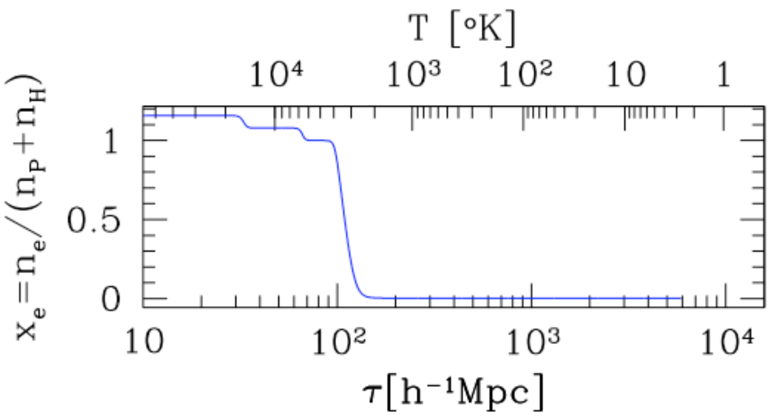

T [°K]
10^4
10^3
10^2
10
1
$x_e = n_e/(n_p + n_H)$
1
0.5
0
10
10^2
10^3
10^4
$\tau [h^{-1}Mpc]$

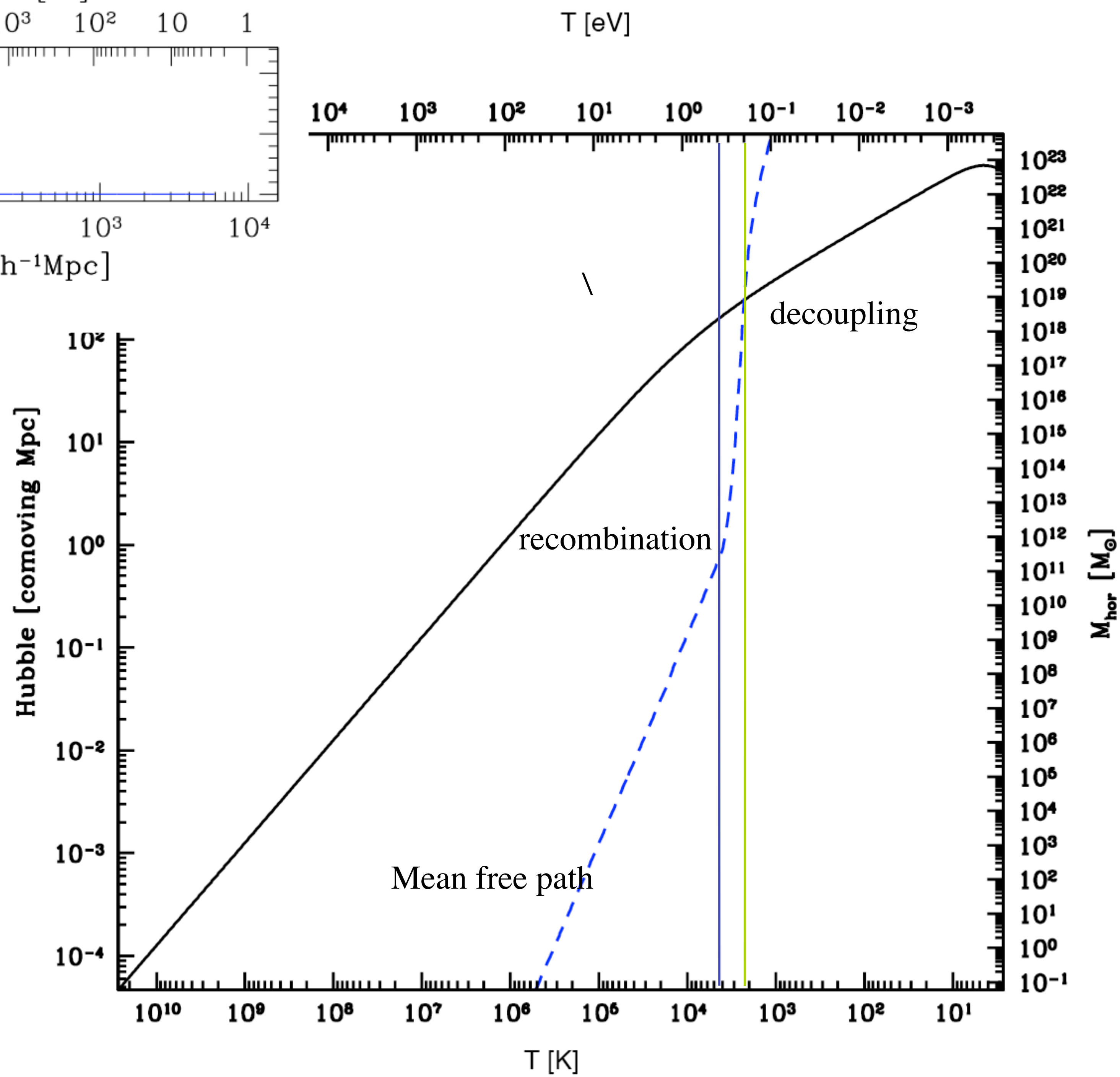

T [eV]
10^4
10^3
10^2
10^1
10^0
10^{-1}
10^{-2}
10^{-3}
decoupling
recombination
Mean free path
Hubble [comoving Mpc]
10^2
10^1
10^0
10^{-1}
10^{-2}
10^{-3}
10^{-4}
M_{hor} [$M_\odot$]
10^{23}
10^{22}
10^{21}
10^{20}
10^{19}
10^{18}
10^{17}
10^{16}
10^{15}
10^{14}
10^{13}
10^{12}
10^{11}
10^{10}
10^9
10^8
10^7
10^6
10^5
10^4
10^3
10^2
10^1
10^0
10^{-1}
T [K]
10^{10}
10^9
10^8
10^7
10^6
10^5
10^4
10^3
10^2
10^1

Components

- Photon-Baryon "fluid"
- Neutrinos
- Cold Dark matter

What determines the temperature of recombination?

$$\frac{\rho_b}{\rho_\gamma} \propto \Omega_b h^2 = \omega_b$$

Dependence is weak.

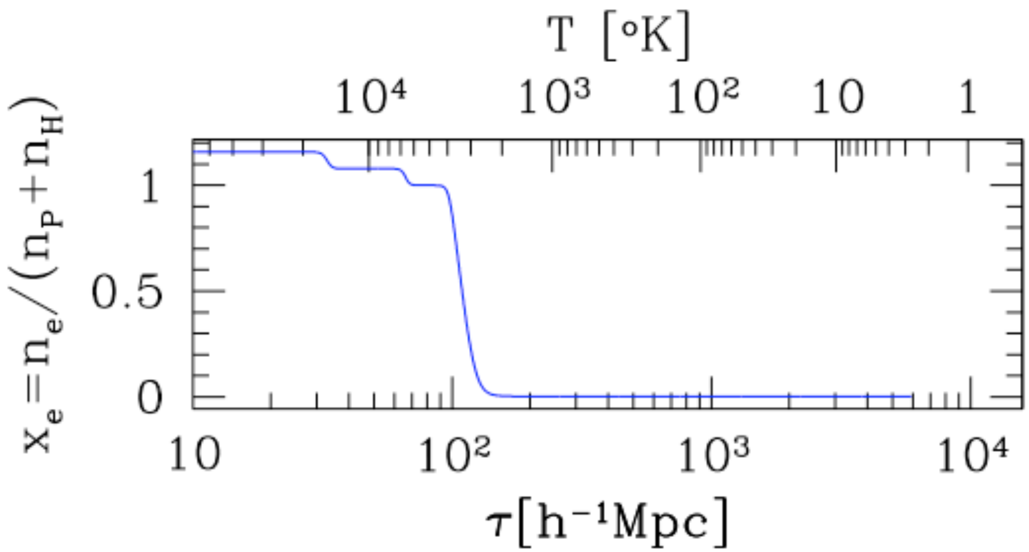

Conformal time depends on total amount of radiation and matter.

$$\tau \propto 1/\mathcal{H} \qquad \mathcal{H}^2 \propto (\rho_\gamma + \rho_\nu + \rho_b + \rho_c)$$

Linear Theory: go to Fourier Space
Note relation between k and angle

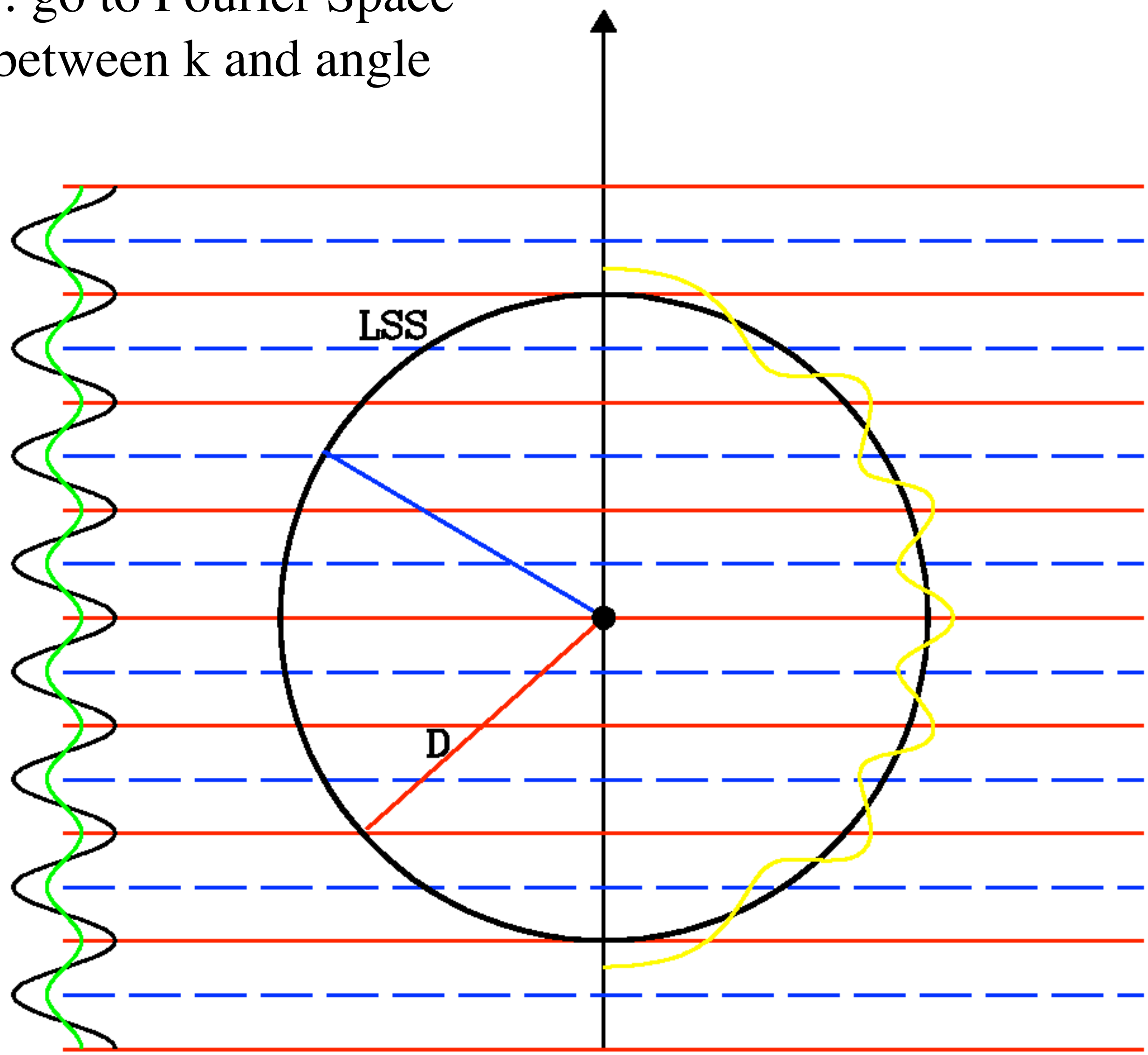

Radiation era (Initial Conditions)

$$\mathcal{H} = \frac{1}{\tau} \qquad \gamma = \frac{1}{\tau^2} \qquad c_\gamma^2 = \frac{1}{3}$$

$$\begin{aligned} \ddot{d}_\gamma + \frac{1}{3}k^2 d_\gamma &= -2k^2\Phi \\ -k^2\tau^2\Phi - 6\Phi &= 2d_\gamma - 6\frac{\dot{d}_\gamma}{k^2\tau} \end{aligned}$$

$$d''_\gamma + \frac{12}{6x + x^3}d'_\gamma + [\frac{1}{3} - \frac{4}{6 + x^2}]d_\gamma = 0$$

$$x = k\tau \qquad ' = \frac{d}{dx}$$

$$x << 1 \rightarrow d_\gamma \propto 1/x \quad ; \quad \text{constant}$$

Radiation era (Initial Conditions)

$$c_\gamma^2 = \frac{1}{3}$$

$$d_\gamma = d_{\gamma,ini}(2\frac{\sin\varphi}{\varphi} - \cos\varphi)$$
$$v_\gamma = d_{\gamma,ini} c_\gamma \frac{(2-\varphi^2)\sin\varphi - 2\varphi\cos\varphi}{\varphi^2}$$
$$\Phi = d_{\gamma,ini}\frac{2(\varphi\cos\varphi - \sin\varphi)}{\varphi^3}$$
$$\varphi = c_\gamma x$$

$$d_\gamma = d_{\gamma,ini}(1 + \frac{\varphi^2}{6} + \cdots)$$
$$v_\gamma = -d_{\gamma,ini} c_\gamma \frac{\varphi}{3} + \cdots$$
$$\Phi = d_{\gamma,ini}(-\frac{2}{9} + \frac{\varphi^2}{45} + \cdots)$$

Only relevant parameter initial amplitude.

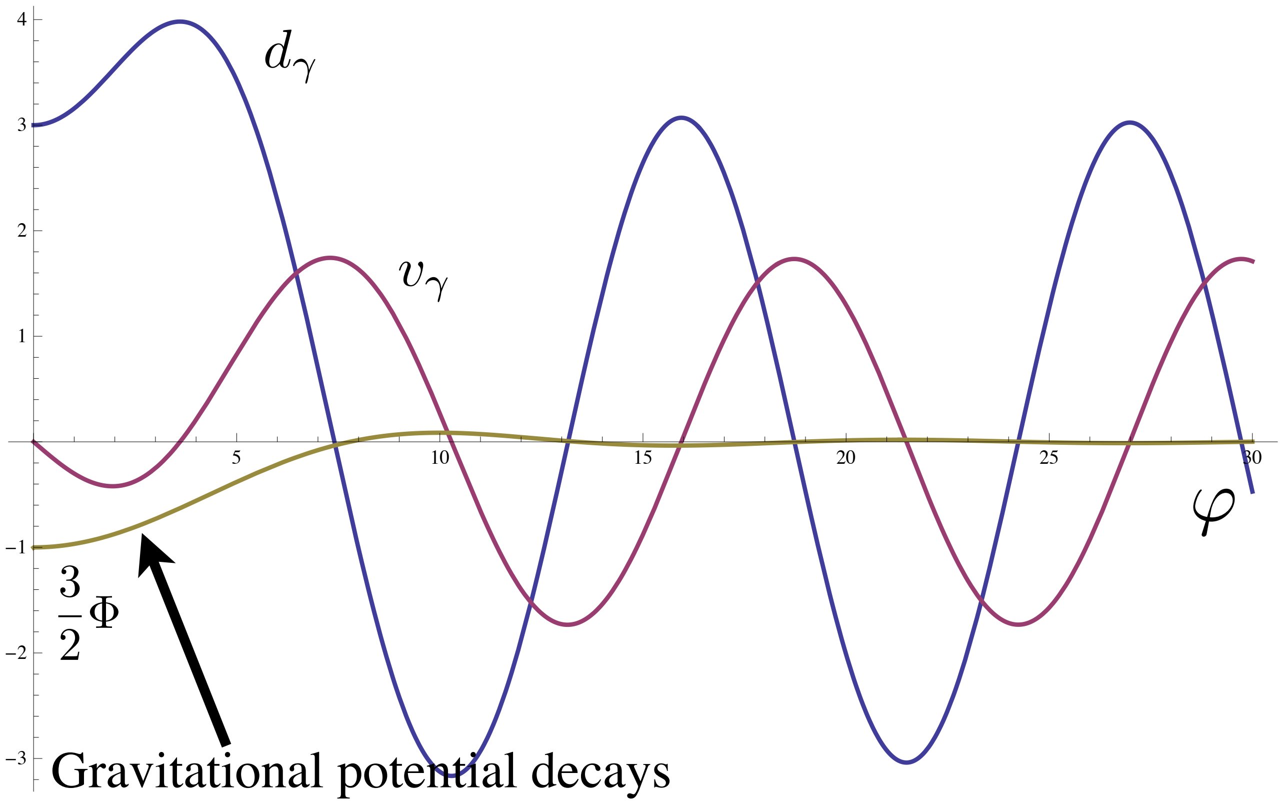

Caution: Quantities outside the horizon are particularly gauge dependent.

Two fluid model

Radiation-matter universe only. Neglect neutrinos (for perturbations).

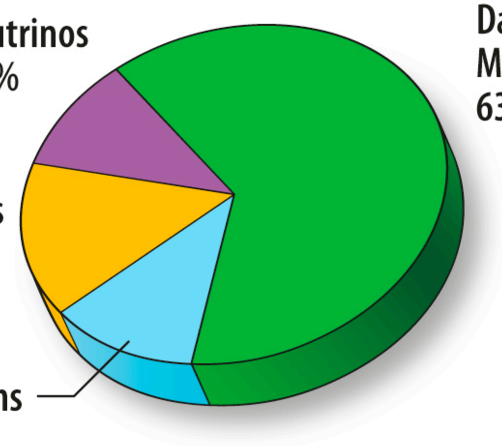

$$\frac{a(\bar{\tau})}{a_{eq}} = \bar{\tau} + \frac{\bar{\tau}^2}{4}$$

$$\bar{\tau} = 2(\sqrt{2}-1)\frac{\tau}{\tau_{eq}} \equiv \frac{\tau}{\tau_e}$$

$$c_c^2 = 0 \qquad \pi_c = 0$$

$$\ddot{d}_c + \mathcal{H}\dot{d}_c = -k^2\Phi$$

$$c_{\gamma b}^2 = \frac{1}{3(1+R_b)} \qquad R_b = \frac{3\rho_b}{4\rho_\gamma} \qquad \pi_{\gamma b} = 0$$

$$\ddot{d}_{\gamma b} + \frac{\mathcal{H}R_b}{(1+R_b)}\dot{d}_{\gamma b} + c_{\gamma b}^2 k^2 d_{\gamma b} = -k^2\frac{2+R_b}{(1+R_b)}\Phi$$

$$\Phi = -\frac{\gamma}{k^2+3\gamma}(d_\gamma - 3\mathcal{H}\frac{\dot{d}}{k^2})$$

Two fluid model

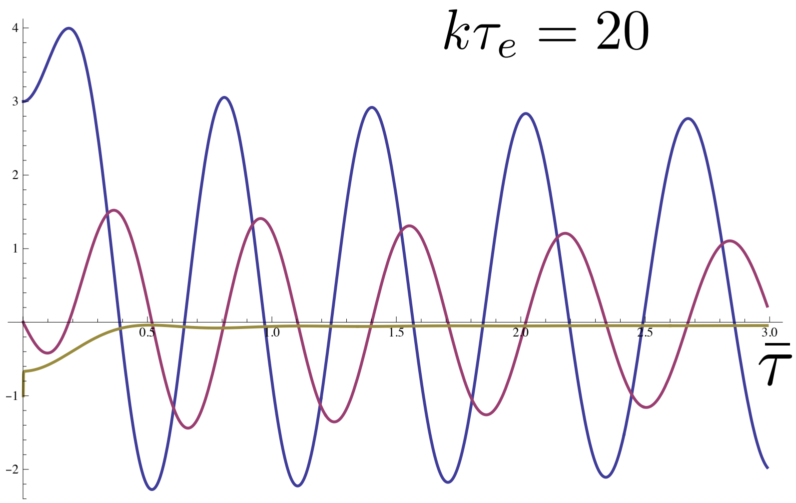

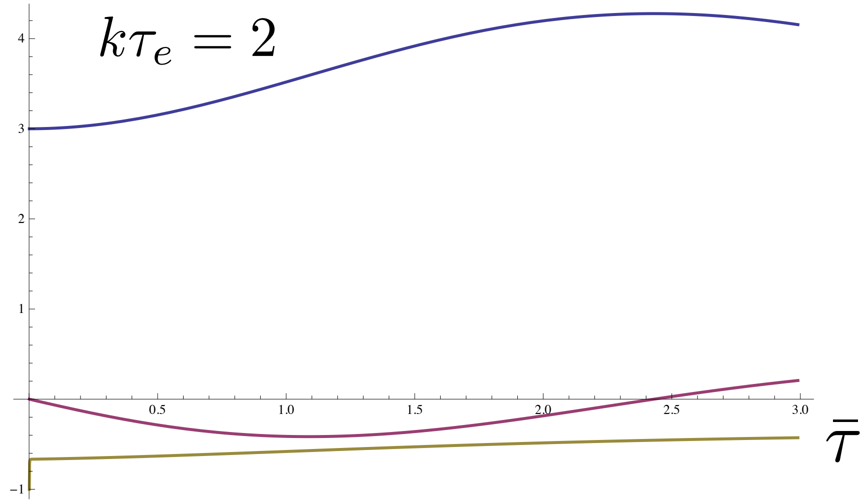

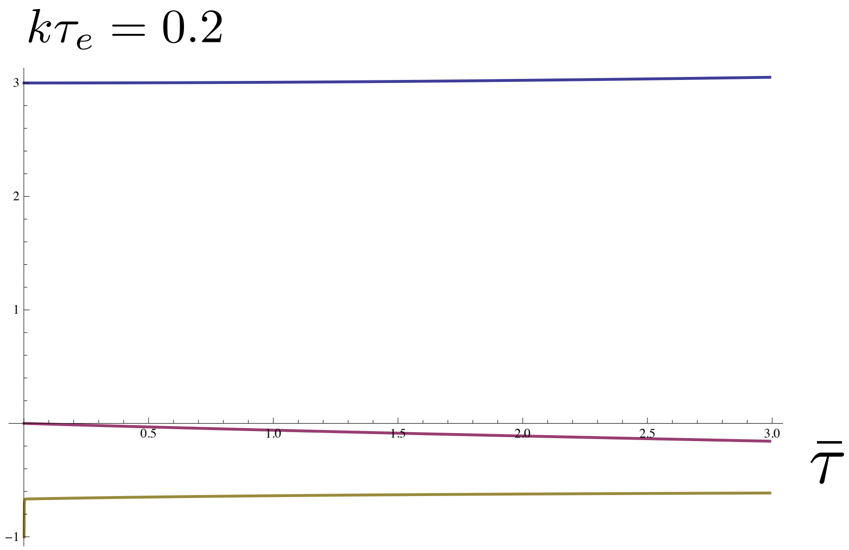

Two fluid model: Damping

$$\ddot{d}_{\gamma b} + \frac{\mathcal{H} R_b}{(1+R_b)}\dot{d}_{\gamma b} + 2\tau_d k^2 \dot{d}_{\gamma b} + c_{\gamma b}^2 k^2 d_{\gamma b} = -k^2 \frac{2+R_b}{(1+R_b)}\Phi$$

$$k\tau_e = 20$$

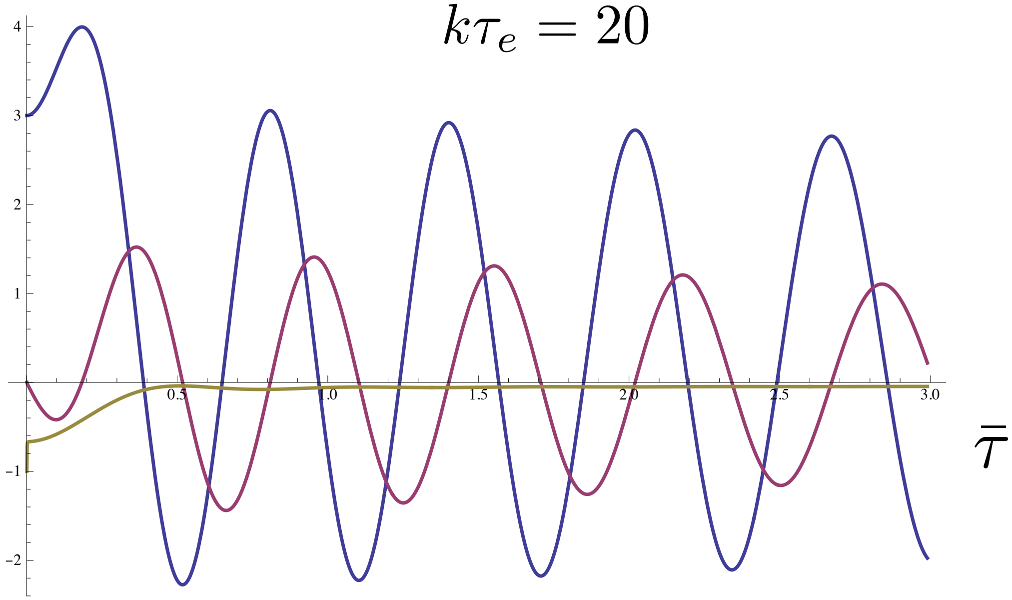

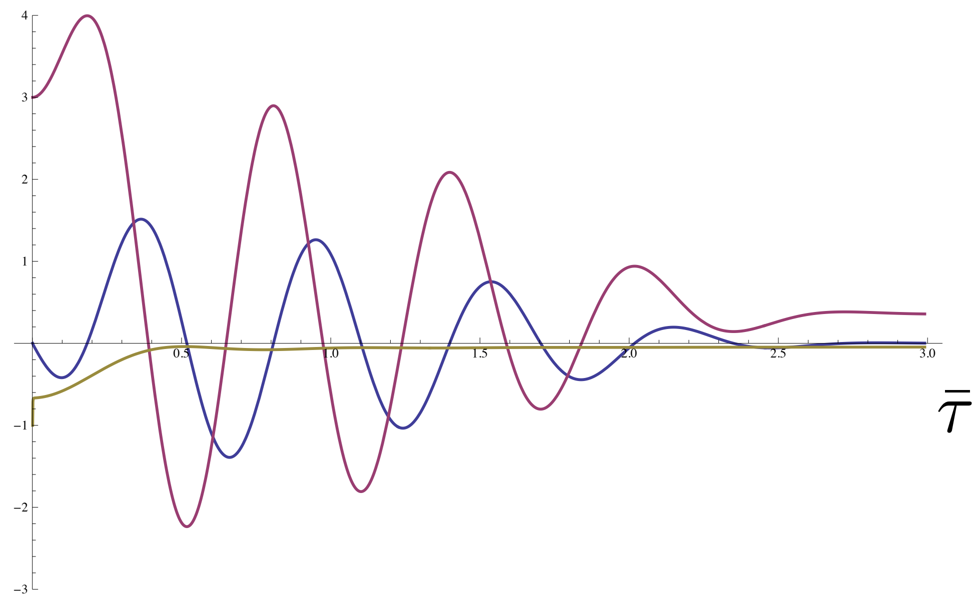

$$\tau_d = \frac{1}{a^2 n_e \sigma_T}\left[\frac{1}{6} - \frac{7}{45(1+R_b)} + \frac{1}{6(1+R_b)^2}\right]$$

$$\Omega_b h^2$$

$$\text{damping} \propto \exp[-\Gamma t] \rightarrow \exp(-k^2 \tau_d \tau)$$

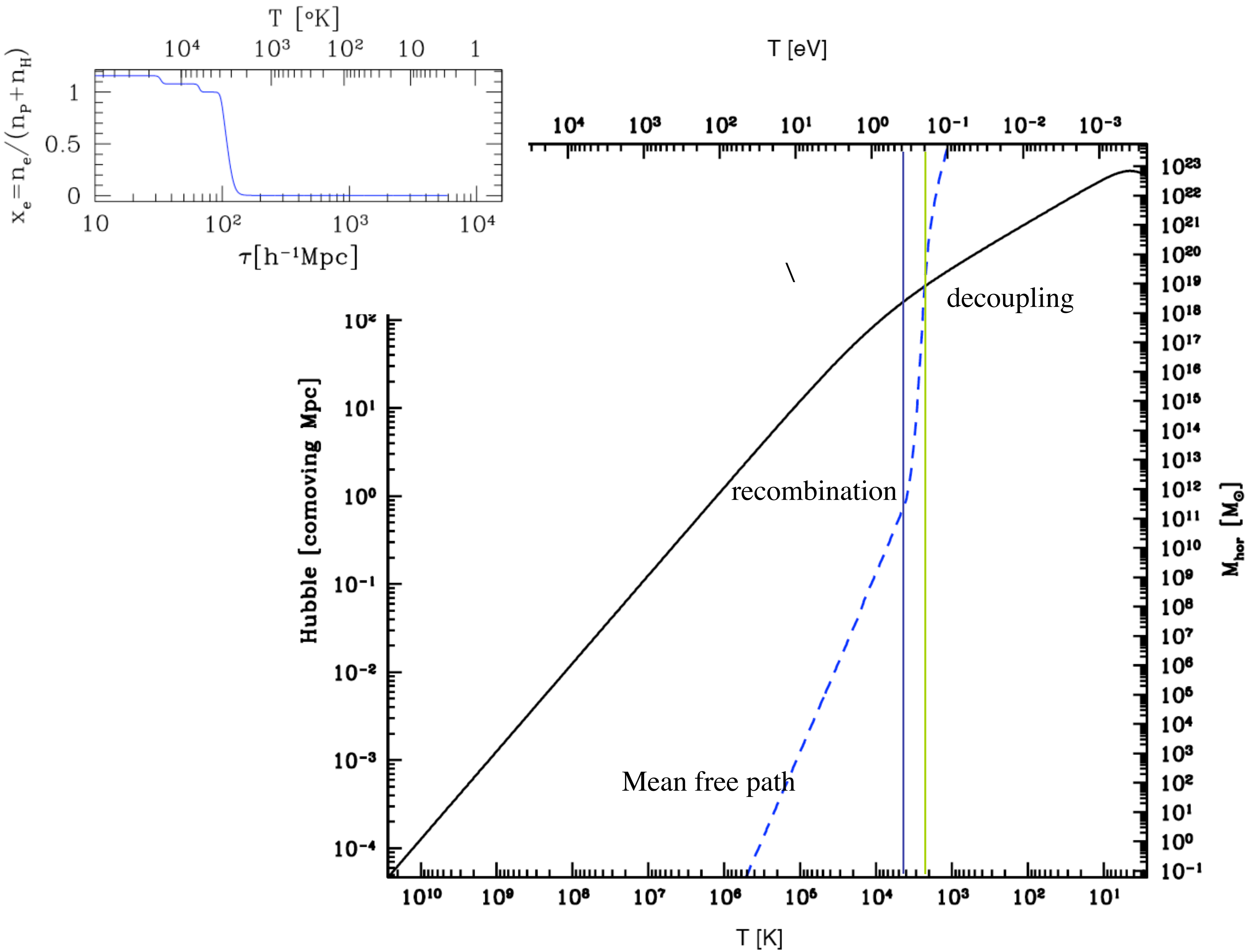
T [°K]
10^4 10^3 10^2 10 1
$x_e = n_e/(n_p+n_H)$
1
0.5
0
10 10^2 10^3 10^4
τ[h^{-1}Mpc]
T [eV]
10^4 10^3 10^2 10^1 10^0 10^{-1} 10^{-2} 10^{-3}
decoupling
recombination
Mean free path
Hubble [comoving Mpc]
10^2 10^1 10^0 10^{-1} 10^{-2} 10^{-3} 10^{-4}
M_{hor} [$M_\odot$]
10^{23} 10^{22} 10^{21} 10^{20} 10^{19} 10^{18} 10^{17} 10^{16} 10^{15} 10^{14} 10^{13} 10^{12} 10^{11} 10^{10} 10^9 10^8 10^7 10^6 10^5 10^4 10^3 10^2 10^1 10^0 10^{-1}
10^{10} 10^9 10^8 10^7 10^6 10^5 10^4 10^3 10^2 10^1
T [K]

Two fluid model

$$\ddot{d}_{\gamma b} + \frac{\mathcal{H} R_b}{(1+R_b)} \dot{d}_{\gamma b} + 2\tau_d k^2 \dot{d}_{\gamma b} + c_{\gamma b}^2 k^2 d_{\gamma b} = -k^2 \frac{2+R_b}{(1+R_b)} \Phi$$

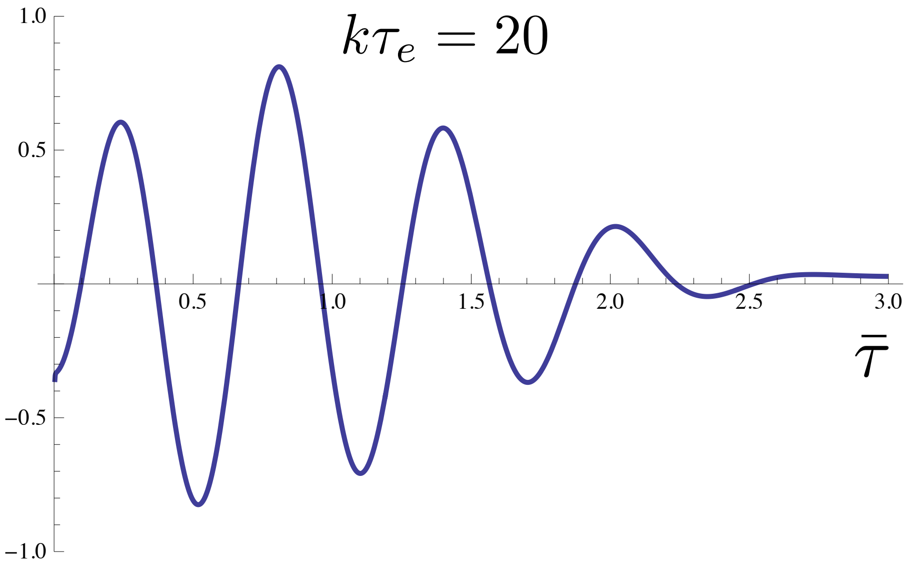

$$\Theta_0^{eff} \equiv \frac{1}{3} d_\gamma + \Phi + \Psi \approx A \frac{e^{-k^2 x_S^2}}{(1+R_b)^{1/4}} \cos(kS + \delta\varphi) - R_b \Phi$$

$$k u_\gamma = -\frac{\dot{d}_\gamma}{k} \approx A\sqrt{3} \frac{e^{-k^2 x_S^2}}{(1+R_b)^{3/4}} \sin(kS + \delta\varphi)$$

$$S(\tau) = \int_0^\tau c_s d\tau' \qquad x_S^2(\tau) = \int_0^\tau \tau_d d\tau' \qquad A \approx -\frac{d_{\gamma,ini}(1+\Delta_\gamma)}{3}$$

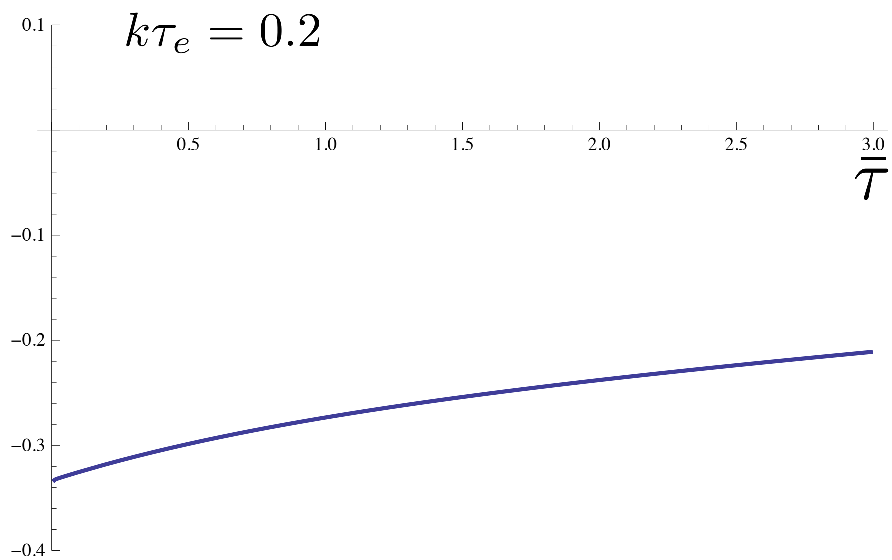

$$\Phi = \Psi = -\frac{1}{5} d_{\gamma,ini} \qquad \Theta_0^{eff} \approx -\frac{1}{15} d_{\gamma,ini} \approx \frac{\Phi}{3}$$

Simple formula

$$ds^2 = a^2(\tau)[-(1+2\Phi)d\tau^2 + (1-2\Psi)dx^2]$$

$$T_{obs} = T_{rec}\frac{P^\mu u_\mu|_{obs}}{P^\mu u_\mu|_{rec}}$$

$$\frac{dP_\mu}{d\lambda} = \frac{1}{2}\partial_\mu g_{\alpha\beta}P^\alpha P^\beta \qquad \frac{1}{P_0}\frac{dP_0}{d\lambda} = \dot{\Phi} + \dot{\Psi}$$

$$\frac{P^\mu u_\mu|_{obs}}{P^\mu u_\mu|_{rec}} = \frac{a_{rec}}{a_{obs}}[1 + \Phi_{rec} - \Phi_{obs} - \hat{n}\cdot\vec{v}_{rec} + \hat{n}\cdot\vec{v}_{obs} + \int d\tau(\dot{\Phi}+\dot{\Psi})]$$

Recombination

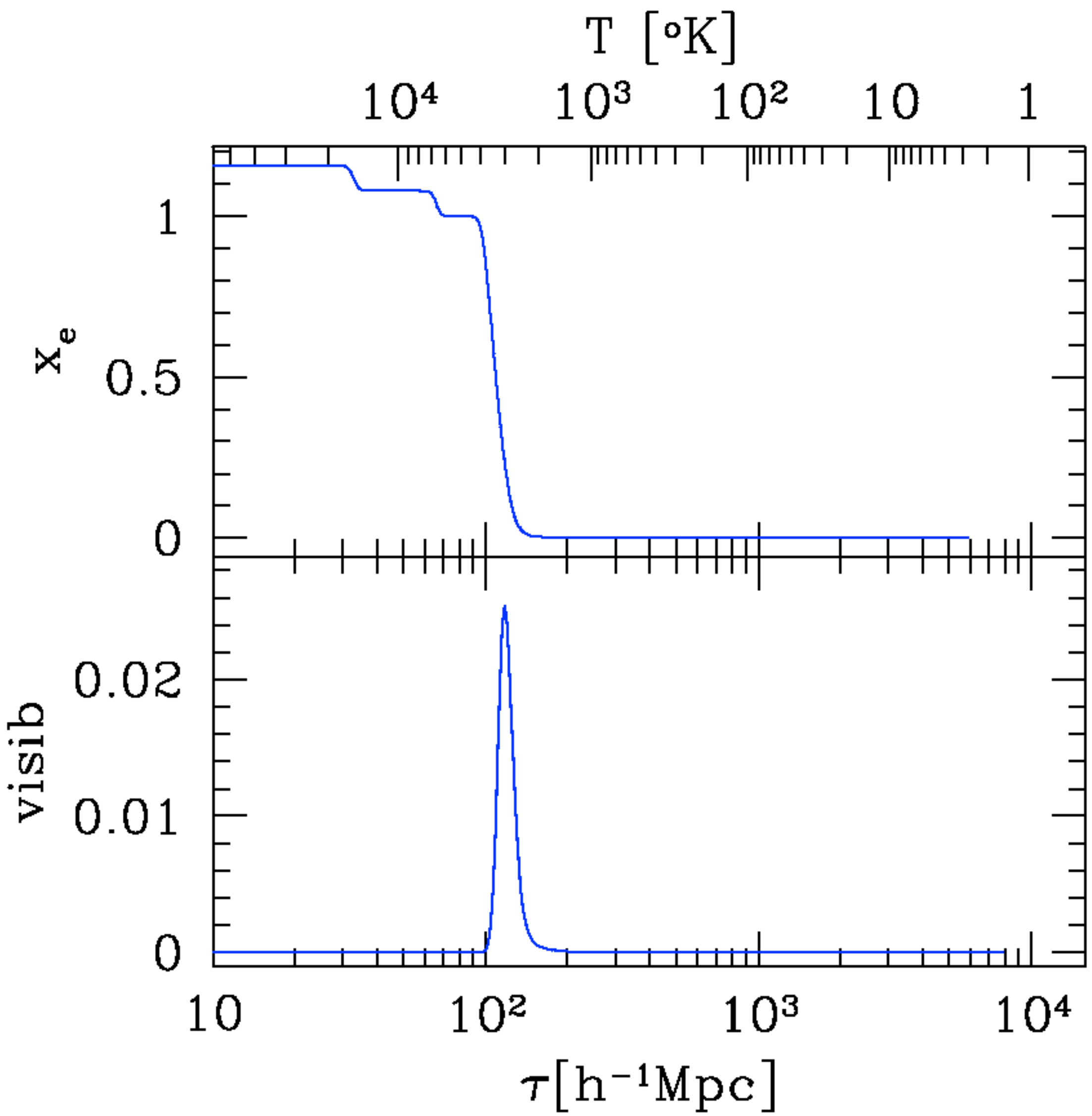

Projection

$$\frac{\delta T}{T}(\hat{n}) \equiv \Theta(\hat{n}) = \sum a_{lm} Y_{lm}(\hat{n})$$

ISW

$$\Theta(\hat{n}) = \int d\tau \dot{g}[\frac{d_\gamma}{3} + \Phi + \Psi - \hat{n} \cdot \vec{v}_\gamma] + g(\dot{\Phi} + \dot{\Psi})$$

$$\Theta(\hat{n}) = \int \frac{d^3k}{(2\pi)^3} \zeta(\vec{k}) \int d\tau [\dot{g}(\Theta_0^{eff} + u_\gamma \frac{\partial}{\partial \tau_0}) + g(\dot{\Phi} + \dot{\Psi})] e^{i(\tau_0 - \tau)\vec{k} \cdot \hat{n}}$$

Two fluid model

$$\ddot{d}_{\gamma b} + \frac{\mathcal{H} R_b}{(1+R_b)}\dot{d}_{\gamma b} + 2\tau_d k^2 \dot{d}_{\gamma b} + c_{\gamma b}^2 k^2 d_{\gamma b} = -k^2 \frac{2+R_b}{(1+R_b)}\Phi$$

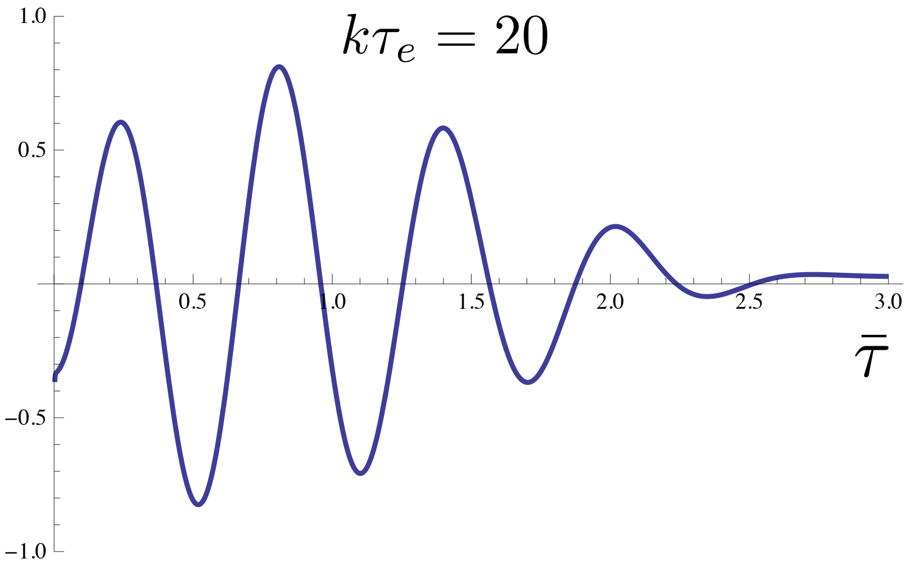

$$\Theta_0^{eff} \equiv \frac{1}{3}d_\gamma + \Phi + \Psi \approx A\frac{e^{-k^2 x_S^2}}{(1+R_b)^{1/4}}\cos(kS+\delta\varphi) - R_b\Phi$$

$$ku_\gamma = -\frac{\dot{d}_\gamma}{k} \approx A\sqrt{3}\frac{e^{-k^2 x_S^2}}{(1+R_b)^{3/4}}\sin(kS+\delta\varphi)$$

$$S(\tau) = \int_0^\tau c_s d\tau' \qquad x_S^2(\tau) = \int_0^\tau \tau_d d\tau' \qquad A \approx -\frac{d_{\gamma,ini}(1+\Delta_\gamma)}{3}$$

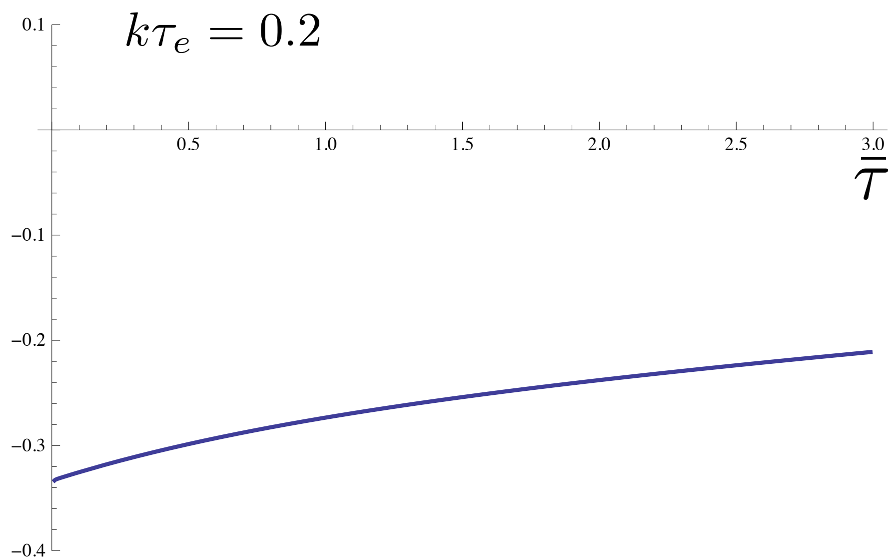

$$\Phi = \Psi = -\frac{1}{5}d_{\gamma,ini} \qquad \Theta_0^{eff} \approx -\frac{1}{15}d_{\gamma,ini} \approx \frac{\Phi}{3}$$

Two fluid model

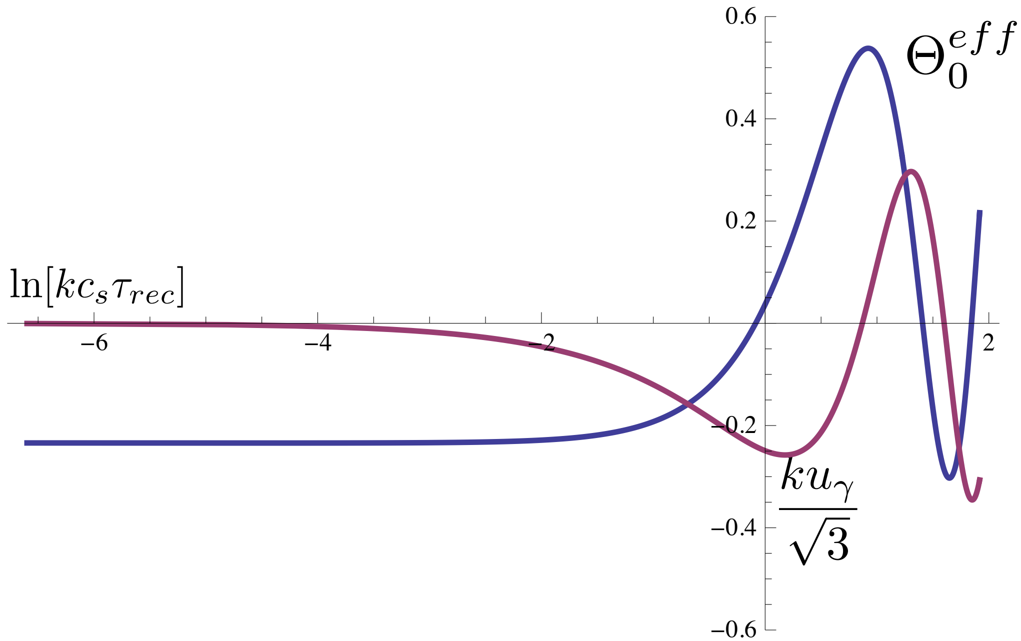

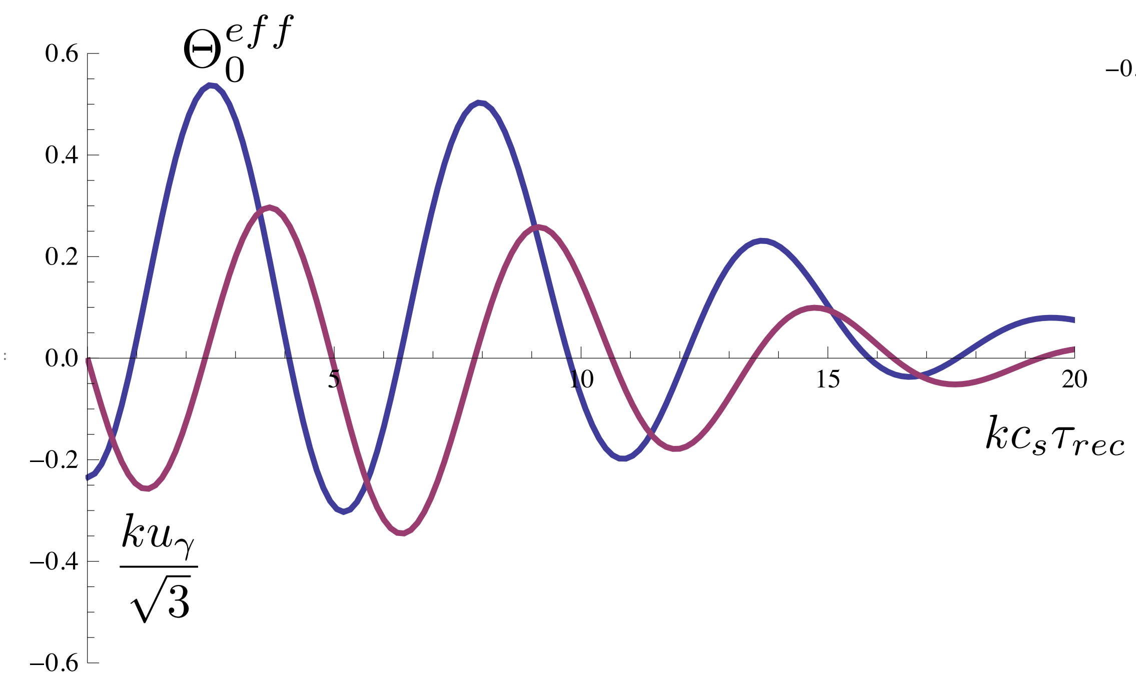

Beware:
The observed spectrum will have additional damping due to the finite width of the last scattering surface.

Planck Spectra

We now know what the state of the plasma was at recombination. We still need to connect it with what we observe.

What is the relation of the peaks in the previous transparency and the power spectrum?

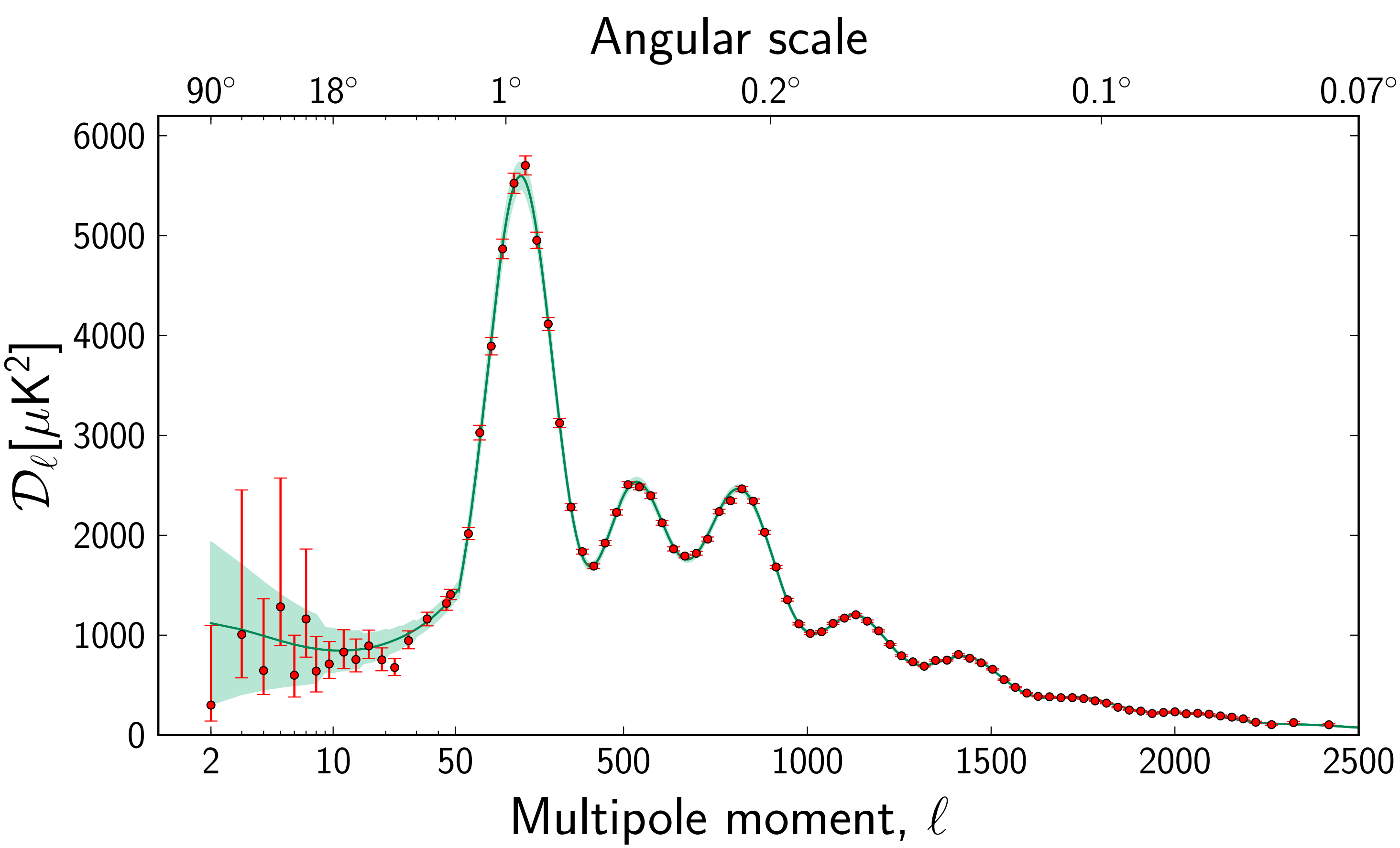

Projection

$$\langle \zeta(k_1)\zeta(k_2)\rangle = (2\pi)^3 \delta^D(k_1 - k_2) P_\zeta(k)$$

$$C_l = \frac{2}{\pi}\int k^2 dk P_\zeta(k) \left| \int d\tau [\dot{g}(\Theta_0^{eff} + u_\gamma \frac{\partial}{\partial \tau_0}) + g(\dot{\Phi} + \dot{\Psi})] j_l(k(\tau_0 - \tau))\right|^2$$

$$C_l \approx \frac{2}{\pi}\int k^2 dk P_\zeta(k) |\Theta_0^{eff}|^2 j_l(kD)^2 + |k u_\gamma|^2 j_l'(kD)^2$$

$$\int \frac{dx}{x} j_l(x)^2 = \frac{1}{2l(l+1)}$$

$$\int \frac{dx}{x} j_l'(x)^2 = \frac{1}{6(l-1)(l+2)}$$

$$\int \frac{dx}{x} j_l(x) j_l'(x) = \frac{\pi}{(2l-1)(2l-1)(2l+3)}$$

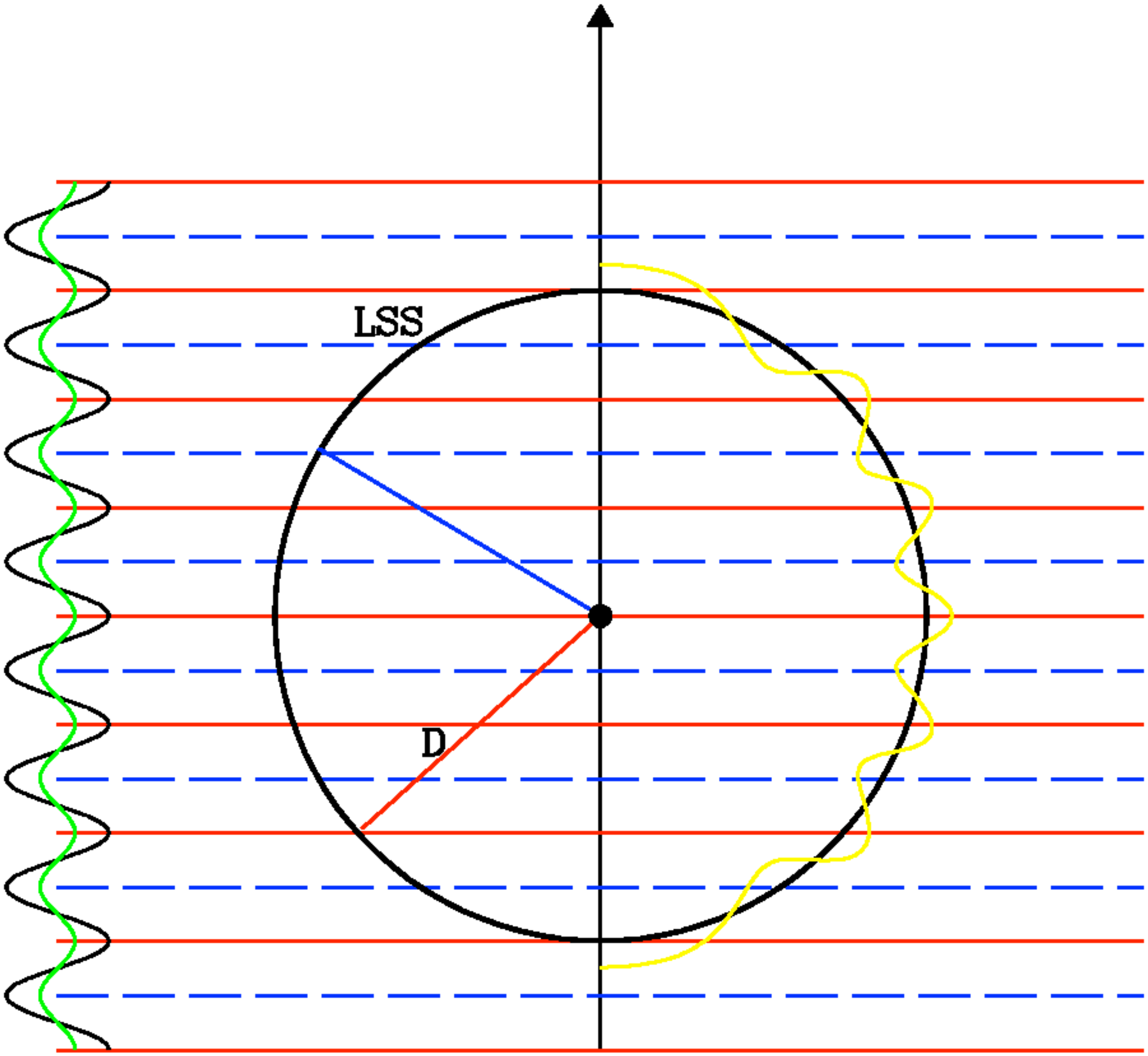
LSS
D

Projection Kernels

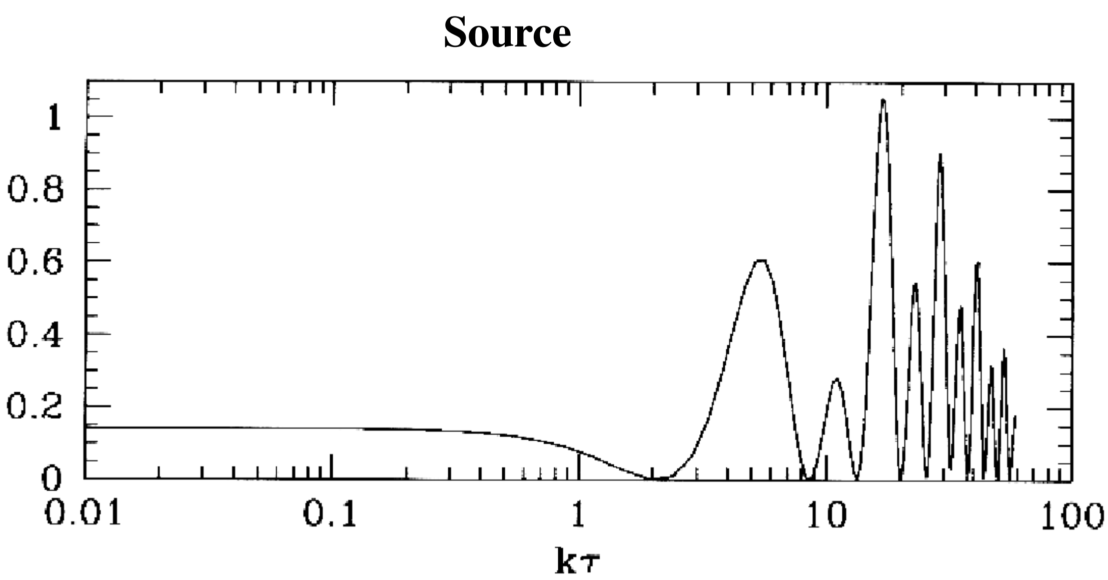

Structure on scales

$$k \sim \frac{1}{\tau_{rec}}$$

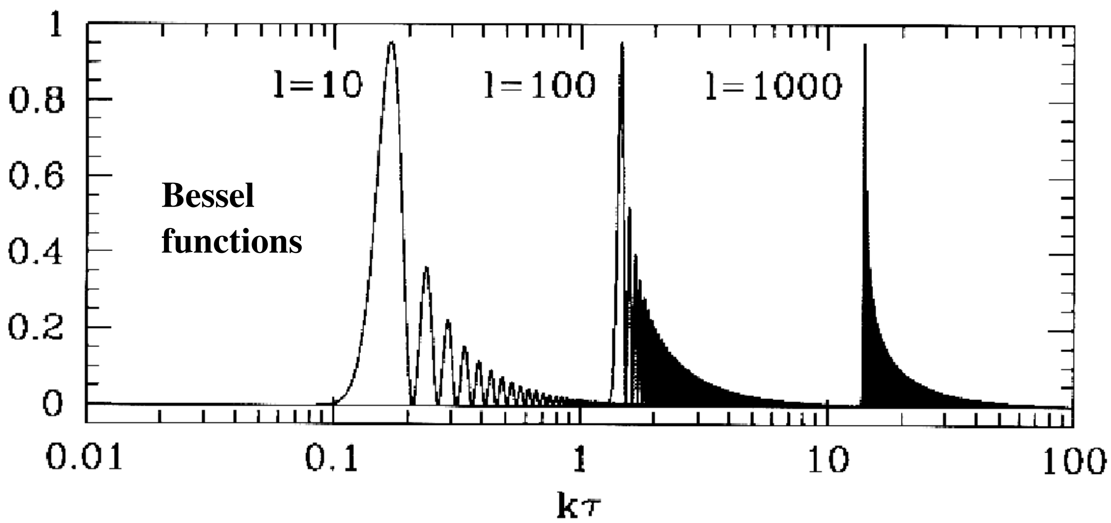

Structure on scales

$$k \sim \frac{1}{(\tau_0 - \tau_{rec})}$$

Observational Results

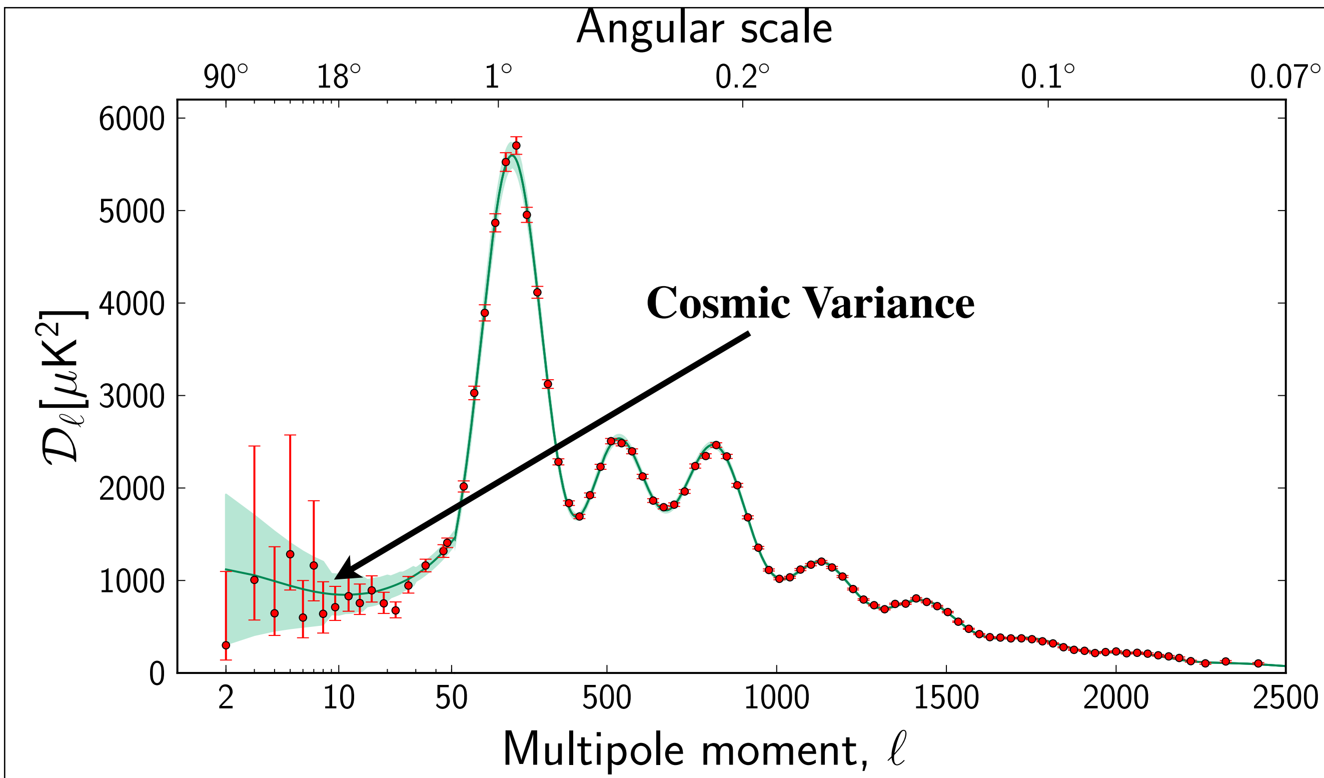

Recombination

Late times

Initial Conditions

Derived parameters

	Planck		*Planck*+WP	
Parameter	Best fit	68% limits	Best fit	68% limits
$\Omega_b h^2$	0.022068	0.02207 ± 0.00033	0.022032	0.02205 ± 0.00028
$\Omega_c h^2$	0.12029	0.1196 ± 0.0031	0.12038	0.1199 ± 0.0027
$100\theta_{MC}$	1.04122	1.04132 ± 0.00068	1.04119	1.04131 ± 0.00063
τ	0.0925	0.097 ± 0.038	0.0925	$0.089^{+0.012}_{-0.014}$
n_s	0.9624	0.9616 ± 0.0094	0.9619	0.9603 ± 0.0073
$\ln(10^{10} A_s)$	3.098	3.103 ± 0.072	3.0980	$3.089^{+0.024}_{-0.027}$
Ω_Λ	0.6825	0.686 ± 0.020	0.6817	$0.685^{+0.018}_{-0.016}$
Ω_m	0.3175	0.314 ± 0.020	0.3183	$0.315^{+0.016}_{-0.018}$
σ_8	0.8344	0.834 ± 0.027	0.8347	0.829 ± 0.012
z_{re}	11.35	$11.4^{+4.0}_{-2.8}$	11.37	11.1 ± 1.1
H_0	67.11	67.4 ± 1.4	67.04	67.3 ± 1.2
$10^9 A_s$	2.215	2.23 ± 0.16	2.215	$2.196^{+0.051}_{-0.060}$
$\Omega_m h^2$	0.14300	0.1423 ± 0.0029	0.14305	0.1426 ± 0.0025
Age/Gyr	13.819	13.813 ± 0.058	13.8242	13.817 ± 0.048
z_*	1090.43	1090.37 ± 0.65	1090.48	1090.43 ± 0.54
$100\theta_*$	1.04139	1.04148 ± 0.00066	1.04136	1.04147 ± 0.00062
z_{eq}	3402	3386 ± 69	3403	3391 ± 60

Parameter dependencies

http://space.mit.edu/home/tegmark/cmb/movies.html

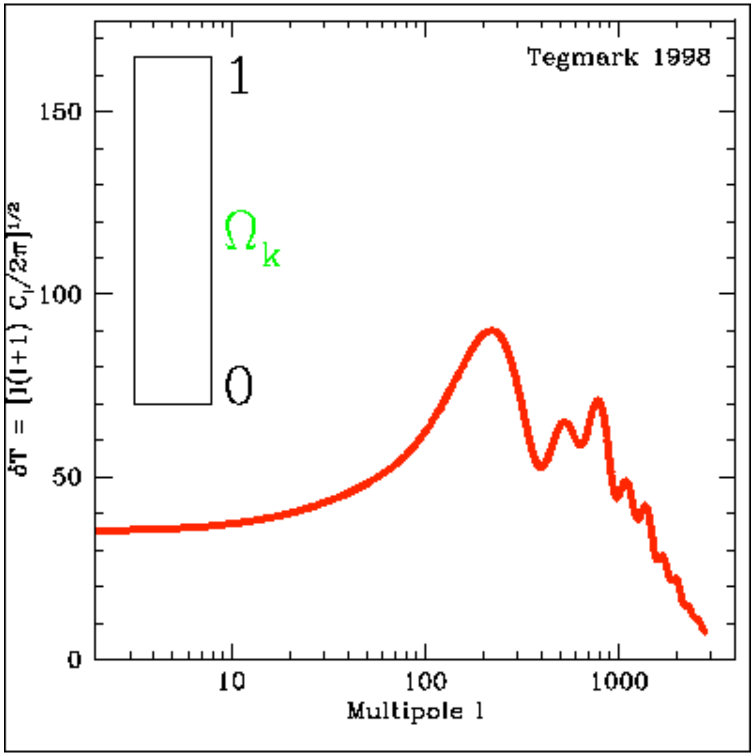

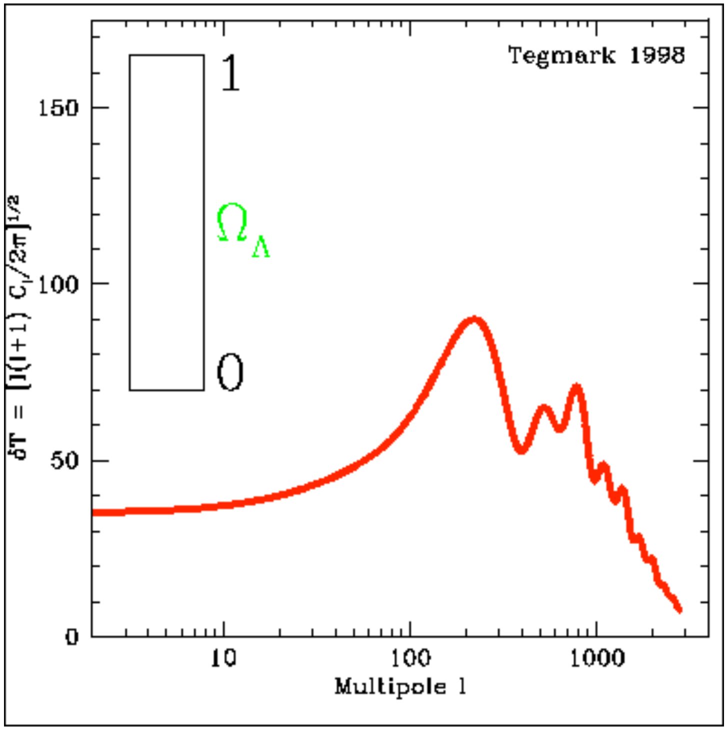

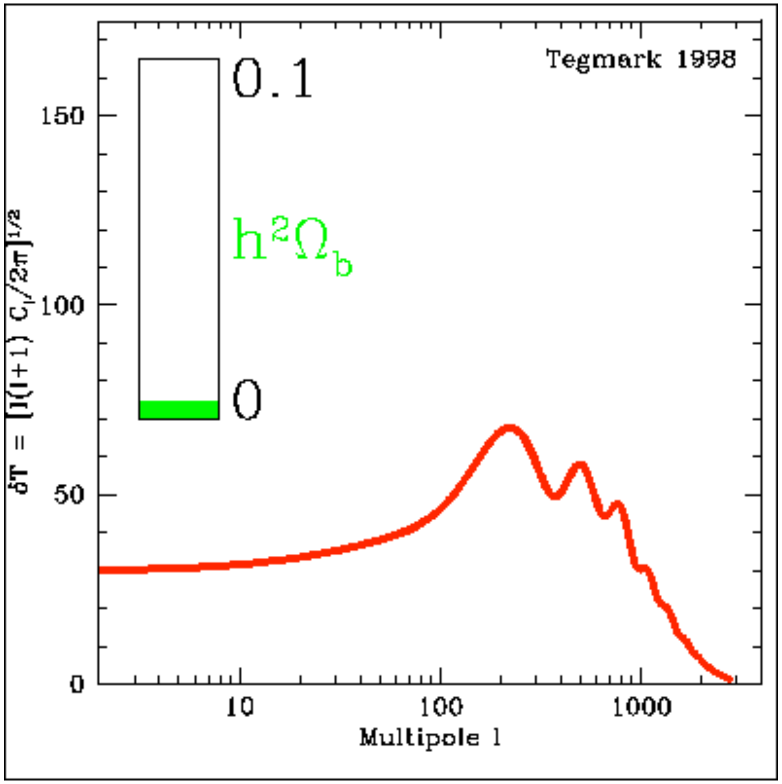

What is Cosmic Variance?

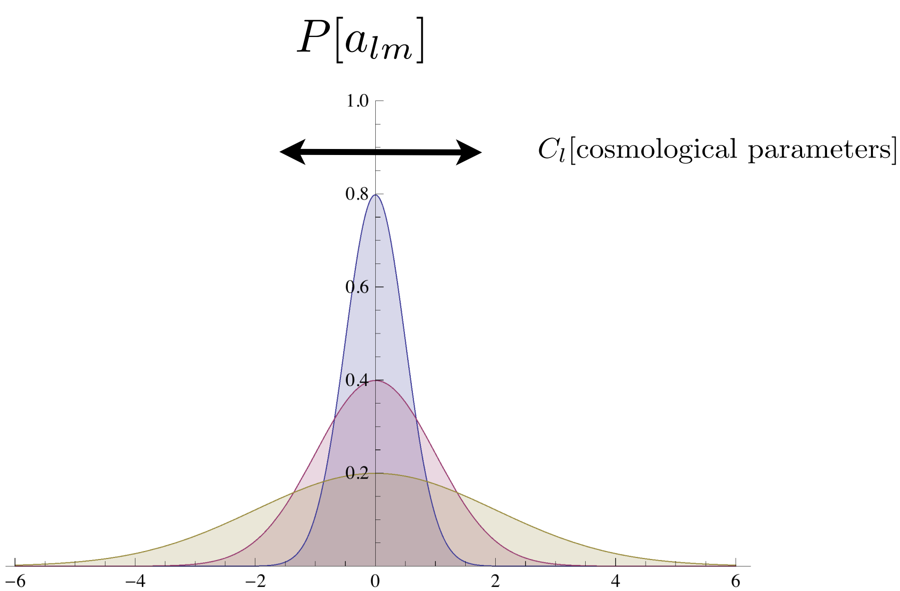

(2l+1) if had all sky

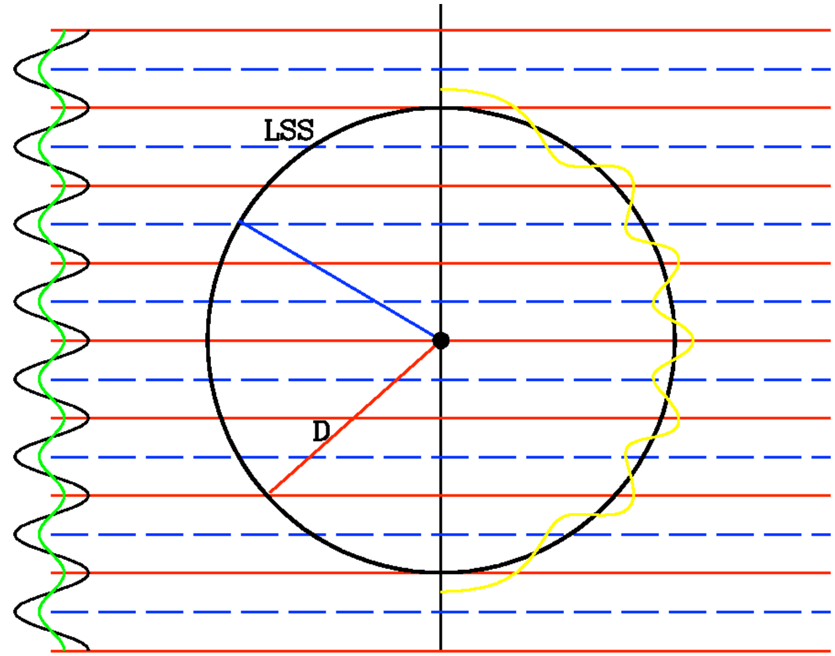

$$\Theta(\hat{n}) = \int \frac{d^3k}{(2\pi)^3}\zeta(\vec{k}) \int d\tau [\dot{g}(\Theta_0^{eff} + u_\gamma \frac{\partial}{\partial\tau_0}) + g(\dot{\Phi} + \dot{\Psi})] e^{i(\tau_0 - \tau)\vec{k}\cdot\hat{n}}$$

$$\langle \zeta(k_1)\zeta(k_2) \rangle = (2\pi)^3 \delta^D(k_1 - k_2) P_\zeta(k)$$

Statistical nature of predictions is also an issue when dealing with anomalies

Planck constrains on LCDM

Parameter	*Planck* Best fit	*Planck* 68% limits	*Planck*+lensing Best fit	*Planck*+lensing 68% limits	*Planck*+WP Best fit	*Planck*+WP 68% limits
$\Omega_b h^2$	0.022068	0.02207 ± 0.00033	0.022242	0.02217 ± 0.00033	0.022032	0.02205 ± 0.00028
$\Omega_c h^2$	0.12029	0.1196 ± 0.0031	0.11805	0.1186 ± 0.0031	0.12038	0.1199 ± 0.0027
$100\theta_{MC}$	1.04122	1.04132 ± 0.00068	1.04150	1.04141 ± 0.00067	1.04119	1.04131 ± 0.00063
τ	0.0925	0.097 ± 0.038	0.0949	0.089 ± 0.032	0.0925	$0.089^{+0.012}_{-0.014}$
n_s	0.9624	0.9616 ± 0.0094	0.9675	0.9635 ± 0.0094	0.9619	0.9603 ± 0.0073
$\ln(10^{10} A_s)$	3.098	3.103 ± 0.072	3.098	3.085 ± 0.057	3.0980	$3.089^{+0.024}_{-0.027}$

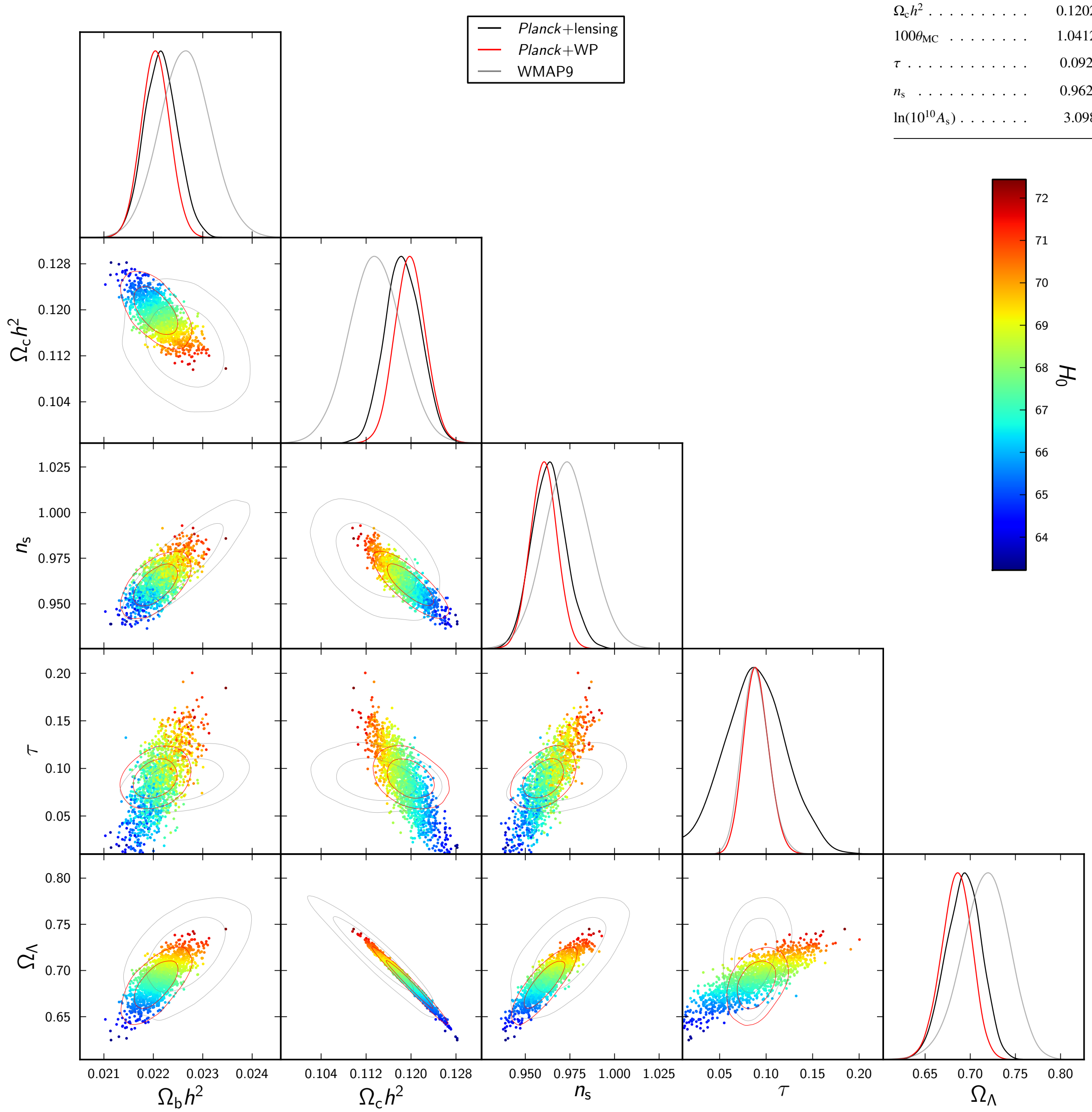

Fig. 2. Comparison of the base ΛCDM model parameters for *Planck*+lensing only (colour-coded samples), and the 68% and 95% constraint contours adding *WMAP* low-ℓ polarization (WP; red contours), compared to *WMAP*-9 (Bennett et al. 2012; grey contours).

Geometric Degeneracy

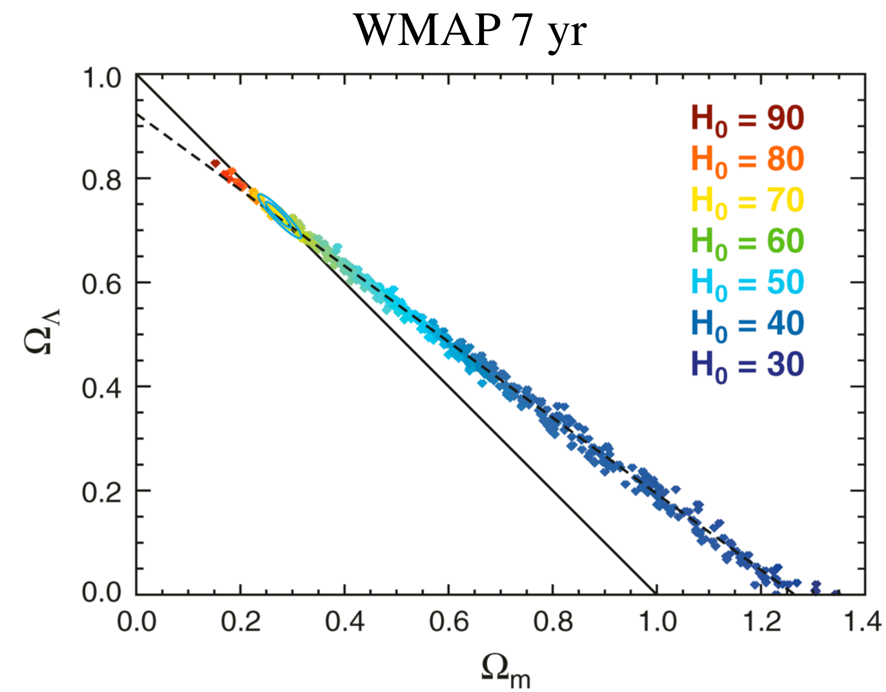

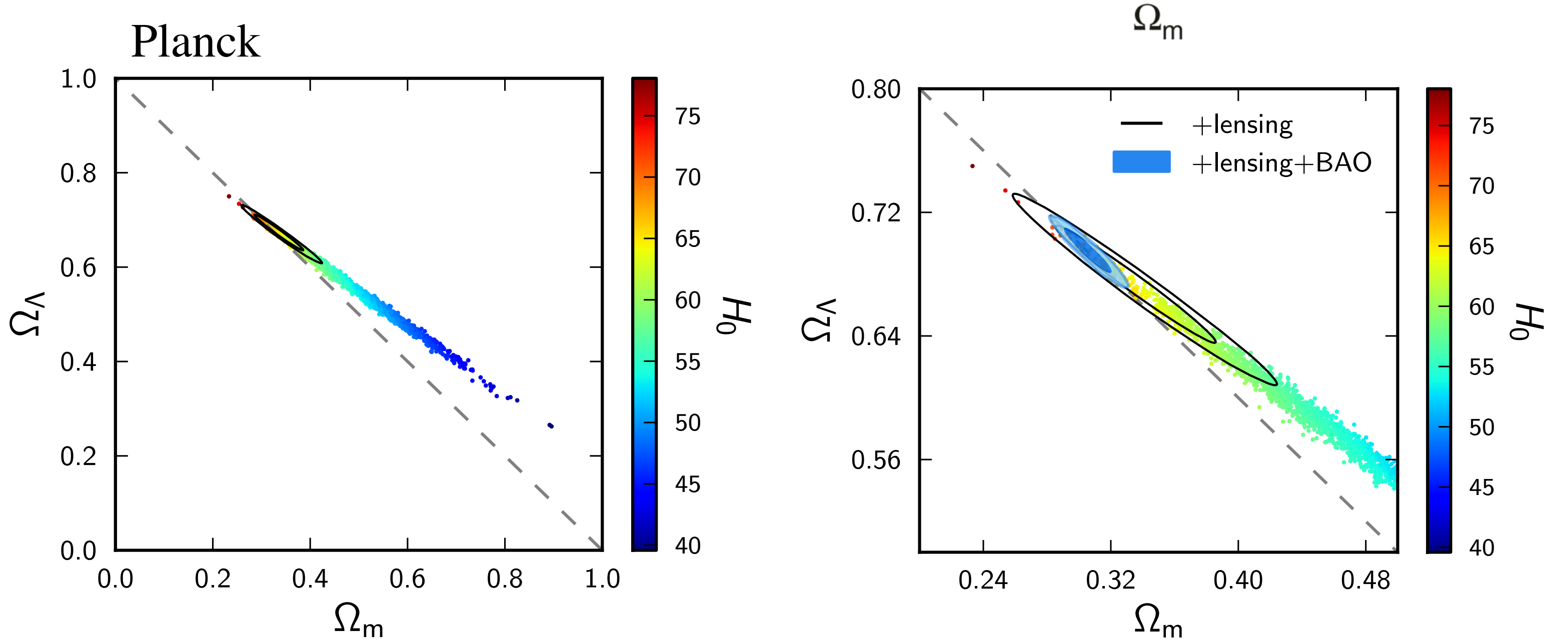

Fig. 25. The *Planck*+WP+highL data combination (samples; colour-coded by the value of H_0) partially breaks the geometric degeneracy between Ω_m and Ω_Λ due to the effect of lensing in the temperature power spectrum. These limits are significantly improved by the inclusion of the *Planck* lensing reconstruction (black contours). Combining also with BAO (right; solid blue contours) tightly constrains the geometry to be nearly flat.

Additional observable from recombination: polarization

Secondary effects: Lensing, ISW, SZ effect, kSZ, polarization from the EOR

Gravitational lensing by the large scale structure

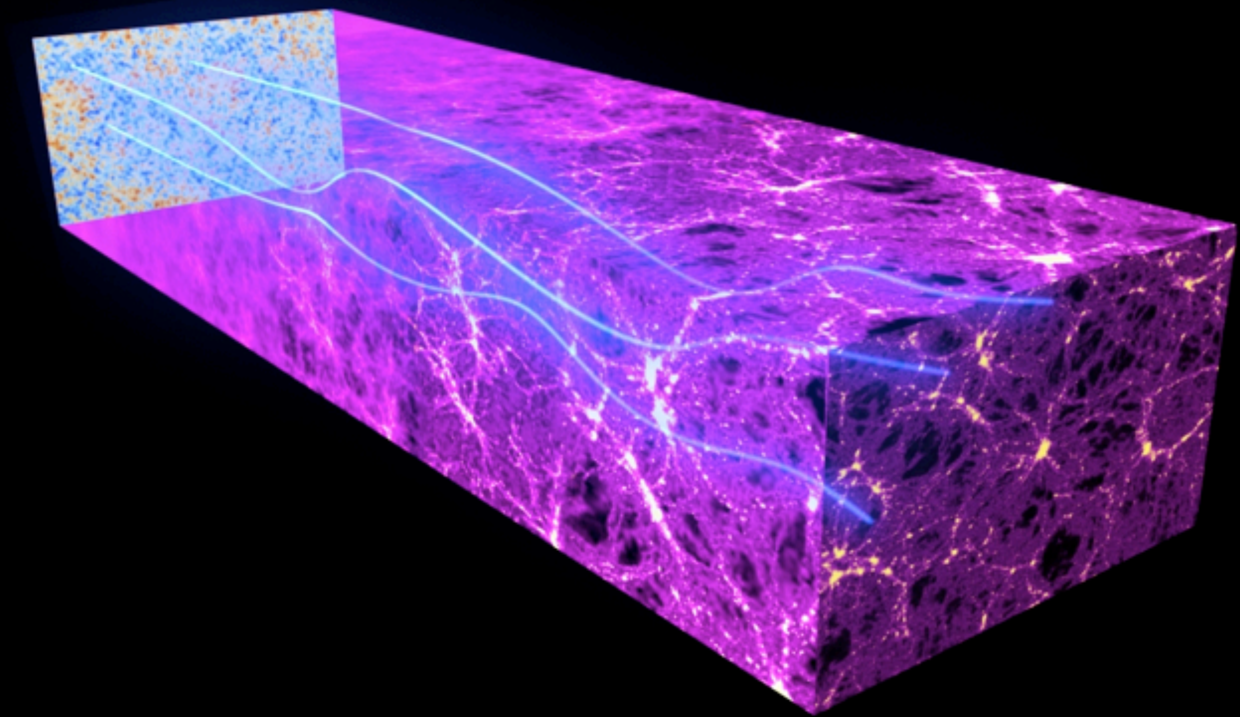

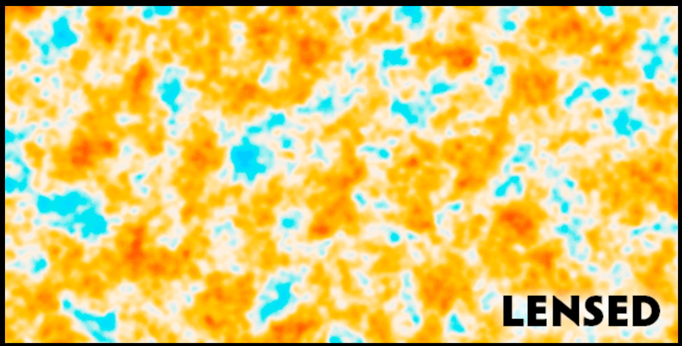

Tracing the lenses with dusty galaxies

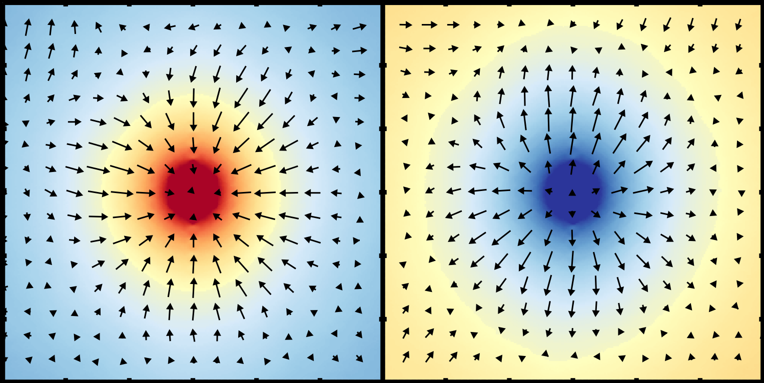

Map of dark matter produced by Planck

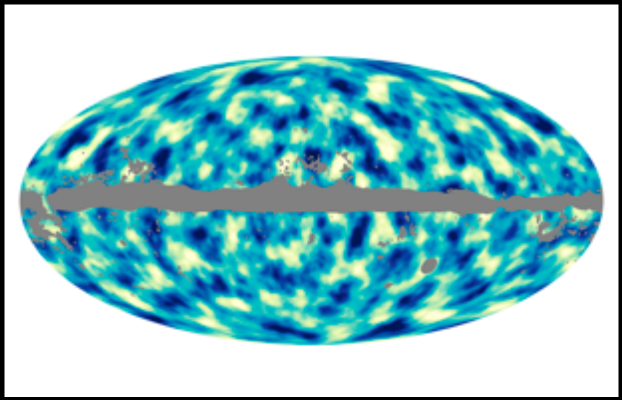

$$\delta\beta = -2\delta\chi\nabla_\perp\Psi,$$

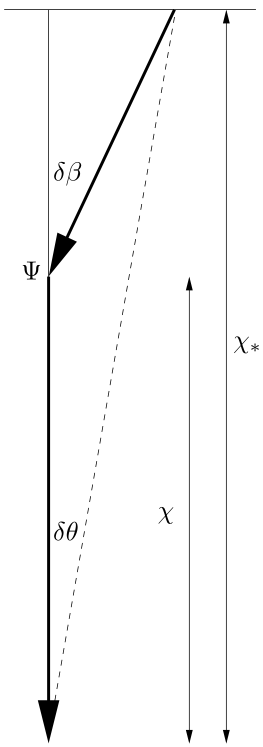

$$\delta\theta_\chi = \frac{f_K(\chi_* - \chi)\delta\beta}{f_K(\chi_*)} = -\frac{f_K(\chi_* - \chi)}{f_K(\chi_*)}2\delta\chi\nabla_\perp\Psi$$

$$f_K(\chi) = \begin{cases} K^{-1/2}\sin(K^{1/2}\chi) & \text{for } K > 0, \text{ closed,} \\ \chi & \text{for } K = 0, \text{ flat,} \\ |K|^{-1/2}\sinh(|K|^{1/2}\chi) & \text{for } K < 0, \text{ open.} \end{cases}$$

$$\boldsymbol{\alpha} = -2\int_0^{\chi_*} \mathrm{d}\chi \frac{f_K(\chi_* - \chi)}{f_K(\chi_*)}\boldsymbol{\nabla}_\perp\Psi(\chi\hat{\mathbf{n}};\eta_0 - \chi).$$

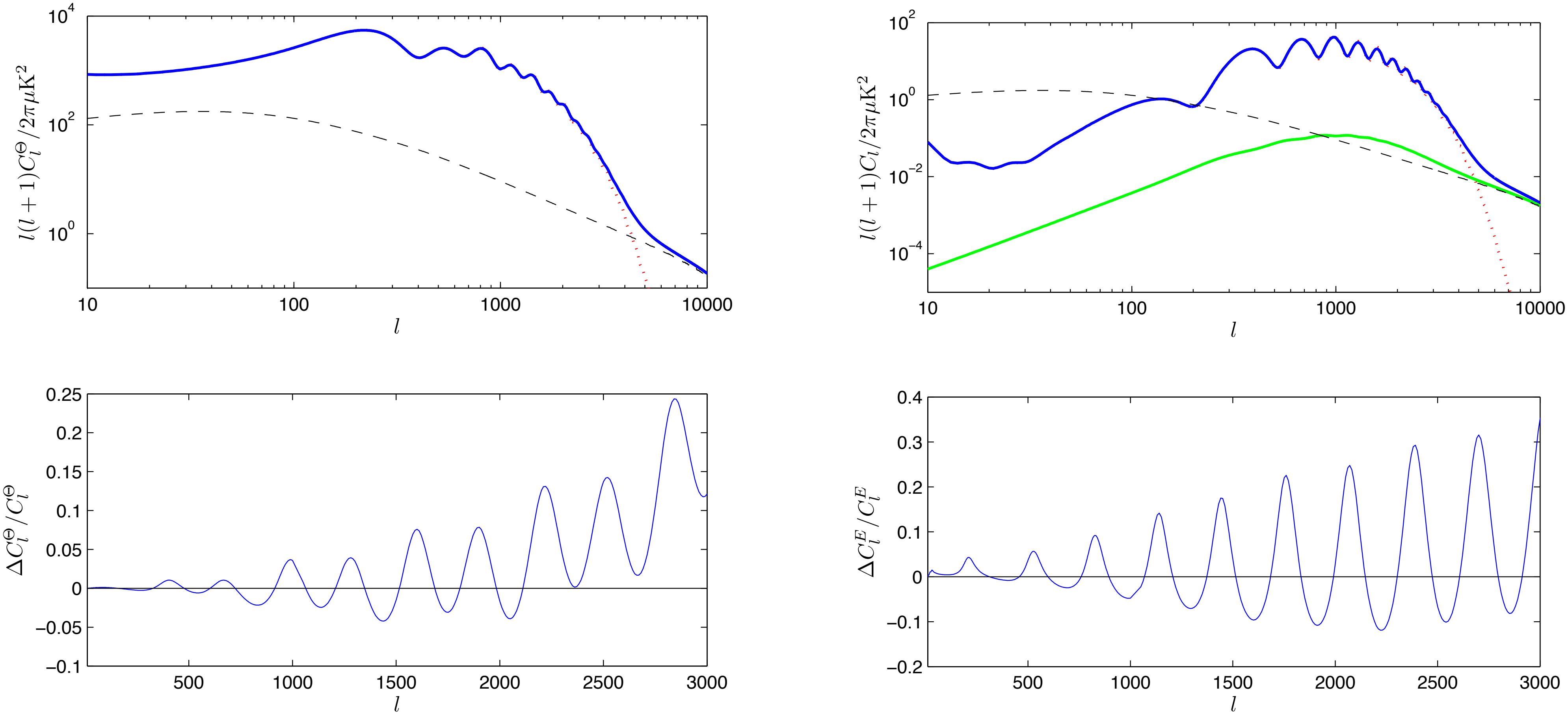
$l(l+1)C_l^{\Theta}/2\pi\mu K^2$
l
$l(l+1)C_l/2\pi\mu K^2$
l
$\Delta C_l^{\Theta}/C_l^{\Theta}$
l
$\Delta C_l^{E}/C_l^{E}$
l

Geometric Degeneracy

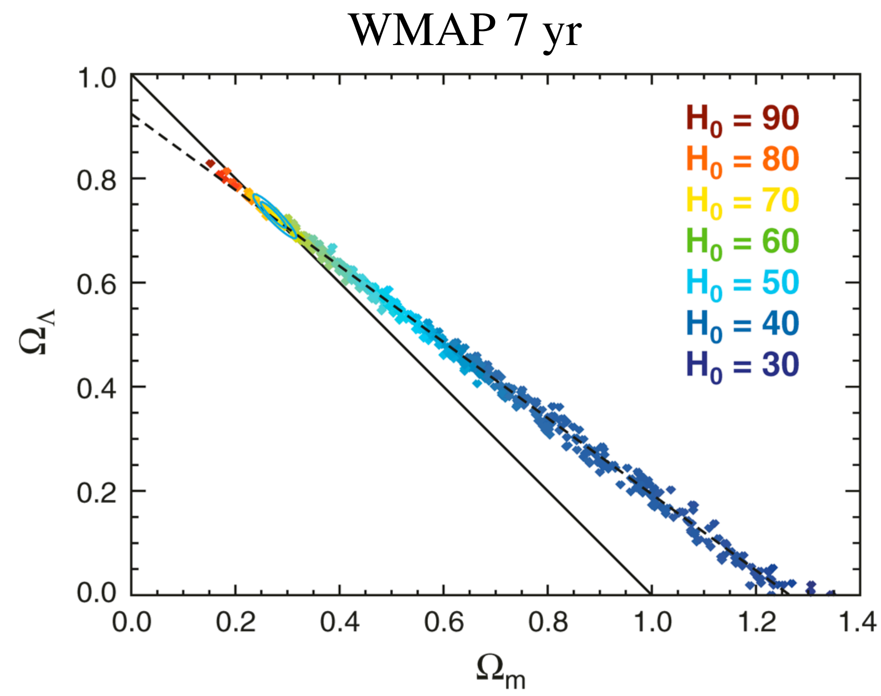

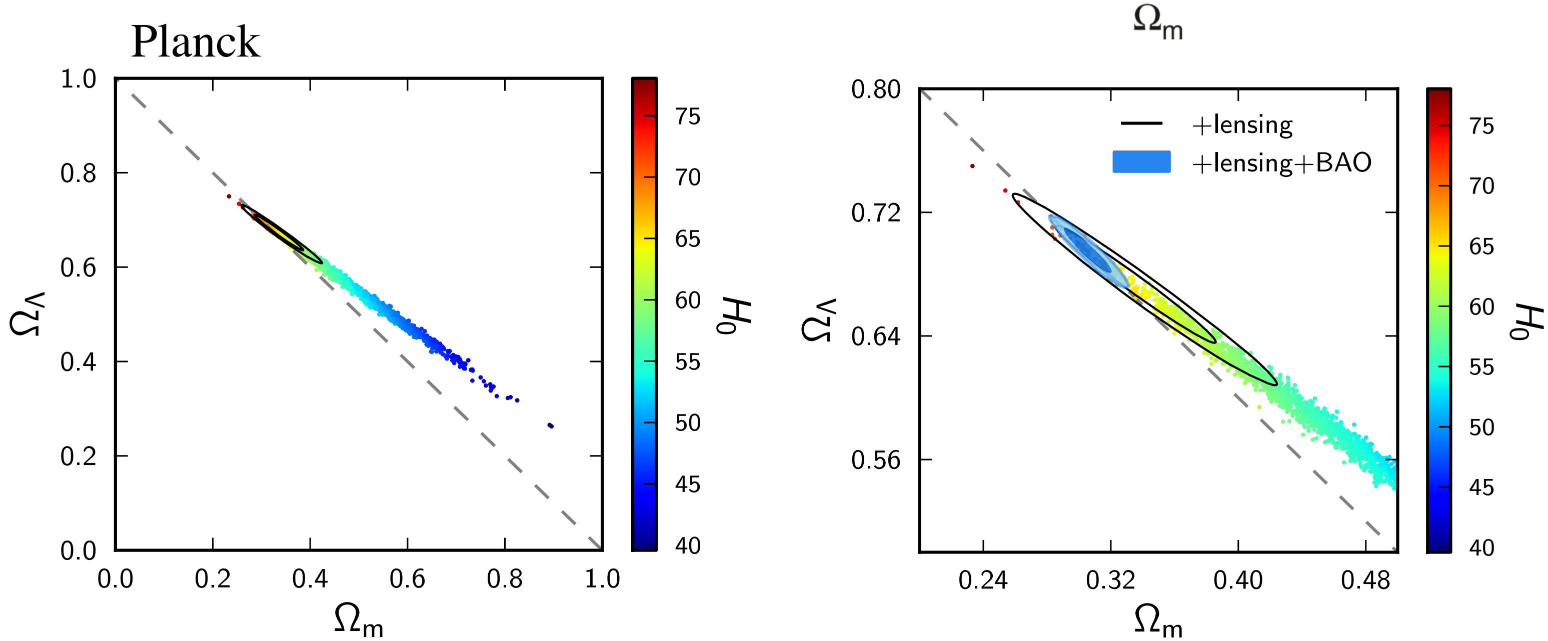

Fig. 25. The *Planck*+WP+highL data combination (samples; colour-coded by the value of H_0) partially breaks the geometric degeneracy between Ω_m and Ω_Λ due to the effect of lensing in the temperature power spectrum. These limits are significantly improved by the inclusion of the *Planck* lensing reconstruction (black contours). Combining also with BAO (right; solid blue contours) tightly constrains the geometry to be nearly flat.

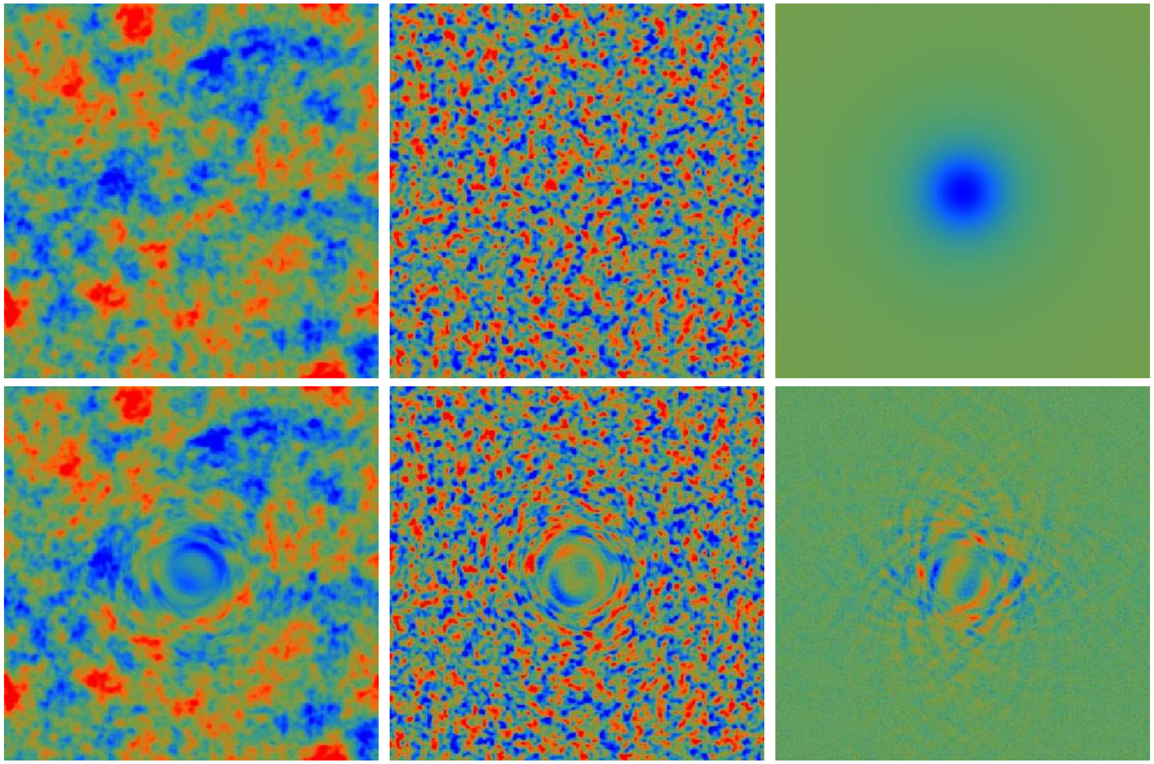

FIG. 1.— An exaggerated example of the lensing effect on a $10° \times 10°$ field. Top: (left-to-right) unlensed temperature field, unlensed E-polarization field, spherically symmetric deflection field $d(\mathbf{n})$. Bottom: (left-to-right) lensed temperature field, lensed E-polarization field, lensed B-polarization field. The scale for the polarization and temperature fields differ by a factor of 10.

$$\begin{aligned}\langle\tilde\Theta(\mathbf{l})\tilde\Theta^*(\mathbf{l}-\mathbf{L})\rangle_\Theta &= \delta(\mathbf{L})\,C_l^\Theta - \int\frac{\mathrm{d}^2\mathbf{l}'}{2\pi}\Big[\mathbf{l}'\cdot(\mathbf{l}-\mathbf{l}')\psi(\mathbf{l}-\mathbf{l}')\langle\Theta(\mathbf{l}')\Theta^*(\mathbf{l}-\mathbf{L})\rangle \\ &\quad + \mathbf{l}'\cdot(\mathbf{l}-\mathbf{L}-\mathbf{l}')\psi^*(\mathbf{l}-\mathbf{L}-\mathbf{l}')\langle\Theta(\mathbf{l})\Theta^*(\mathbf{l}')\rangle\Big] + \mathcal{O}(\psi^2) \\ &= \delta(\mathbf{L})\,C_l^\Theta + \frac{1}{2\pi}\Big[(\mathbf{L}-\mathbf{l})\cdot\mathbf{L}\,C^\Theta_{|\mathbf{l}-\mathbf{L}|} + \mathbf{l}\cdot\mathbf{L}\,C_l^\Theta\Big]\,\psi(\mathbf{L}) + \mathcal{O}(\psi^2). \qquad (7.1)\end{aligned}$$

$$\hat\psi(\mathbf{L}) \equiv N(\mathbf{L})\int\frac{\mathrm{d}^2\mathbf{l}}{2\pi}\,\tilde\Theta(\mathbf{l})\tilde\Theta^*(\mathbf{l}-\mathbf{L})g(\mathbf{l},\mathbf{L}),$$

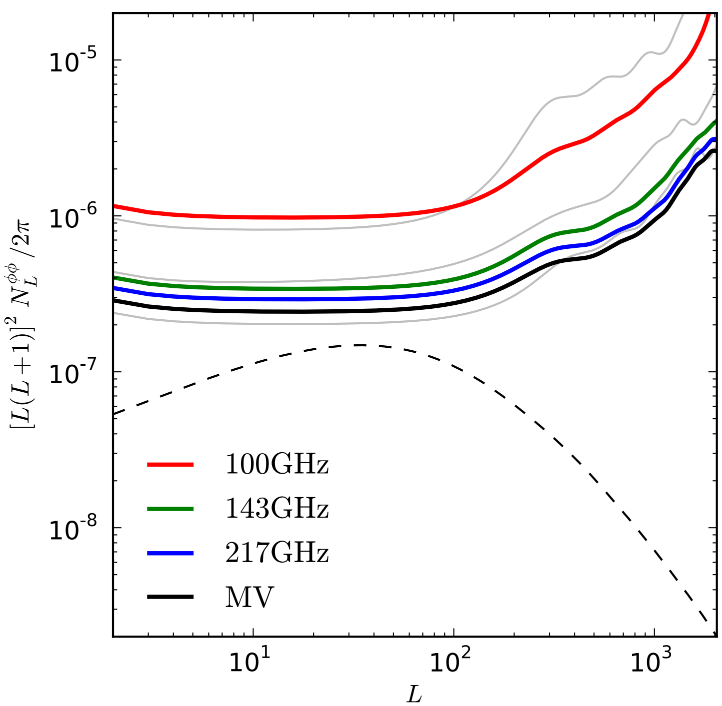

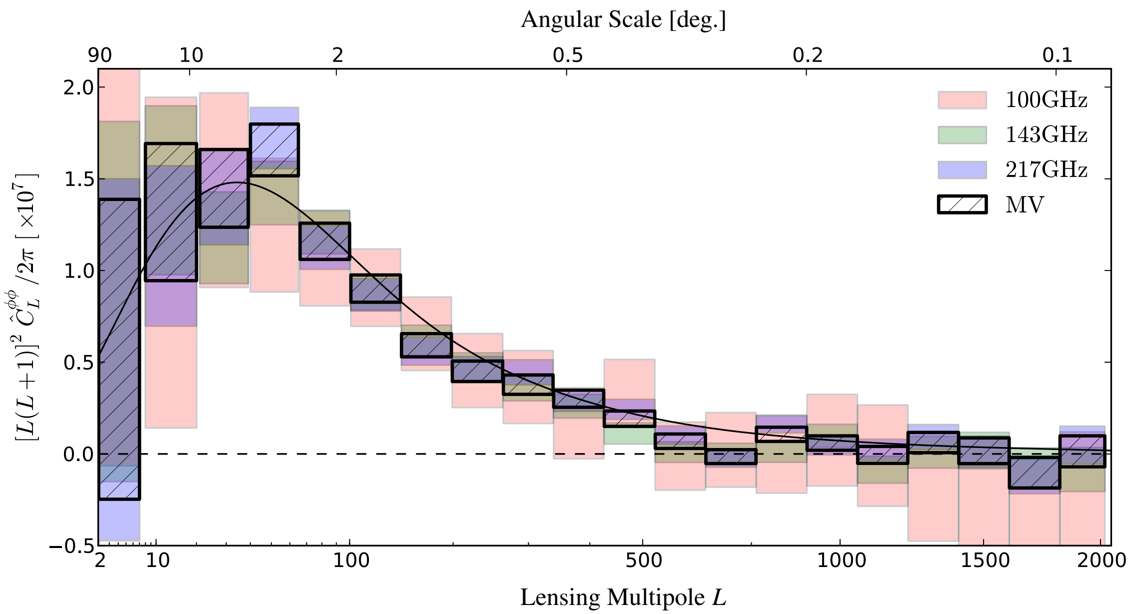

Fig. 10. Lensing potential power spectrum estimates based on the individual 100, 143, and 217 GHz sky maps, as well our fiducial minimum-variance (MV) reconstruction which forms the basis for the *Planck* lensing likelihood. The black line is for the best-fit ΛCDM model of Planck Collaboration XVI (2013).

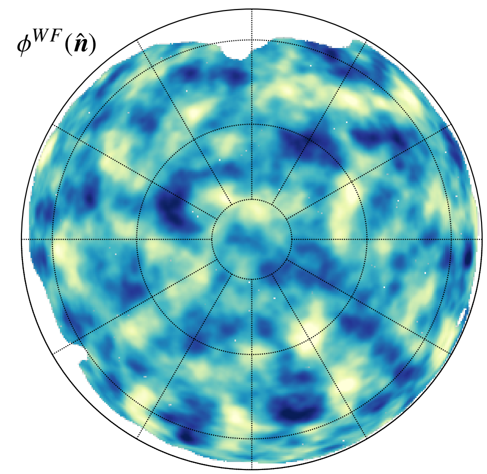

Galactic North

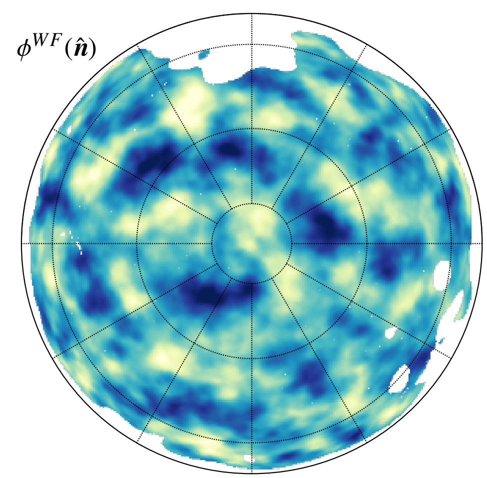

Galactic South

$$A_{\mathrm{L}}^{\phi\phi} = 0.99 \pm 0.05 \quad (68\%;\ \textit{Planck}\text{+lensing+WP+highL}),$$

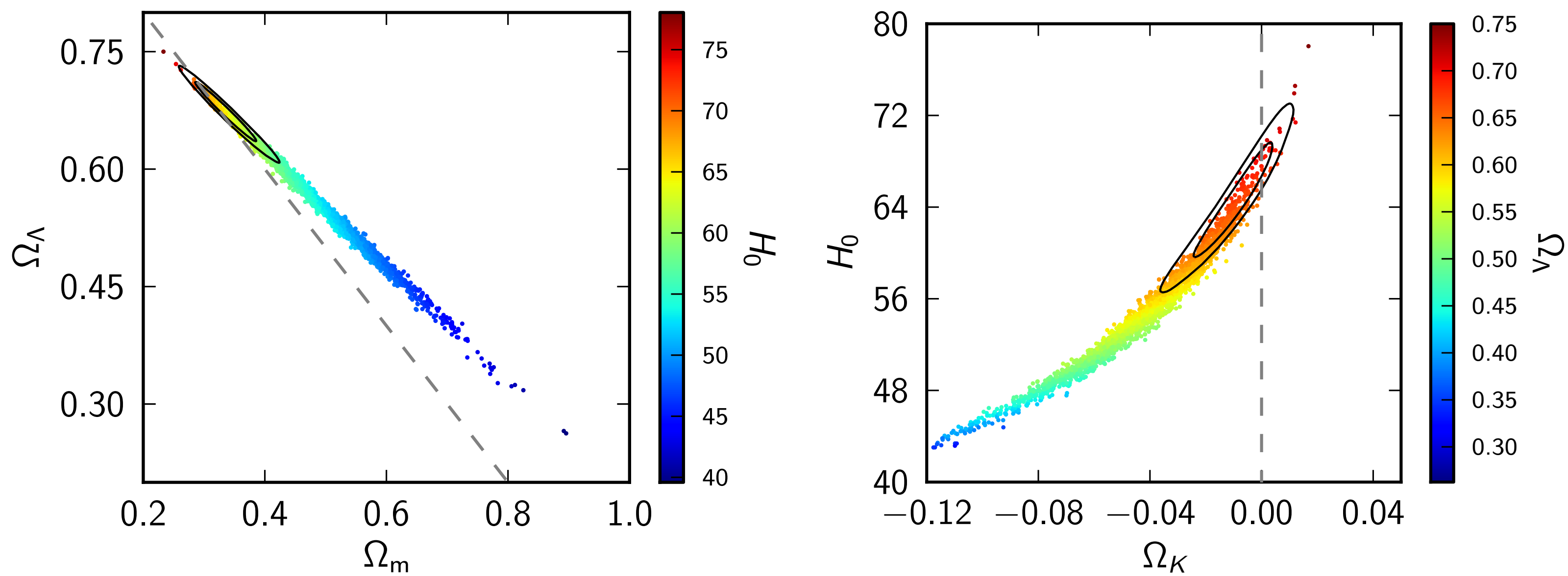

Fig. 15. Two views of the geometric degeneracy in curved ΛCDM models which is partially broken by lensing. *Left*: the degeneracy in the Ω_m-Ω_Λ plane, with samples from *Planck*+WP+highL colour coded by the value of H_0. The contours delimit the 68% and 95% confidence regions, showing the further improvement from including the lensing likelihood. *Right*: the degeneracy in the Ω_K-H_0 plane, with samples colour coded by Ω_Λ. Spatially-flat models lie along the grey dashed lines.

CIB-Lensing

545 GHz

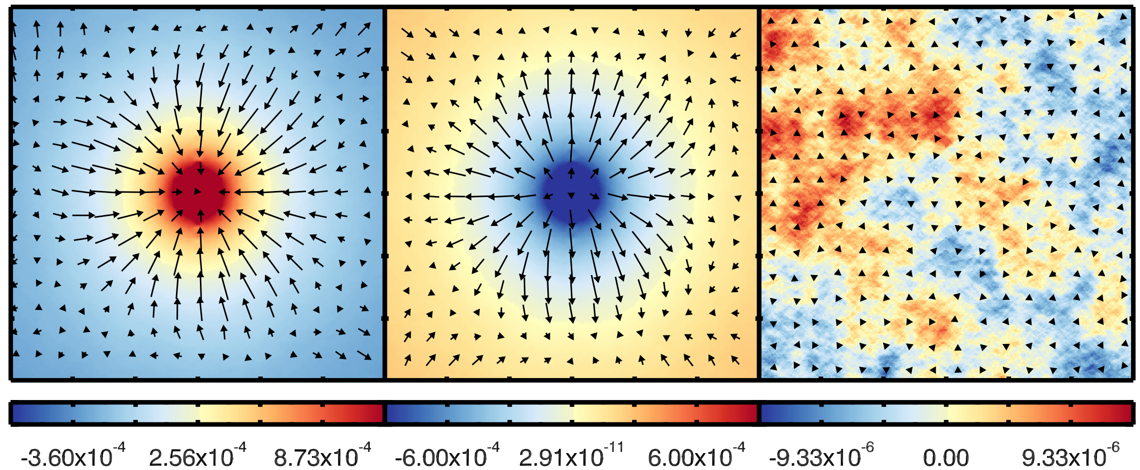

Fig. 4. Temperature maps of size 1 deg^2 at 545 and 857 GHz stacked on the 20,000 brightest peaks (left column), troughs (centre column) and random map locations (right column). The stacked (averaged) temperature maps is in K. The arrows indicate the lensing deflection angle deduced from the gradient of the band-pass filtered lensing potential map stacked on the same peaks. The longest arrow corresponds to a deflection of 6.3″, which is only a fraction of the total deflection angle because of our filtering. This stacking allows us to visualize in real space the lensing of the CMB by the galaxies that generate the CIB. A small and expected offset (≃1′) was corrected by hand when displaying the deflection field.

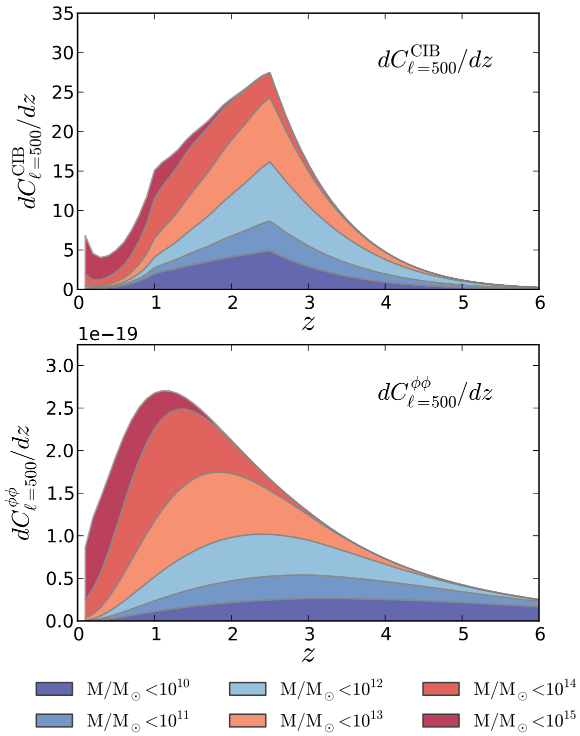

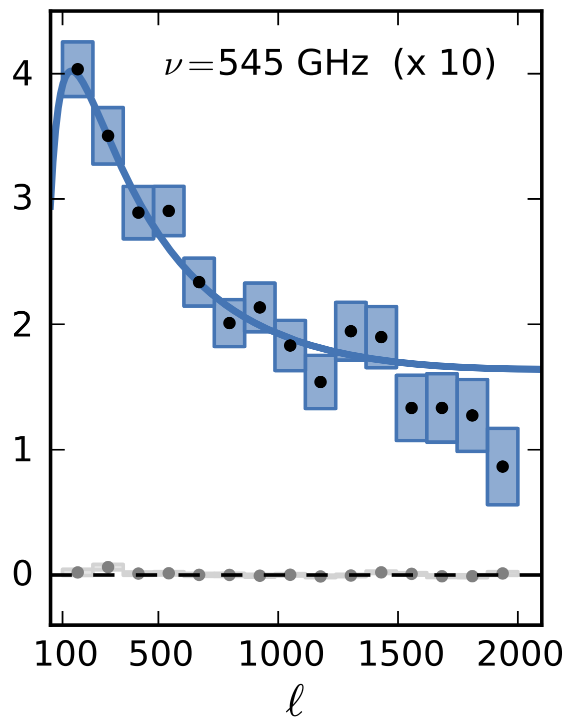

42σ

The Sunyaev Zeldovich effect

A map of the hot gas in the Universe

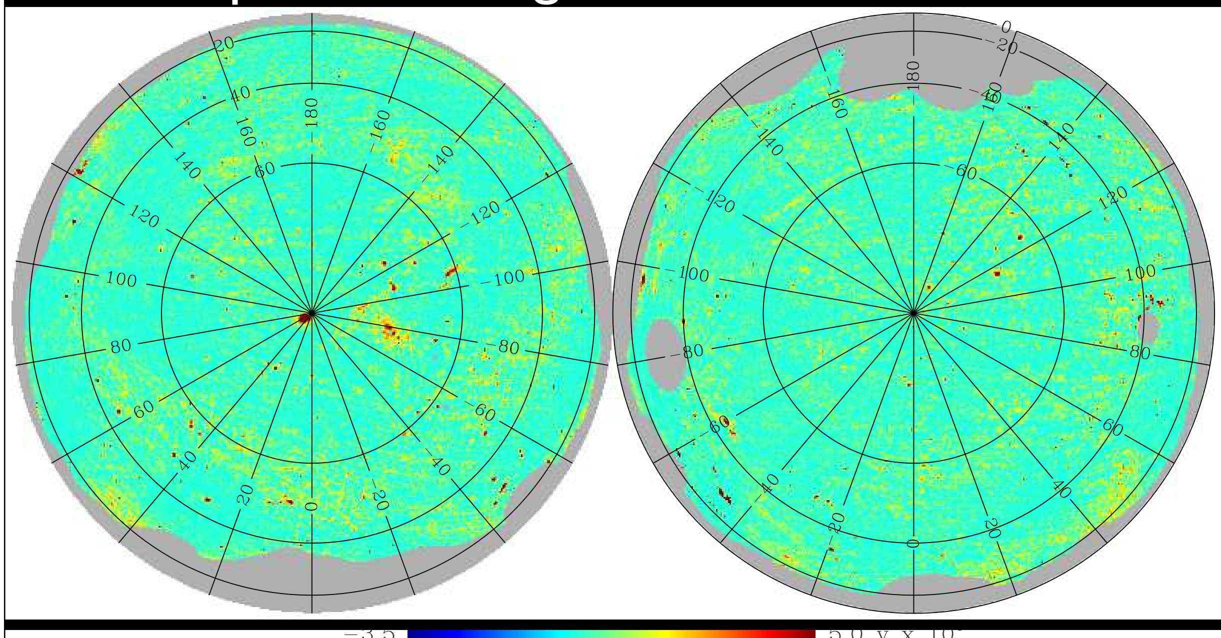

'Bridge' of hot gas connecting two galaxy clusters

Planck catalog of clusters of galaxies

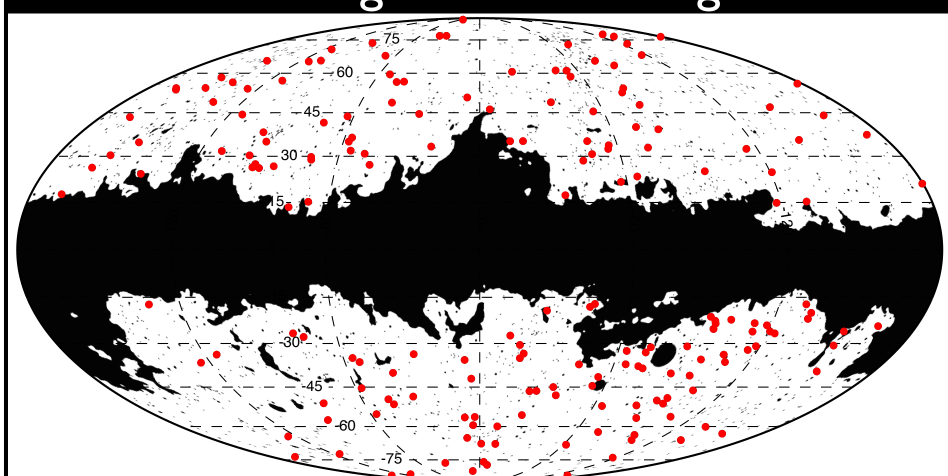

The Polarization of the Cosmic Microwave Background

Overview

- Physical origin of polarization
- The information encoded by polarization
- Summary

The Anisotropies are polarized

DASI

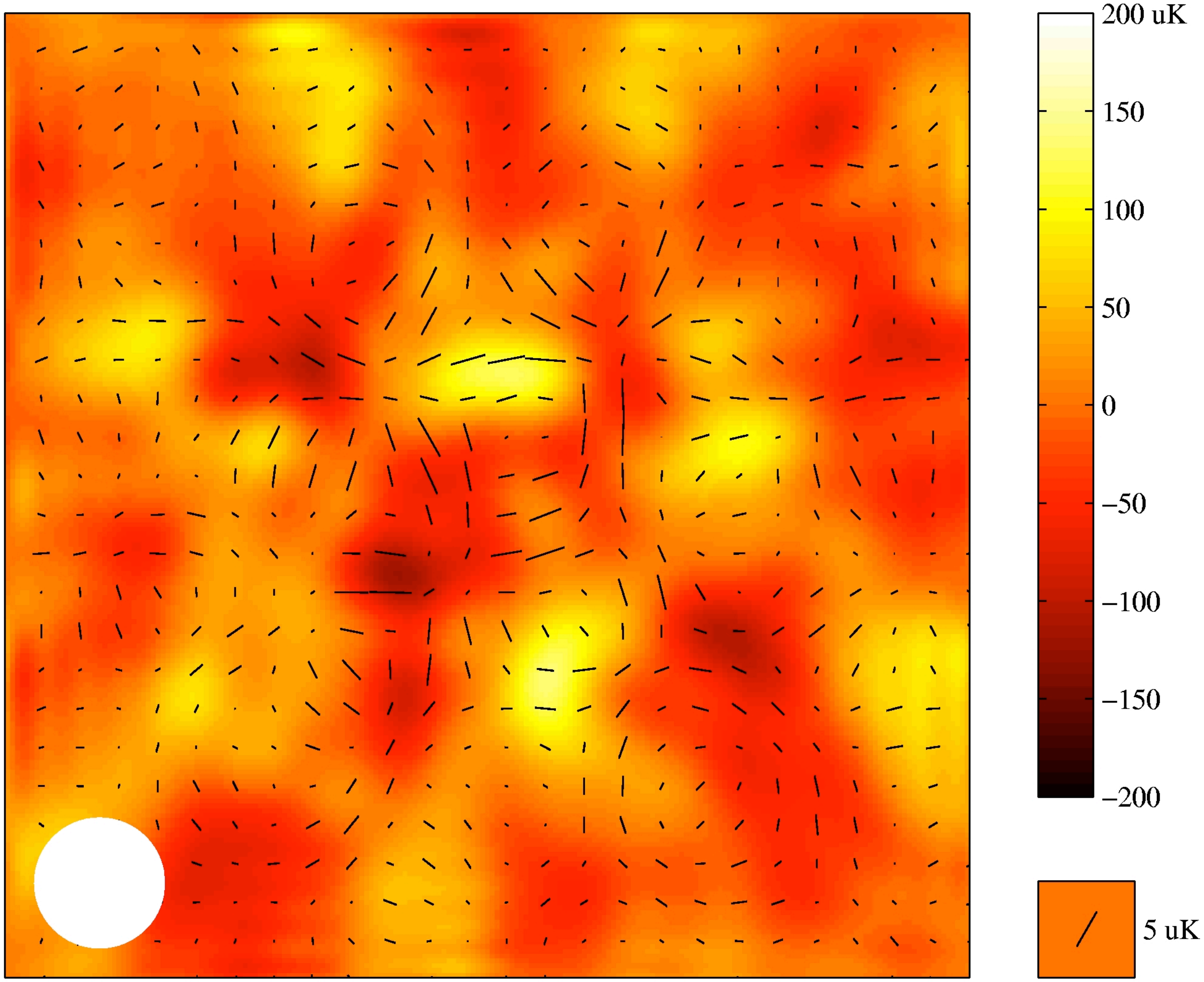

Map is 5 degrees square

Kovac et al.
astro-ph/0209478

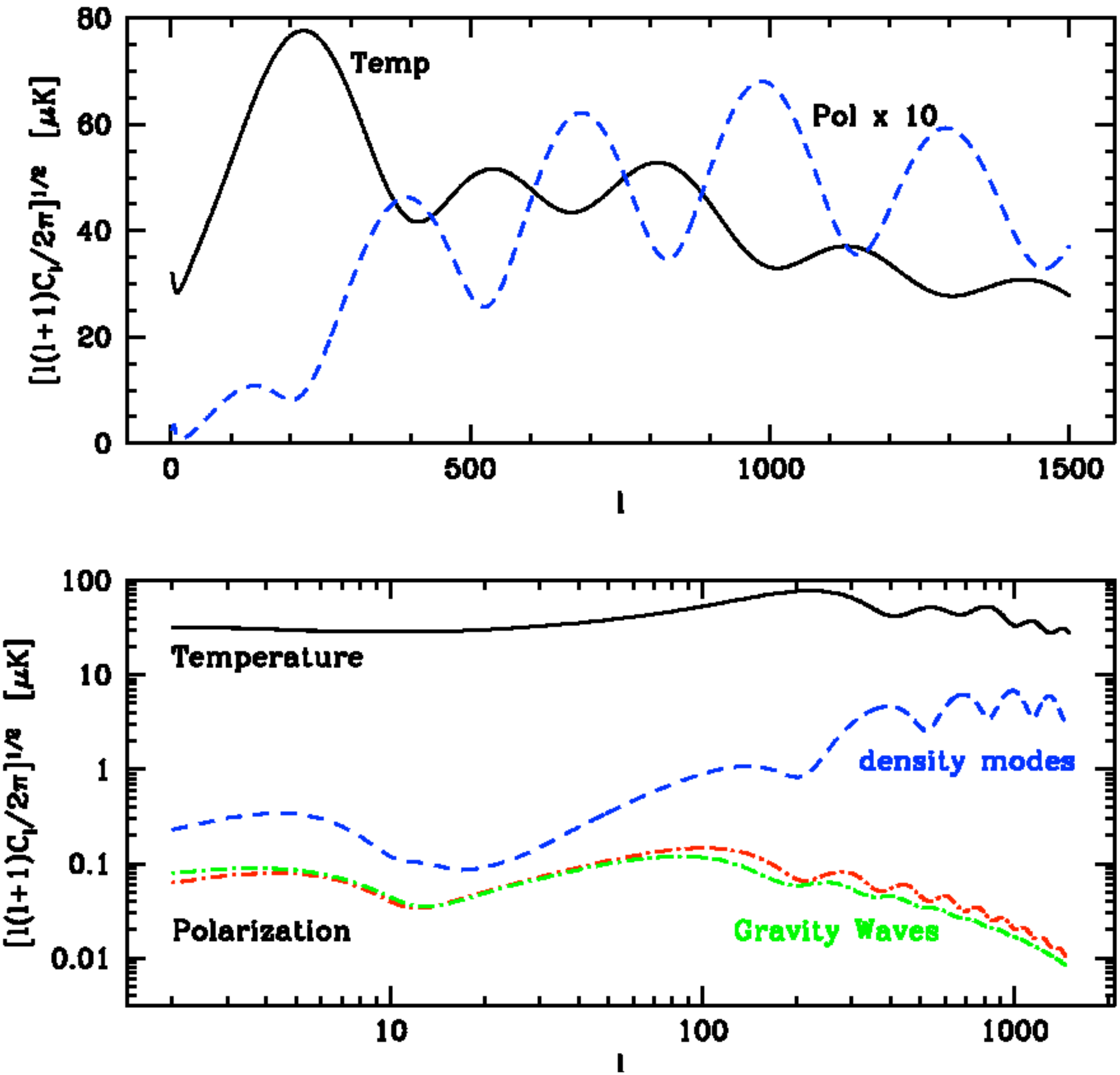

Temp
Pol x 10
[l(l+1)C_l/2π]^1/2 [μK]
l
Temperature
density modes
Polarization
Gravity Waves

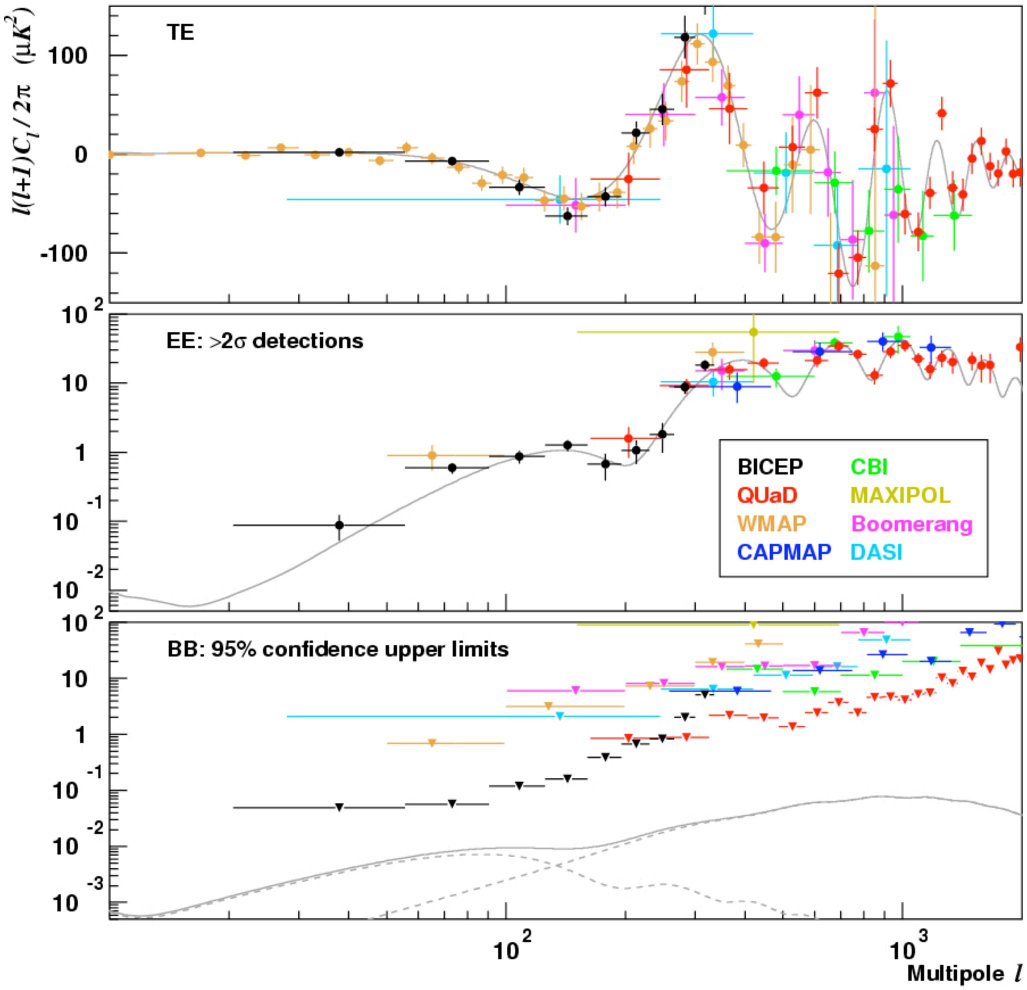

Bicep

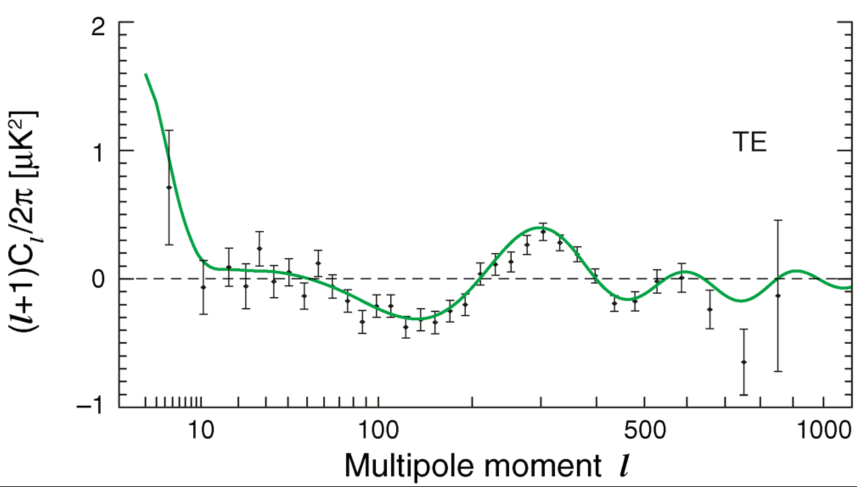

WMAP

The polarization and temperature patterns are correlated.

How is polarization generated?

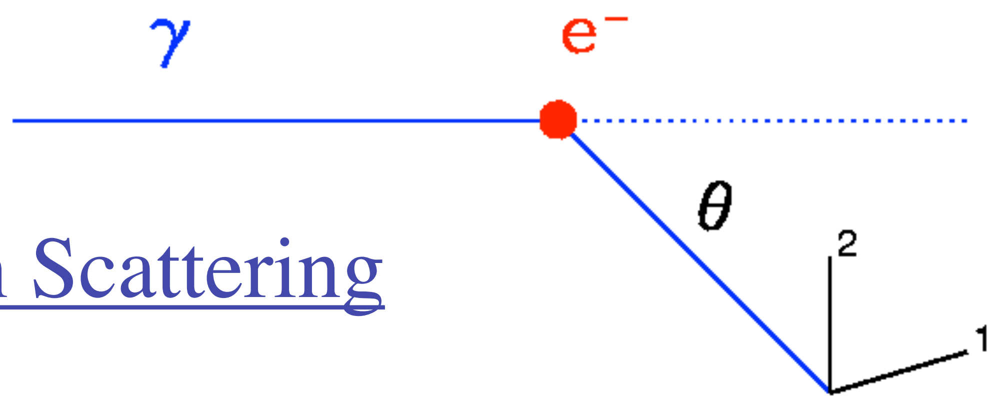

Thomson Scattering

$$I_1 \propto \sigma_{Th} \cos^2\theta$$

$$I_2 \propto \sigma_{Th}$$

THOMSON SCATTERING

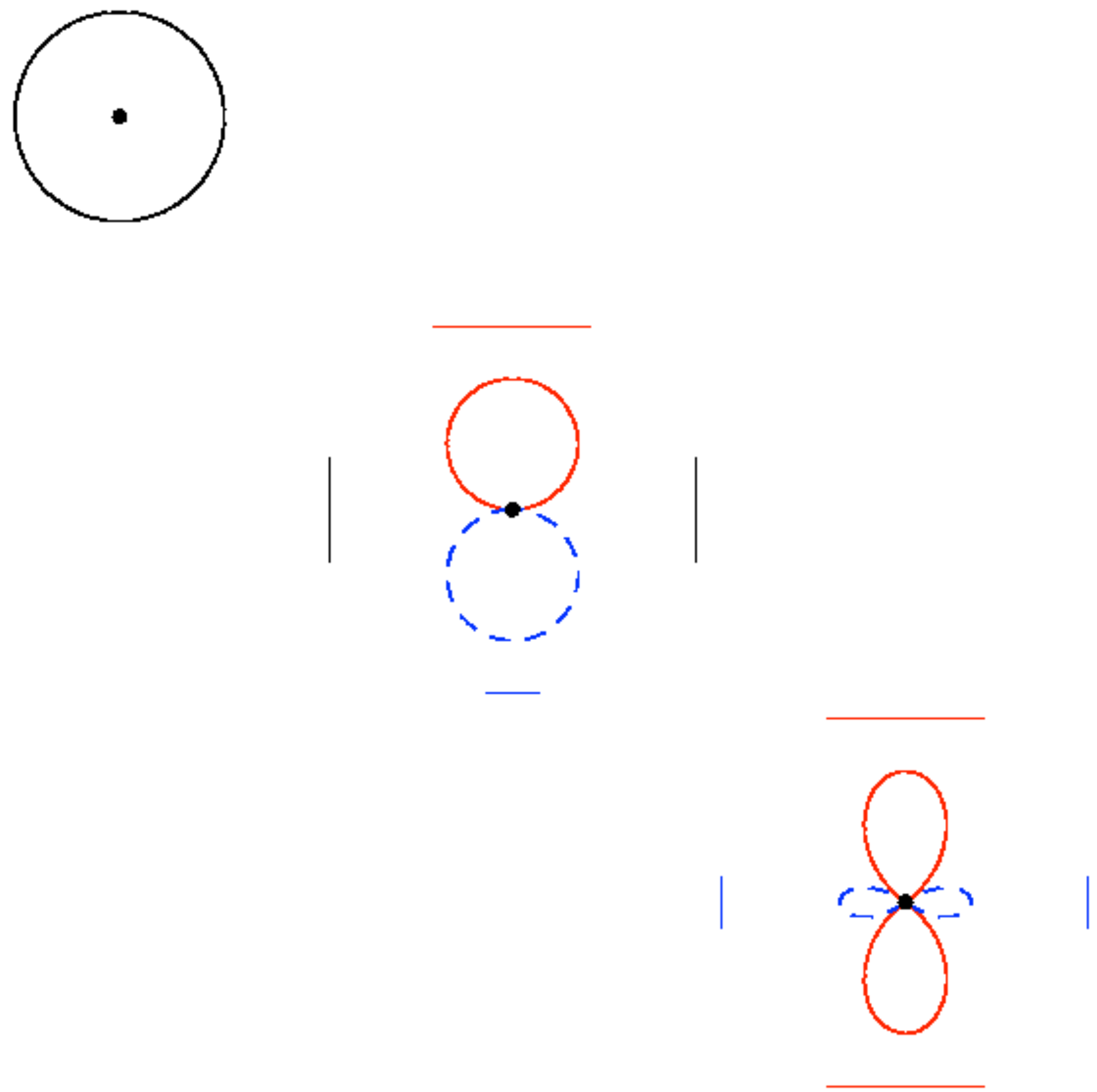

Recombination

T = 0.3 eV << $m_e c^2$

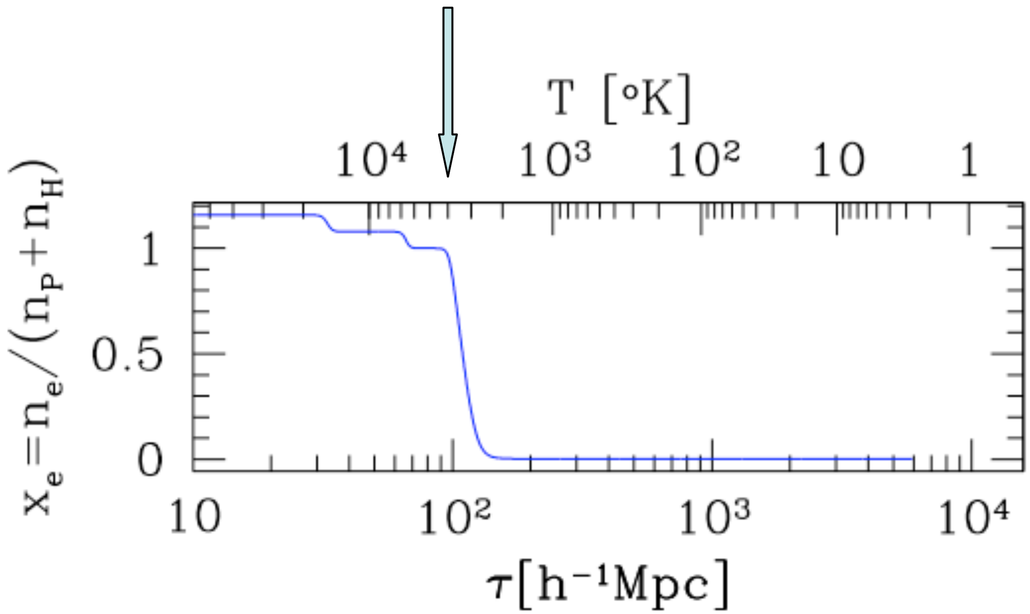

Hydrogen is ionized

Hydrogen is neutral

Thomson Scattering

The quadrupole created by density perturbations

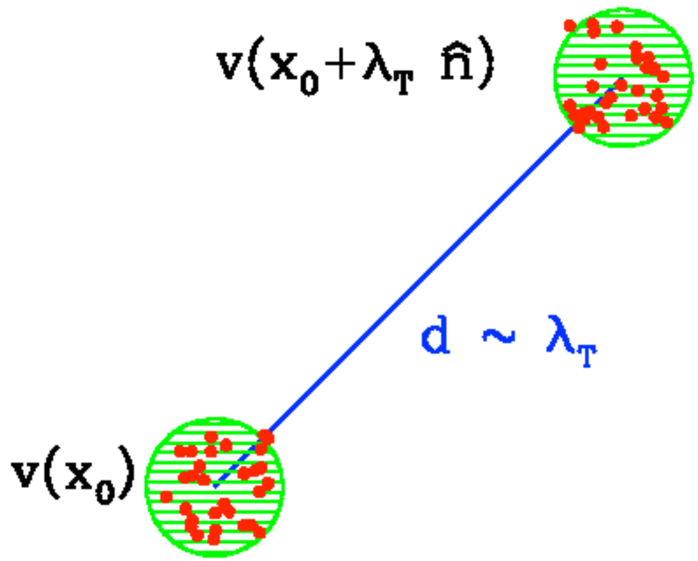

Doppler shift

$$\hat{n} \cdot [v(x_0+\lambda_T\ \hat{n}) - v(x_0)] \sim \lambda_T\ \hat{n}_i\ \hat{n}_j\ v_{i,j}$$

$$\mathrm{Pol} \sim k\ \lambda_T\ v \sim k\ \lambda_T\ c_s\ \delta_\gamma$$

Polarization peaks at smaller scales

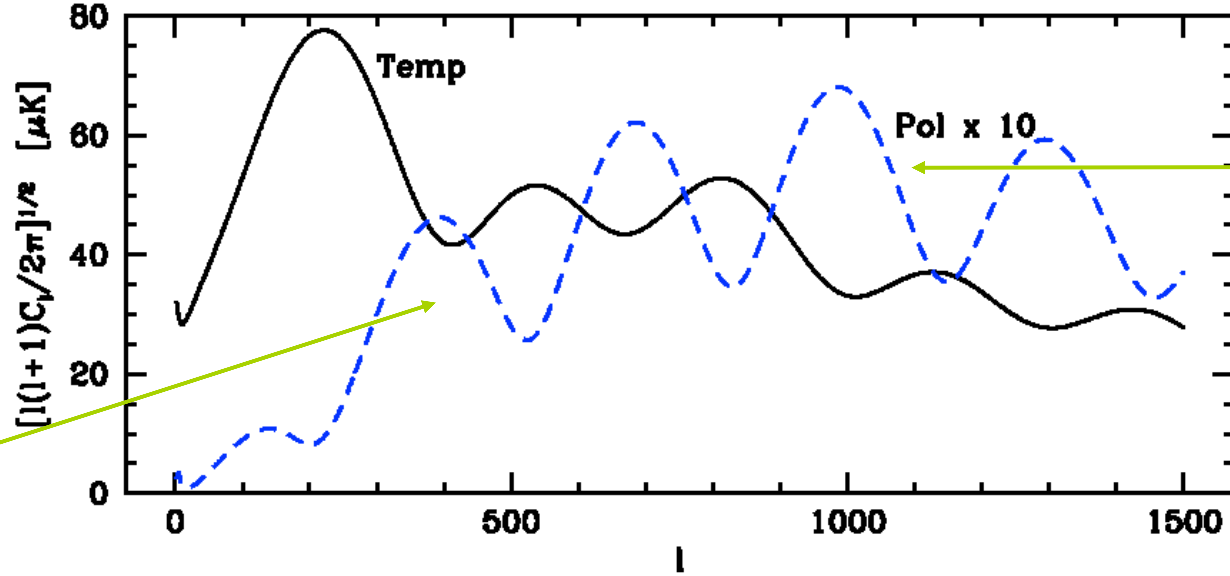

Peaks are out of phase

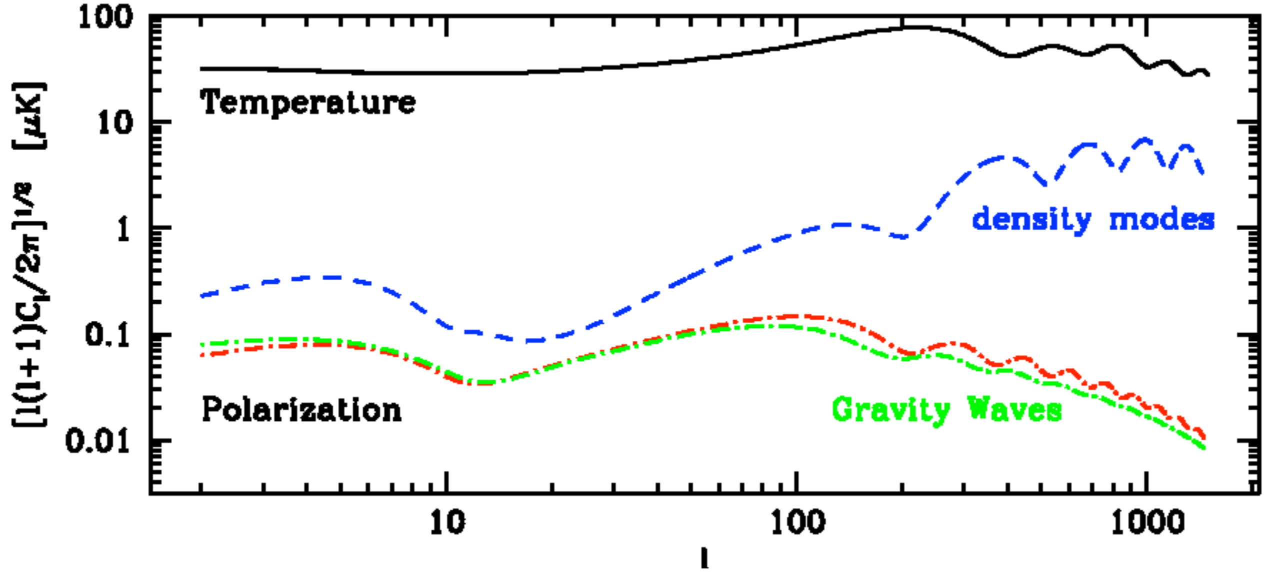

$$\dot{\delta}_\gamma = -\frac{4}{3}kv_\gamma + 4\dot{\phi}$$

When were perturbations created?

Sharp acoustic peaks are difficult to create without inflation

Causal Seeds

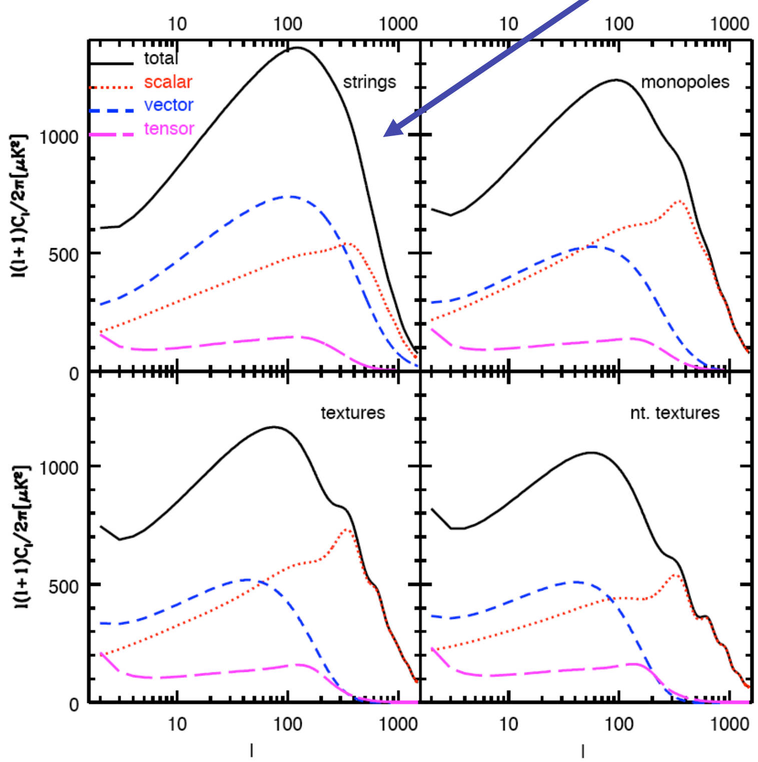

Pen, Seljak & Turok (1997)

WMAP 3yrs

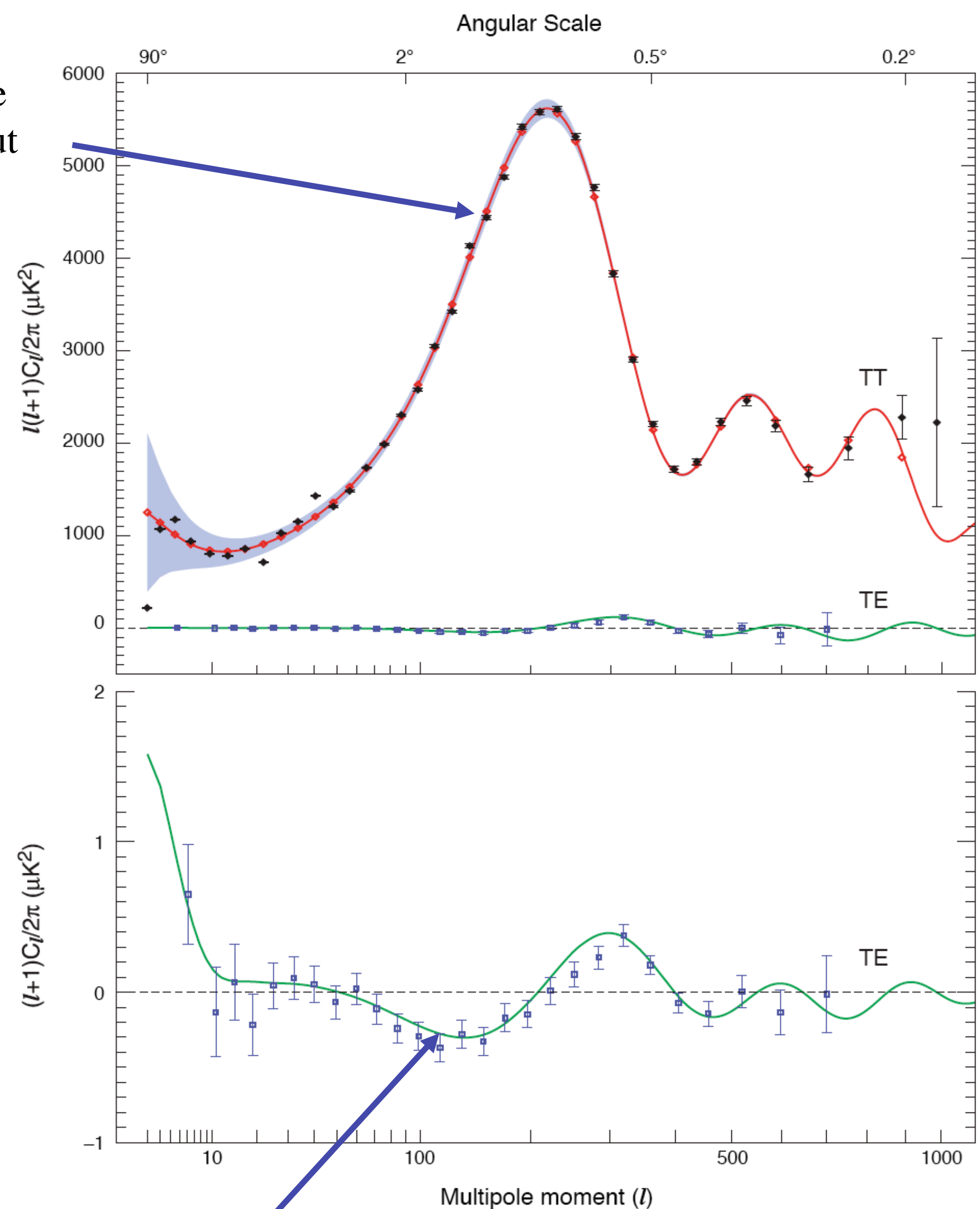

Negative peak imply fluctuations come from outside horizon

Hu & White (1996)
Spergel & MZ (1997)
Pieris et al WMAP (2003)

Scatterings

+

Anisotropies

Density Pert.

Gravity Waves

POLARIZATION

The quadrupole created by GW

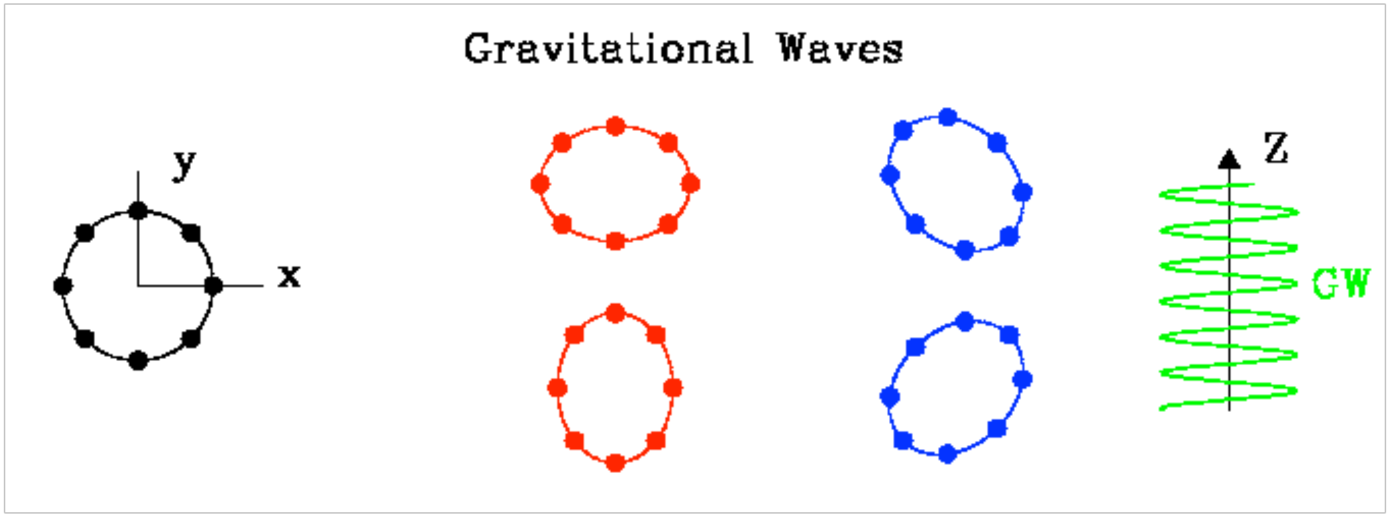

$$\frac{1}{\nu}\frac{d\nu}{d\tau} \propto \frac{1}{2}(1 - \cos^2\theta)e^{\pm i2\phi}\dot{h}_t(\tau)$$

$$P \propto \delta\tau_D \ \dot{h}_t(\tau_D) \sim k\delta\tau_D \ h_t(\tau_D)$$

Anisotropies created by GW

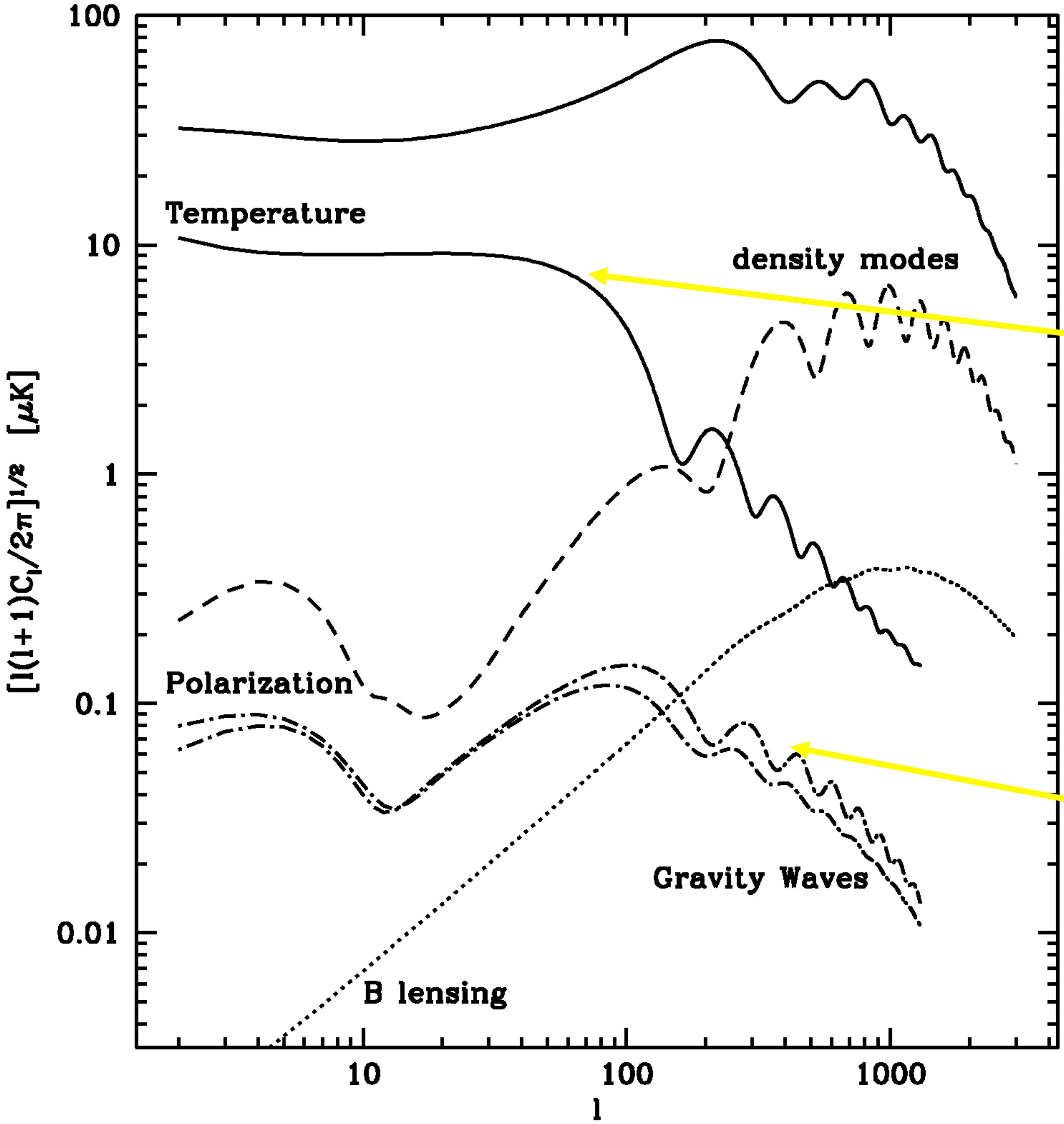

$$h_t(k\tau) \propto \frac{3j_1(k\tau)}{k\tau}$$

ISW like effect, produced after recombination

Polarization is produced at recombination

Density pert.
&
Gravity Waves

Gravity
Waves

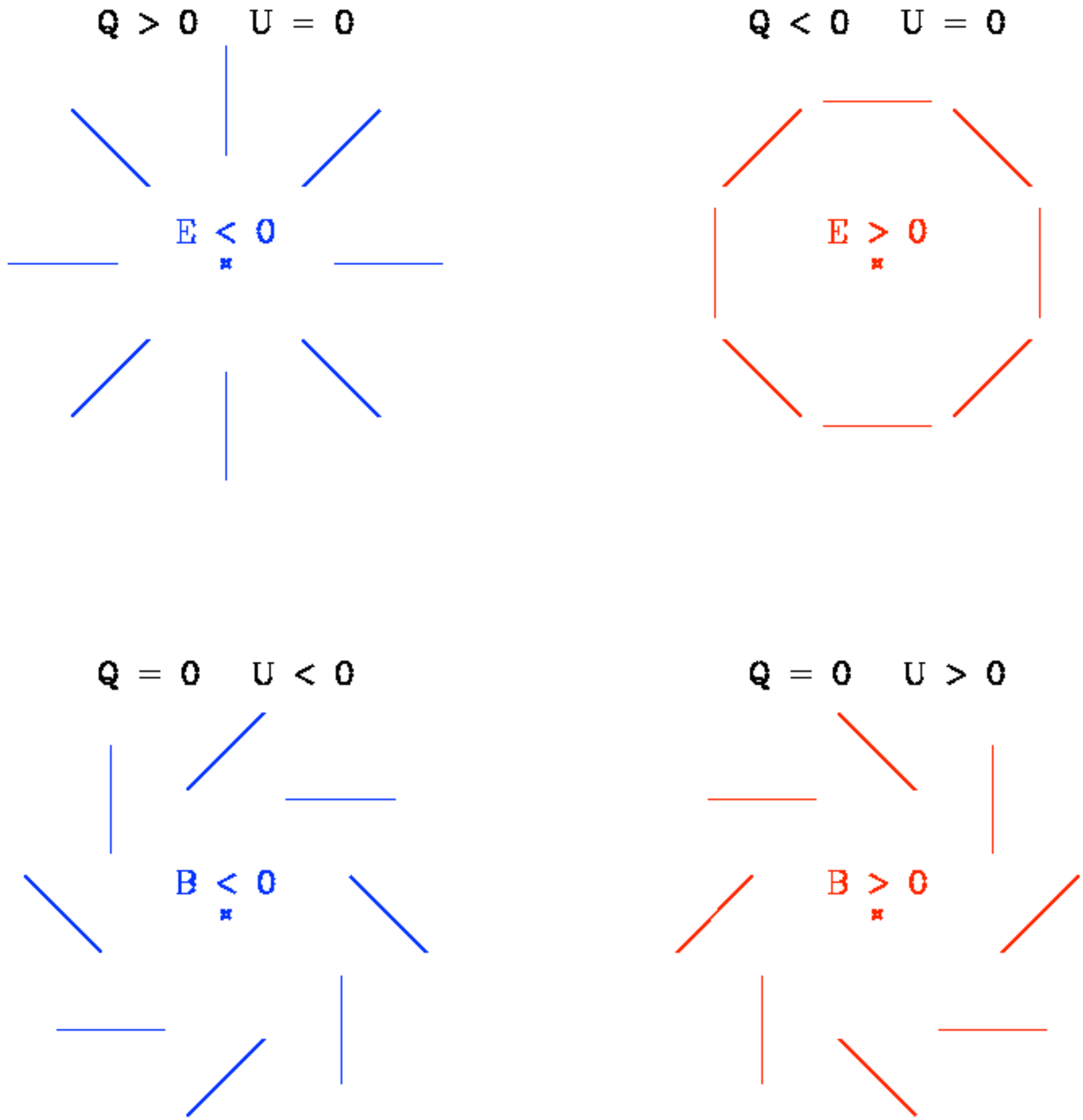

After Recombination

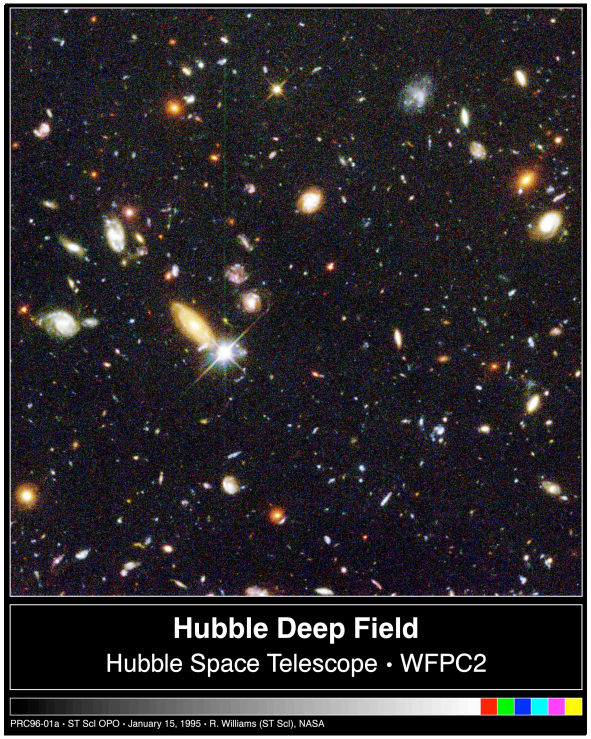

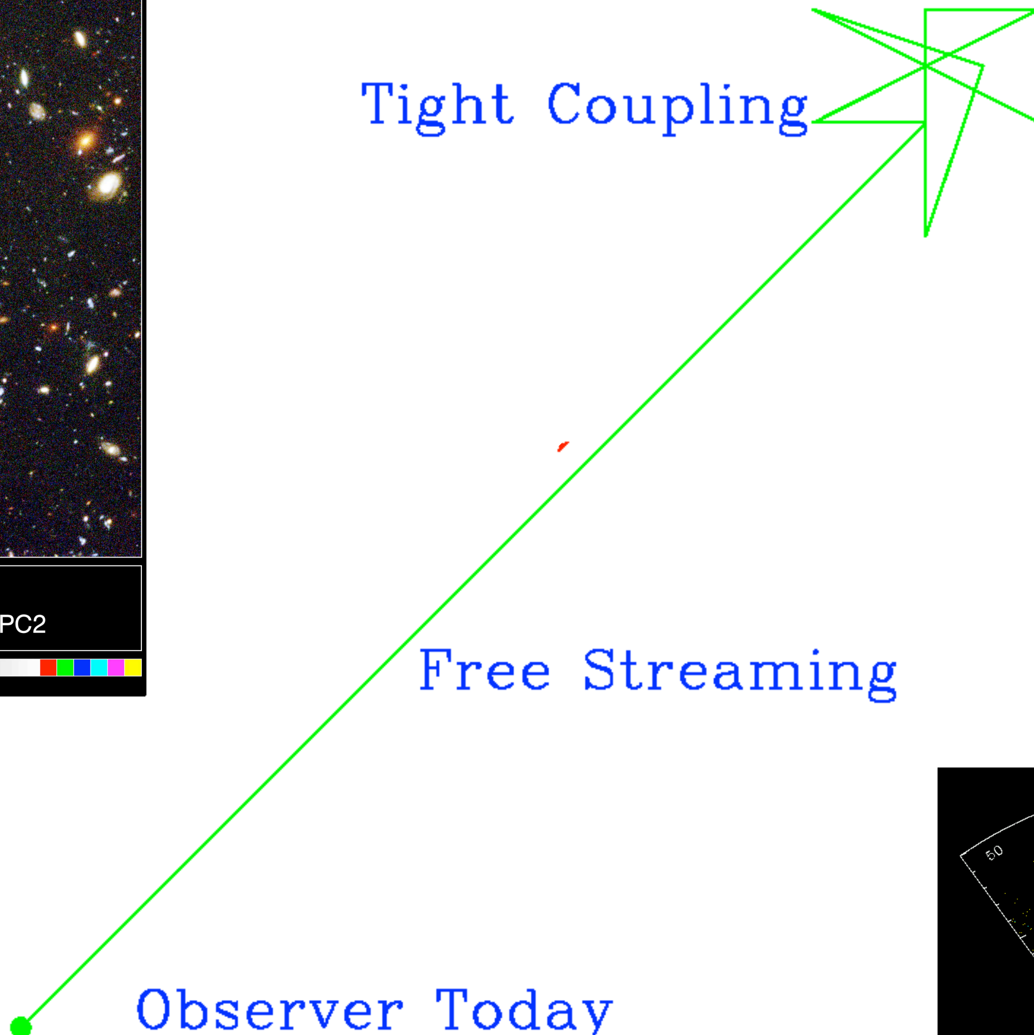

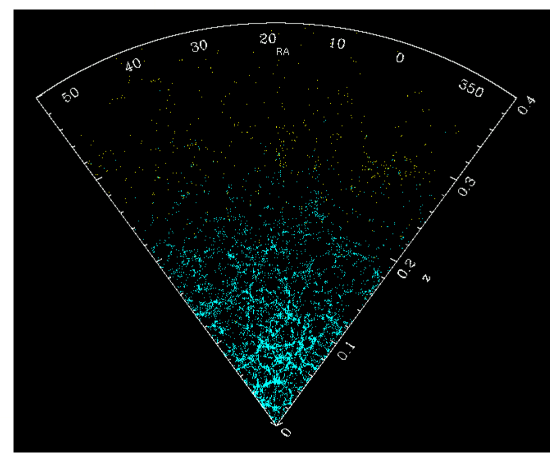

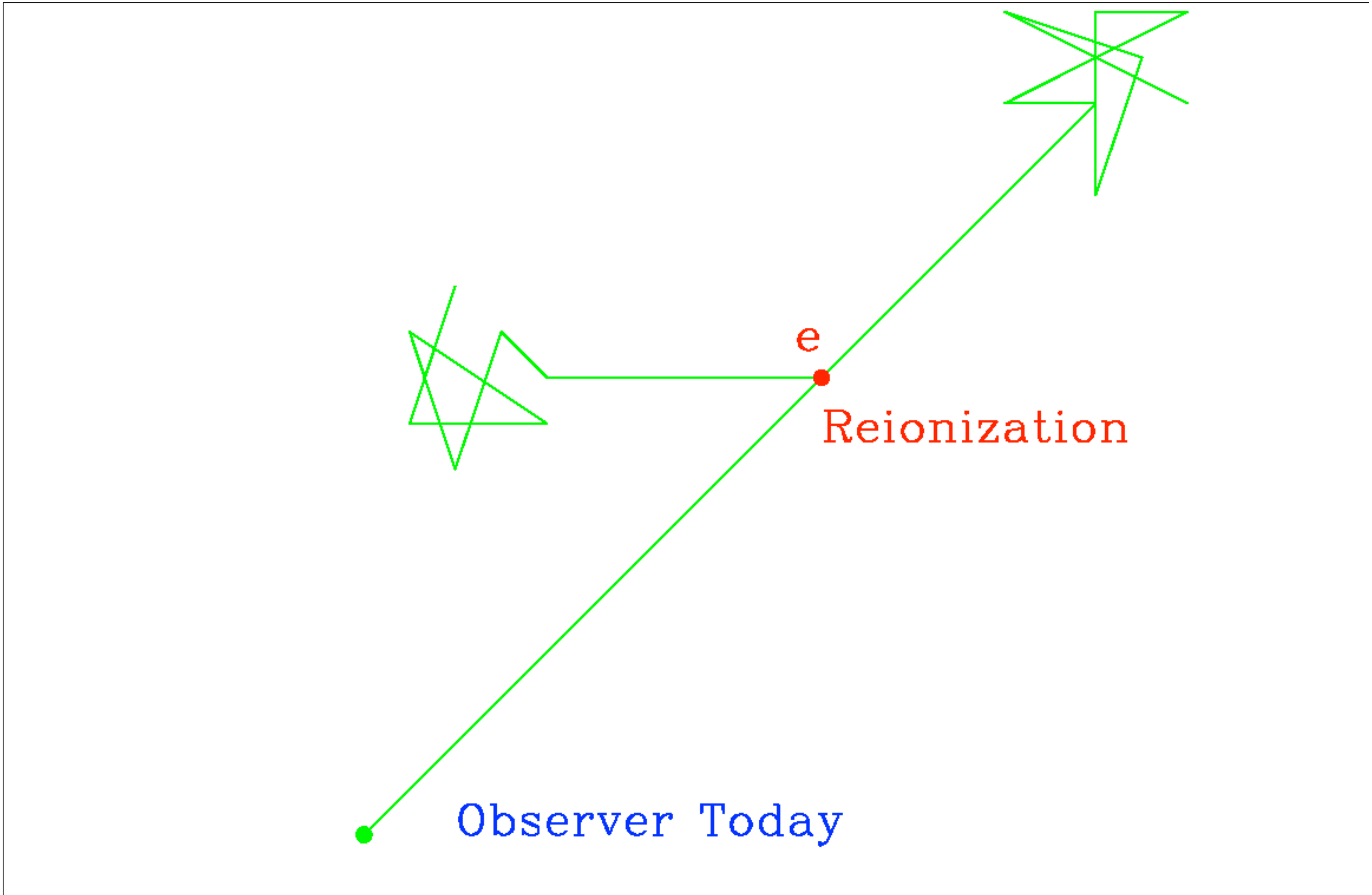
e
Reionization
Observer Today

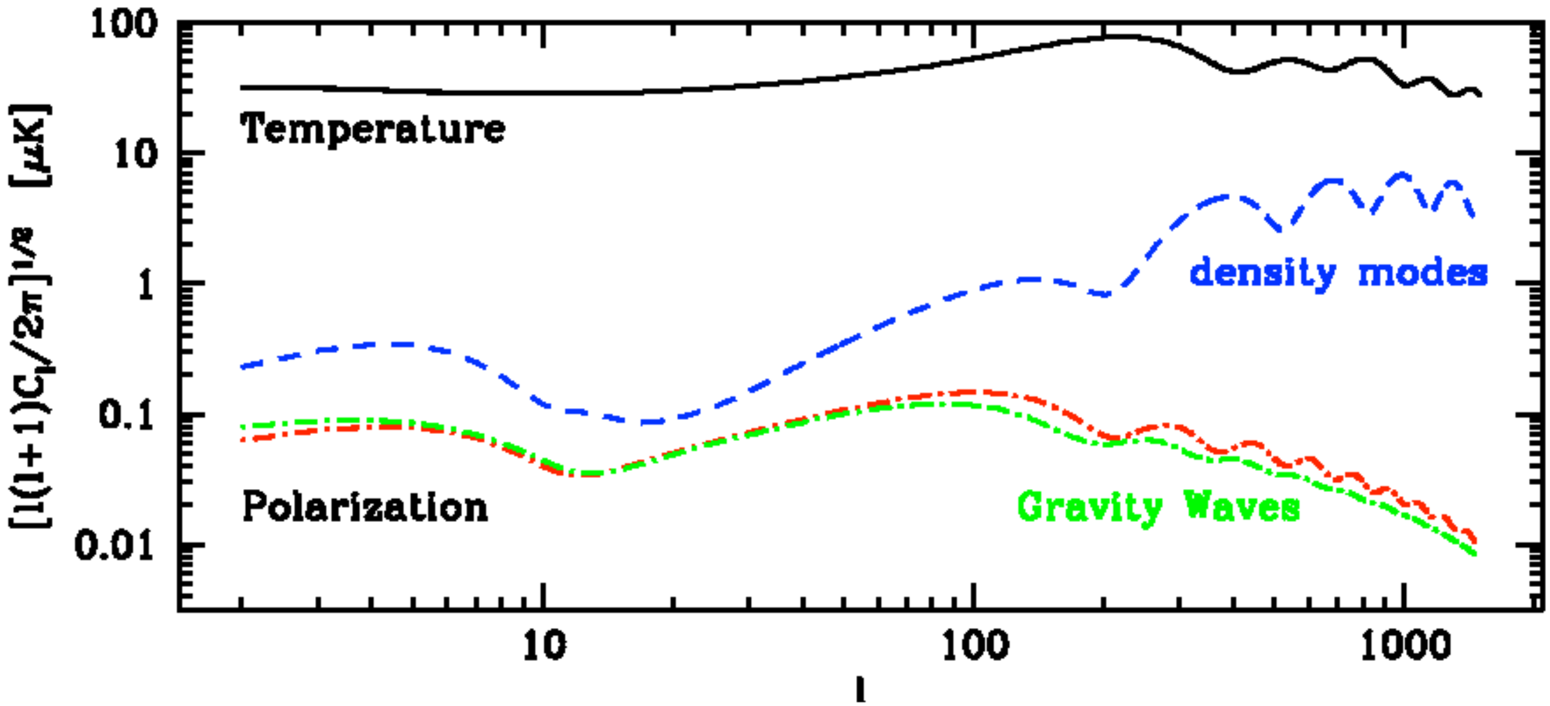

1. The height of the bump is given by the optical depth
2. The quadrupole is produced by the free streaming of the monopole at recombination, $k \sim 2/(\tau_{reio} - \tau_{rec})$ produces the biggest quadrupole
3. Angular scale $l \sim (\tau_o - \tau_{reio})/(\tau_{reio} - \tau_{rec})$

Gravitational Lensing

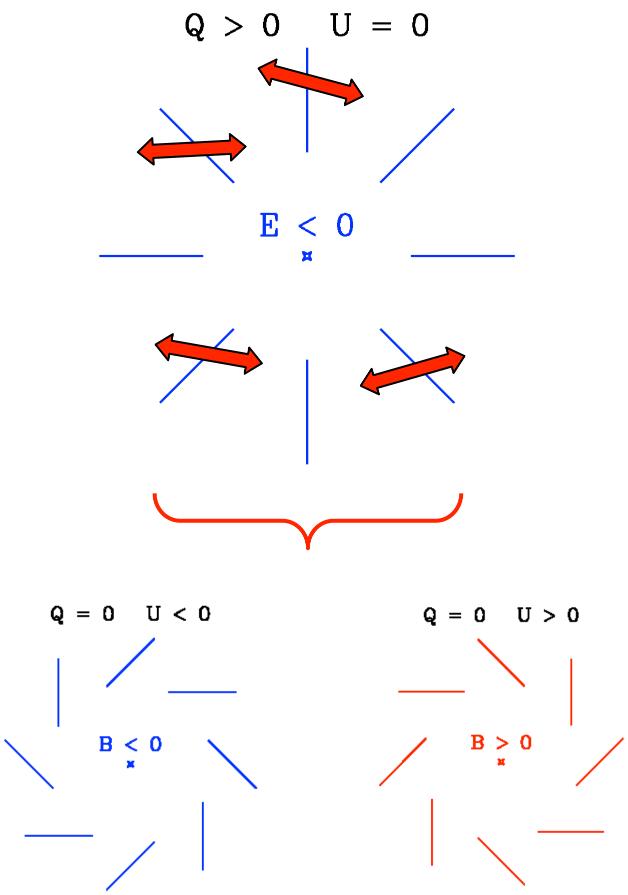

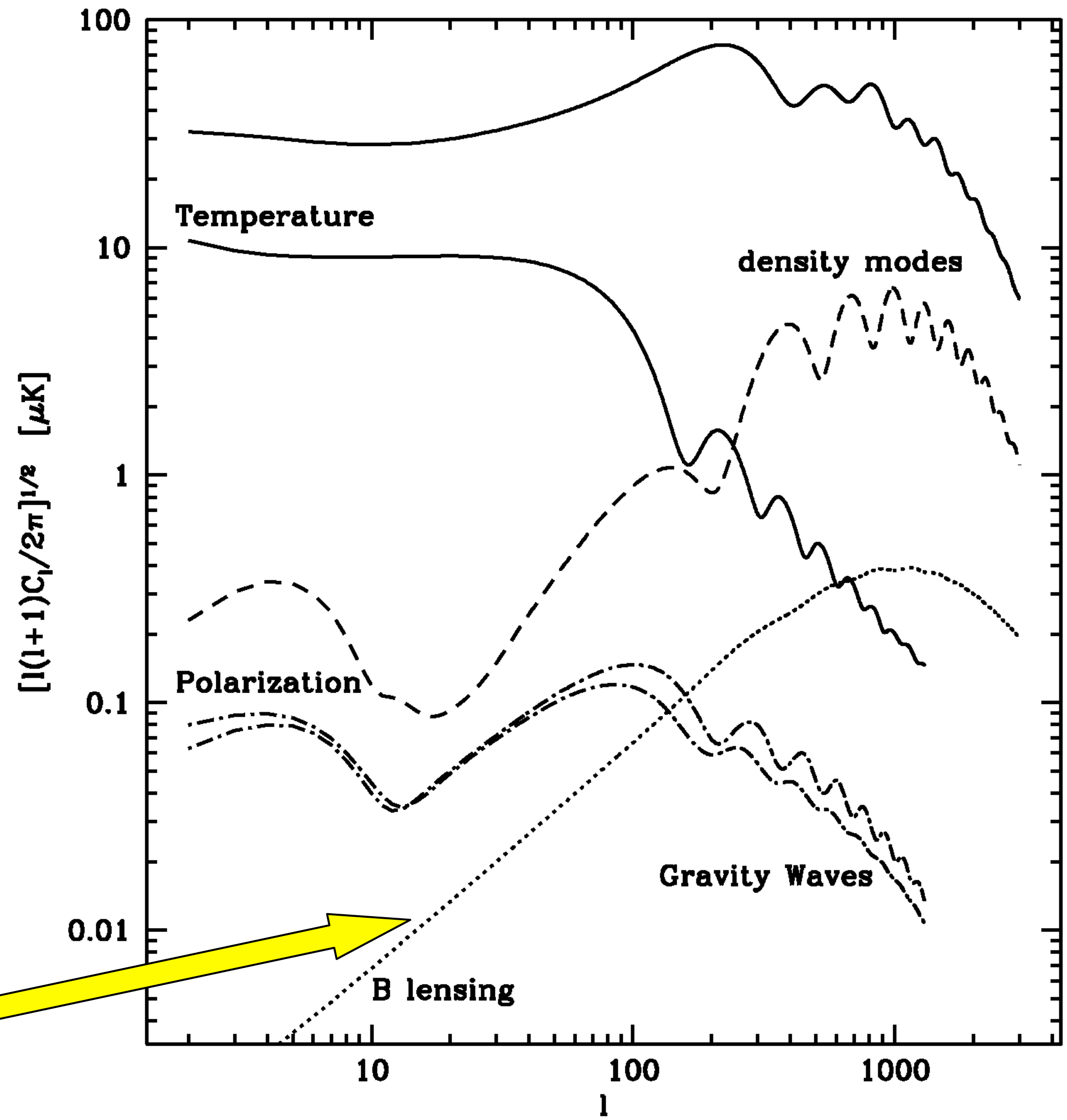

Lensing induced B modes

Structure formation

600 kpc

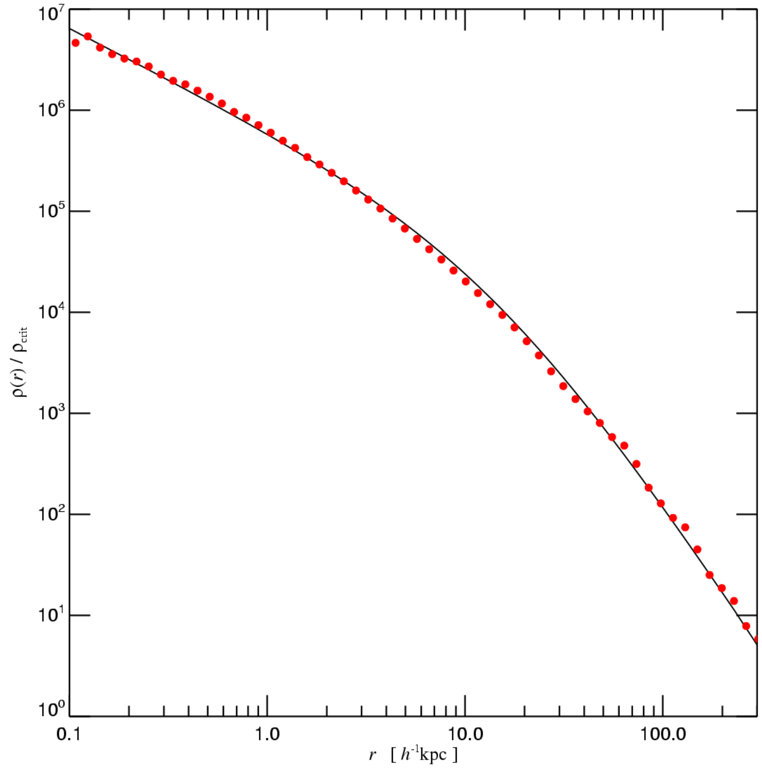

$N_{200} \sim 3 \times 10^7$

Navarro et al 2006

The Core vs. Cusp problem

Weinberg et al. 1306.0913

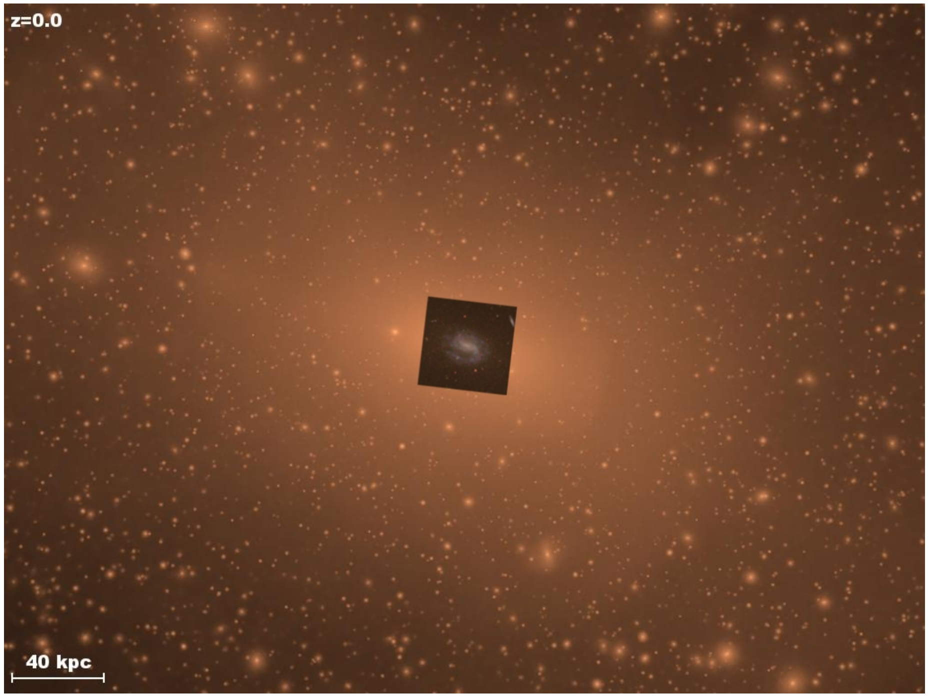

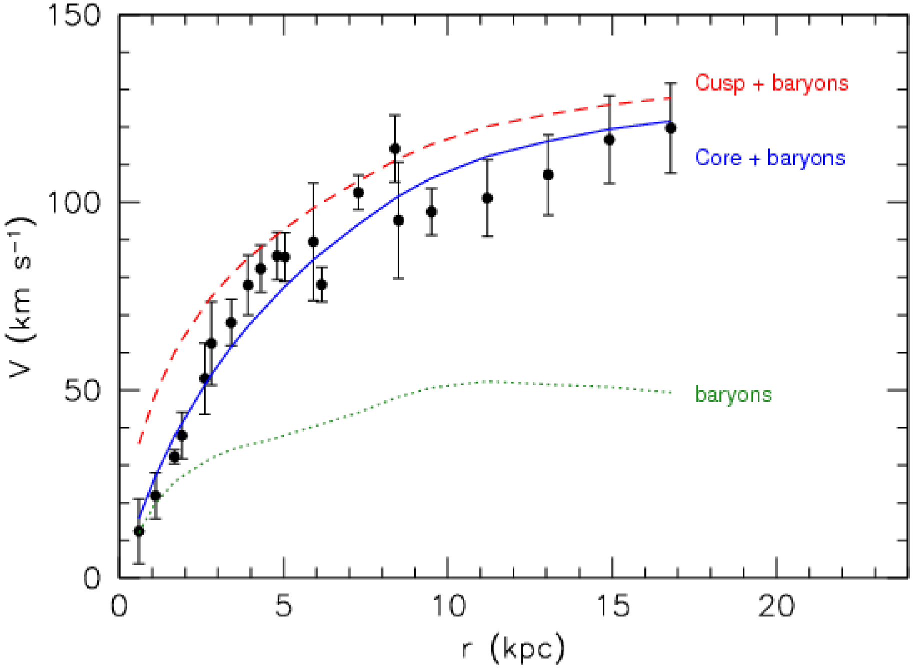

Fig. 1. The cusp-core problem. *(Left)* An optical image of the galaxy F568-3 (small inset, from the Sloan Digital Sky Survey) is superposed on the the dark matter distribution from the "Via Lactea" cosmological simulation of a Milky Way-mass cold dark matter halo (Diemand et al. 2007). In the simulation image, intensity encodes the square of the dark matter density, which is proportional to annihilation rate and highlights low mass substructure. *(Right)* The measured rotation curve of F568-3 (points) compared to model fits assuming a cored dark matter halo (blue solid curve) or a cuspy dark matter halo with an NFW profile (red dashed curve, concentration $c = 9.2$, $V_{200} = 110\,\mathrm{km\,s^{-1}}$). The dotted green curve shows the contribution of baryons (stars+gas) to the rotation curve, which is included in both model fits. An NFW halo profile overpredicts the rotation speed in the inner few kpc. Note that the rotation curve is measured over roughly the scale of the 40 kpc inset in the left panel.

The Satellite problem

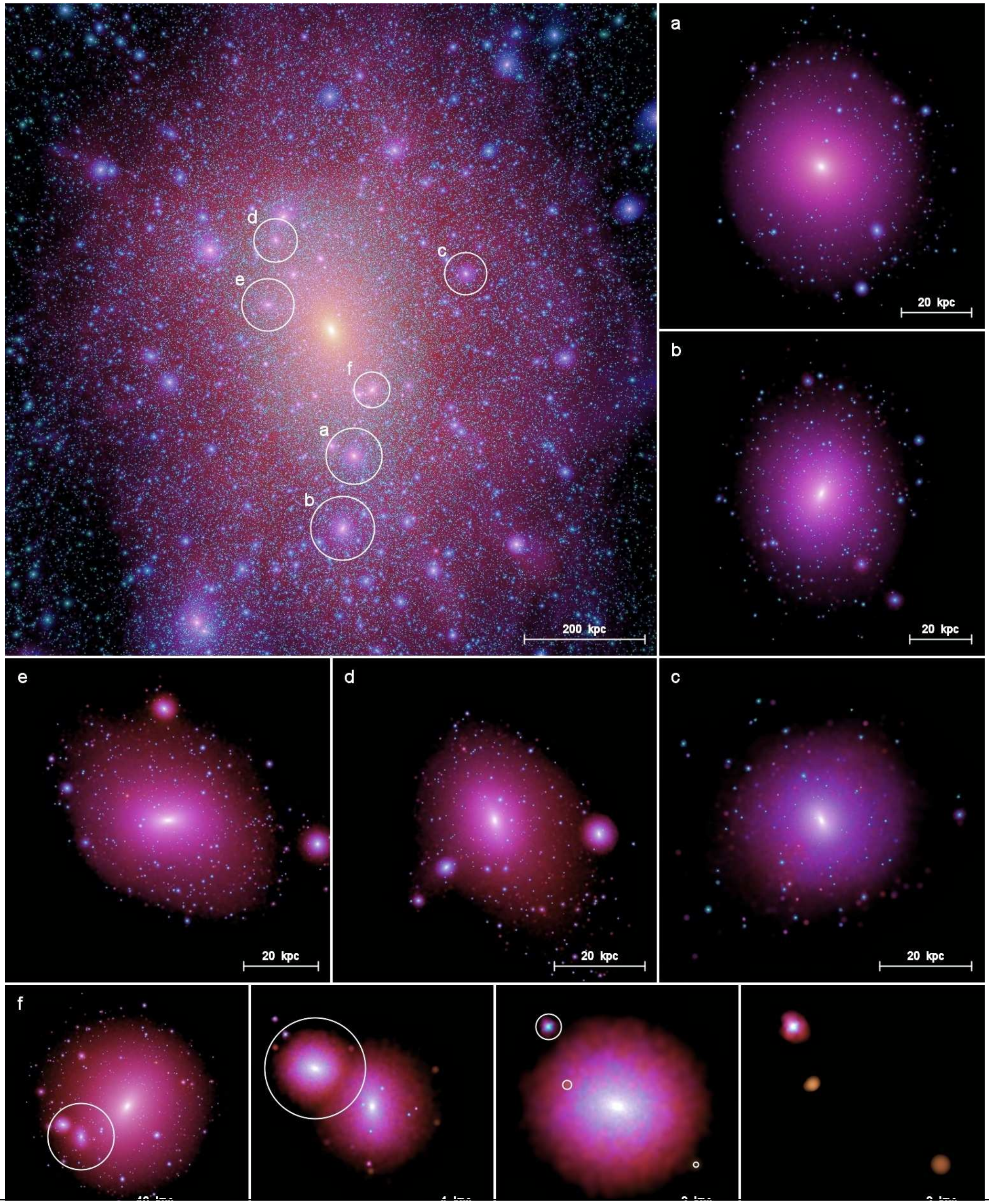

The Satellite problem

Weinberg et al. 1306.0913

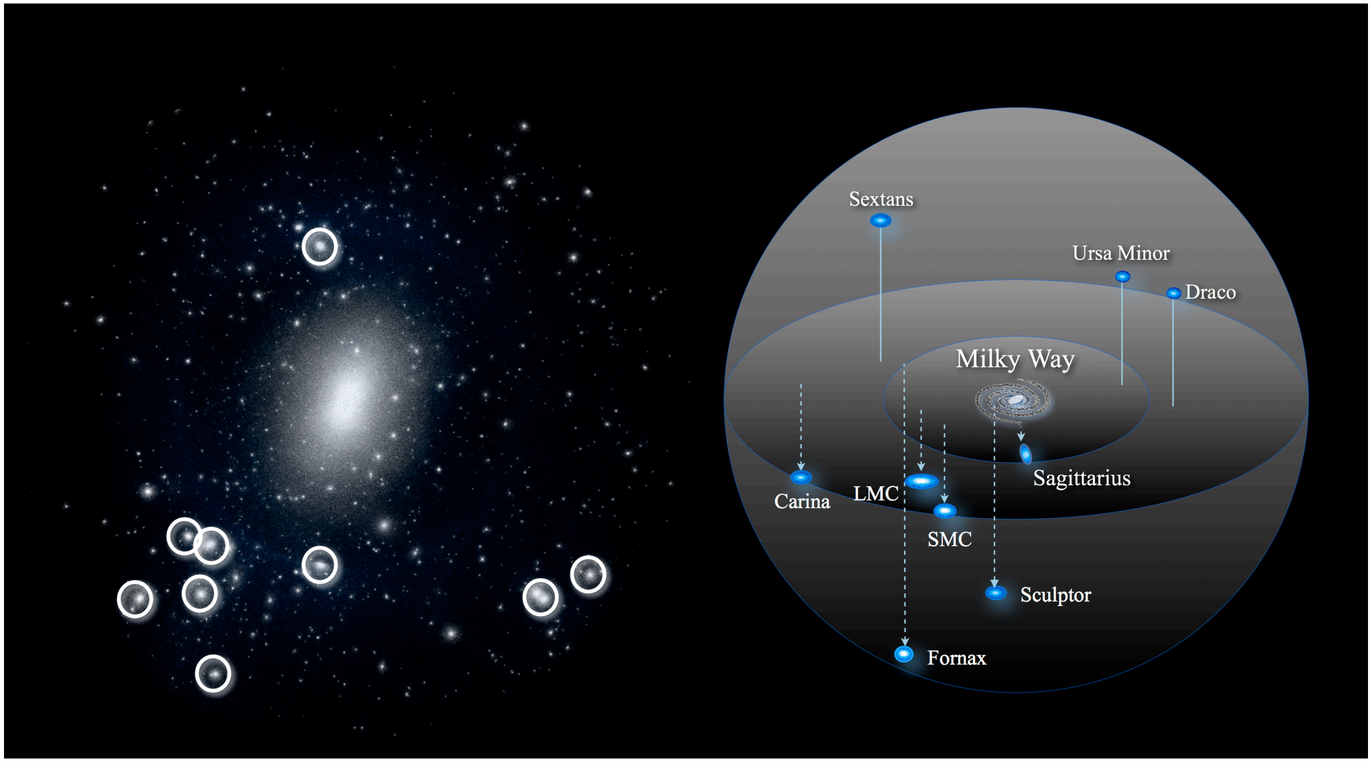

Fig. 2. The missing satellite and "too big to fail" problems. *(Left)* Projected dark matter distribution (600 kpc on a side) of a simulated, $10^{12} M_{\odot}$ CDM halo (Garrison-Kimmel, Boylan-Kolchin, & Bullock, in preparation). As in Figure 1, the numerous small subhalos far exceed the number of known Milky Way satellites. Circles mark the nine most massive subhalos. *(Right)* Spatial distribution of the "classical" satellites of the Milky Way. The central densities of the subhalos in the left panel are too high to host the dwarf satellites in the right panel, predicting stellar velocity dispersions higher than observed. The diameter of the outer sphere in the right panel is 300 kpc; relative to the simulation prediction (and to the Andromeda galaxy) the Milky Way's satellite system is unusually centrally concentrated (Yniguez et al. 2013).

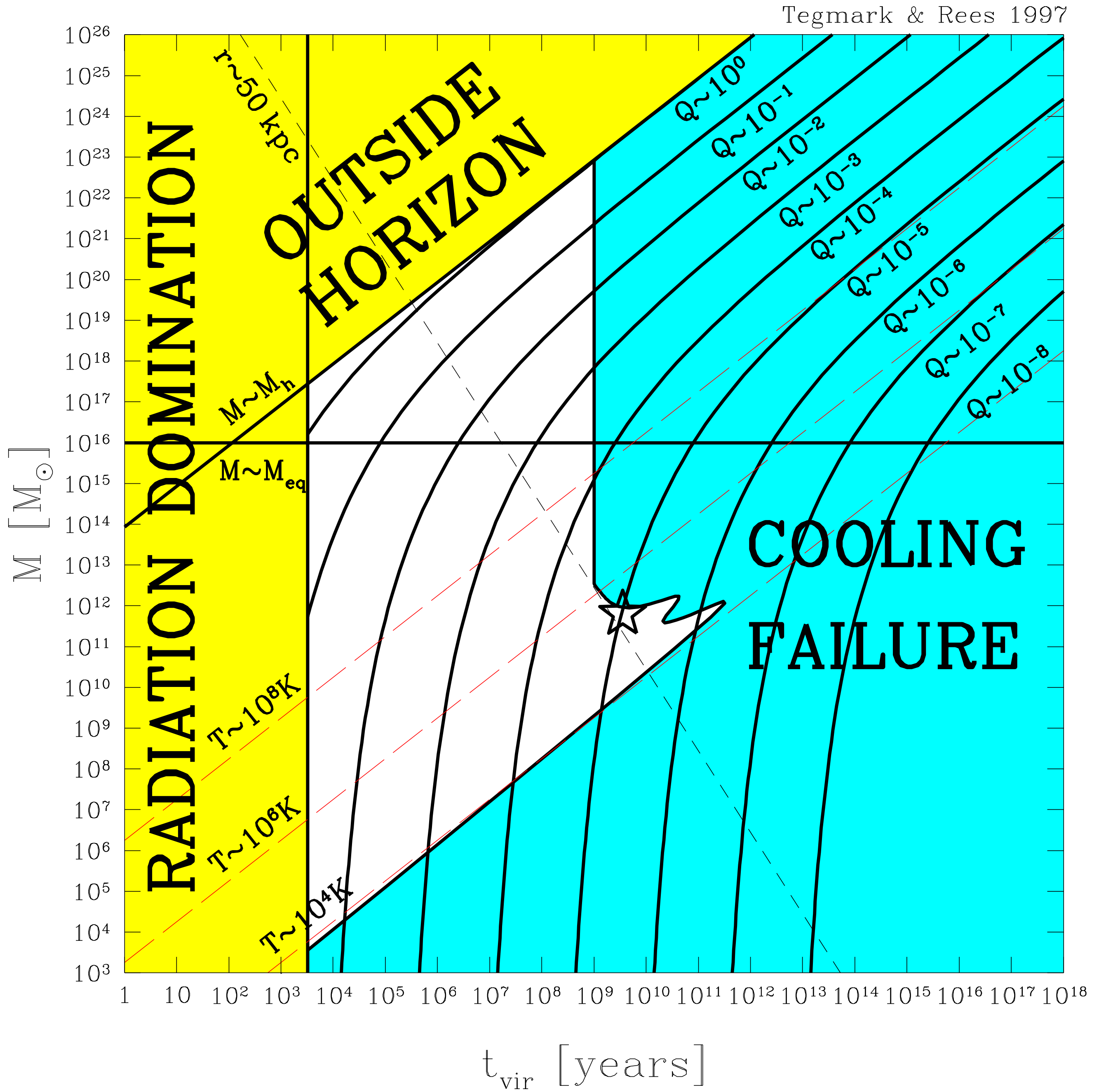

FIG. 1.— The nine rising curves show the largest virialized mass scale as a function of time for different values of Q. Structures with $M \lesssim M_{eq}$ (horizontal line) are seen to all virialize about a factor $Q^{-3/2}$ after the end of the radiation-dominated epoch (shaded, left), whereas for later times, the virialized mass scale asymptotes to about $Q^{3/2}$ times the horizon mass (shaded, upper left). Cooling is inefficient in the

Clusters

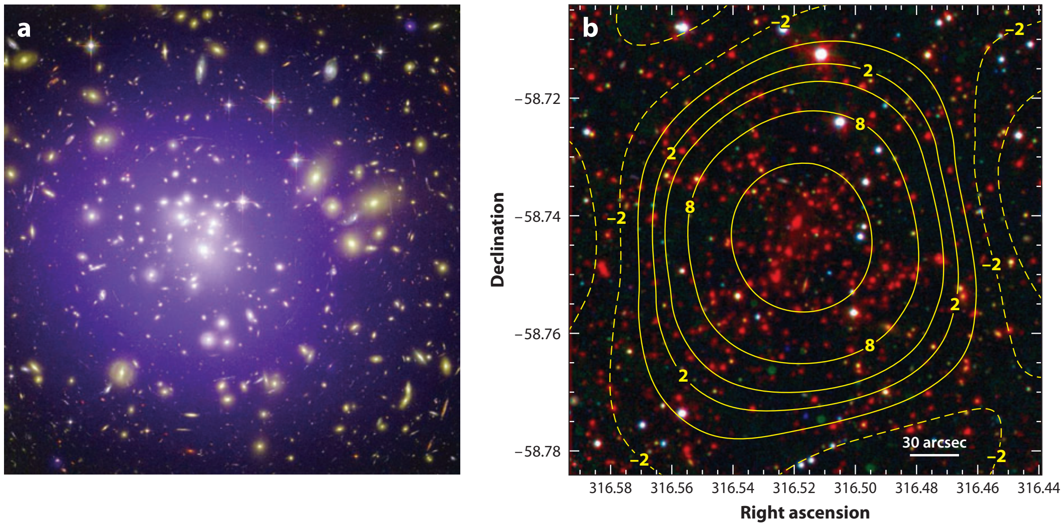

Figure 1

(*a*) The composite X-ray/optical image (556 kpc on a side) of the galaxy cluster Abell 1689 at redshift $z = 0.18$. The purple haze shows X-ray emission of the $T \sim 10^8$ K gas, obtained by the *Chandra X-ray Observatory*. Images of galaxies in the optical band, colored in yellow, are from observations performed with the *Hubble Space Telescope*. The long arcs in the optical image are caused by the gravitational lensing of background galaxies by matter in the galaxy cluster, the largest system of such arcs ever found (Credit: X-ray: NASA/CXC/MIT; Optical: NASA/STScI). (*b*) The galaxy cluster SPT-CL J2106-5844 at $z = 1.133$, the most massive cluster known at $z > 1$ discovered via its Sunyaev-Zel'dovich (SZ) signal ($M_{200} \approx 1.3 \times 10^{15}\ M_{\odot}$). The color image shows the Magellan/LDSS3 optical and *Spitzer*/IRAC mid-IR measurements (corresponding to the blue-green-red color channels). The frame subtends 4.8 × 4.8 arcmin, which corresponds to 2.4 × 2.4 Mpc at the redshift of the cluster. The solid yellow contours correspond to the South Pole Telescope SZ significance values, as labeled, where dashed yellow contours are used for the negative significance values. Adapted from Foley et al. 2011.

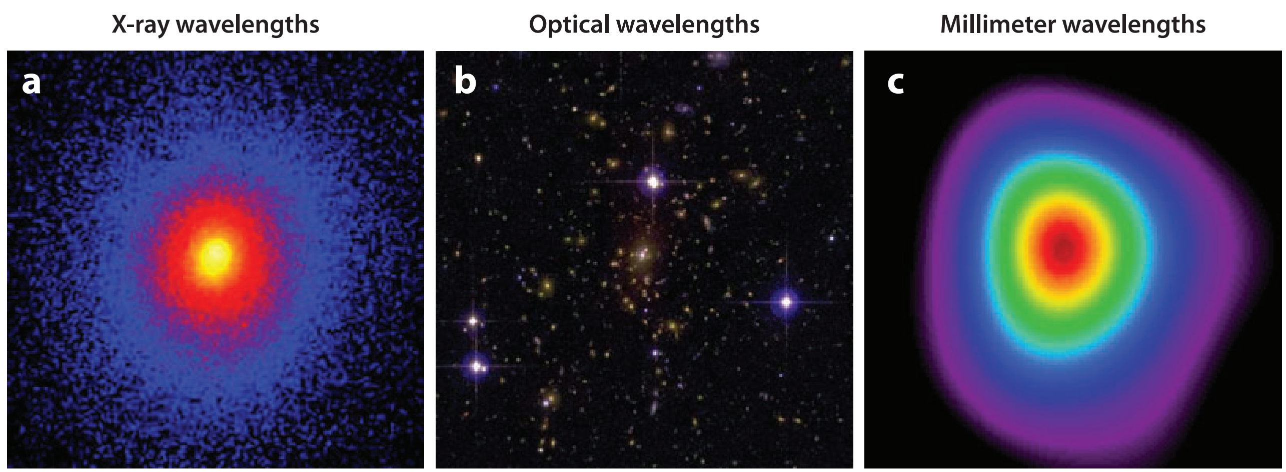

Figure 7

Images of Abell 1835 ($z = 0.25$) at (*a*) X-ray, (*b*) optical, and (*c*) millimeter wavelengths, exemplifying the regular multiwavelength morphology of a massive, dynamically relaxed cluster. All three images are centered on the X-ray peak position and have the same spatial scale, 5.2 arcmin or ∼1.2 Mpc on a side (extending out to $\sim r_{2,500}$; Mantz et al. 2010a). Figure credits: (*a*) X-ray: *Chandra X-ray Observatory*/A. Mantz; (*b*) optical: Canada-France-Hawaii Telescope/A. von der Linden et al.; (*c*) millimeter: Sunyaev Zel'dovich Array/D. Marrone.

Counting clusters

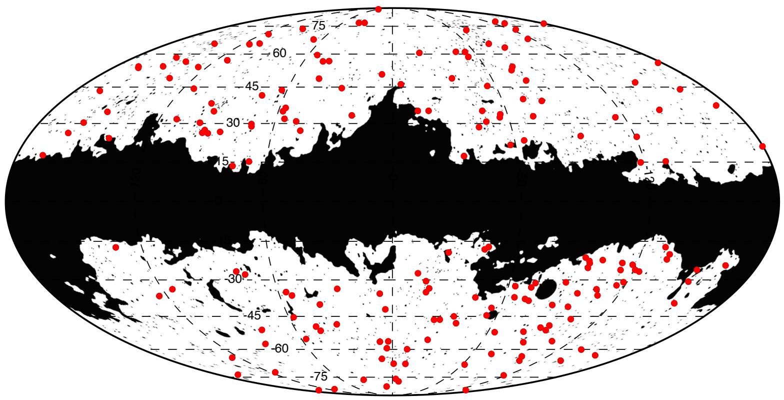

Fig. 1. The distribution on the sky of the *Planck* SZ cluster sub-sample used in this paper, with the 35% mask overlaid.

Planck cluster counts: The σ_8 problem

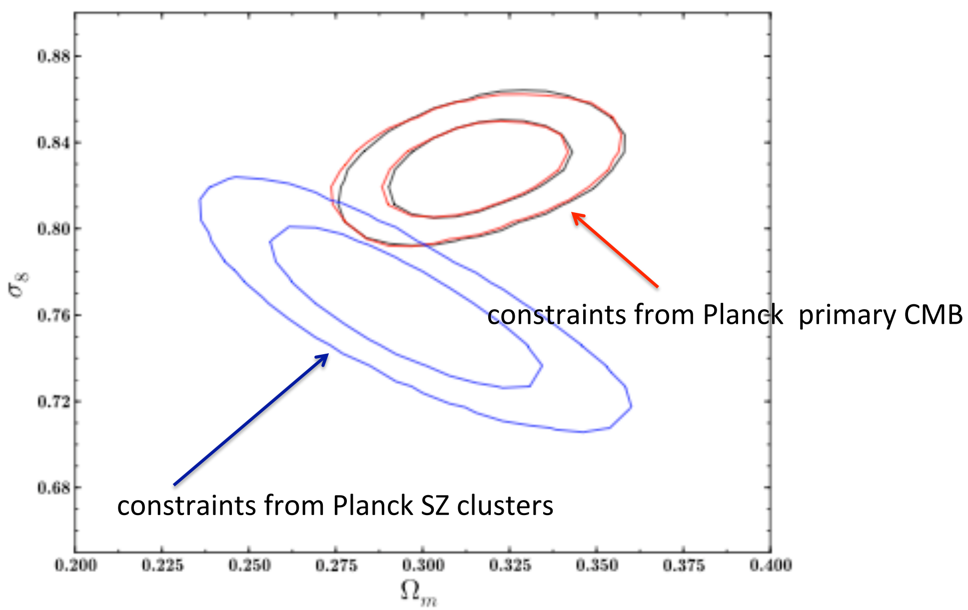

Counting galaxies

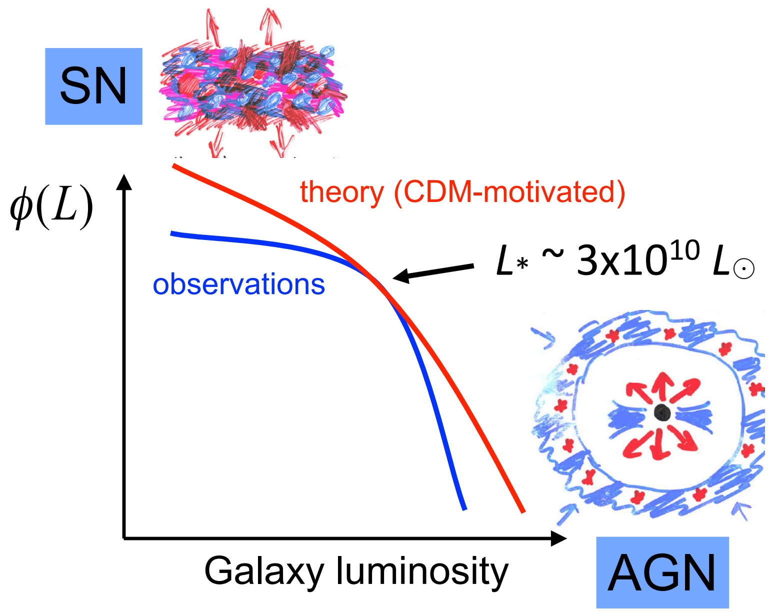

Fig. 1 Role of feedback in modifying the galaxy luminosity function

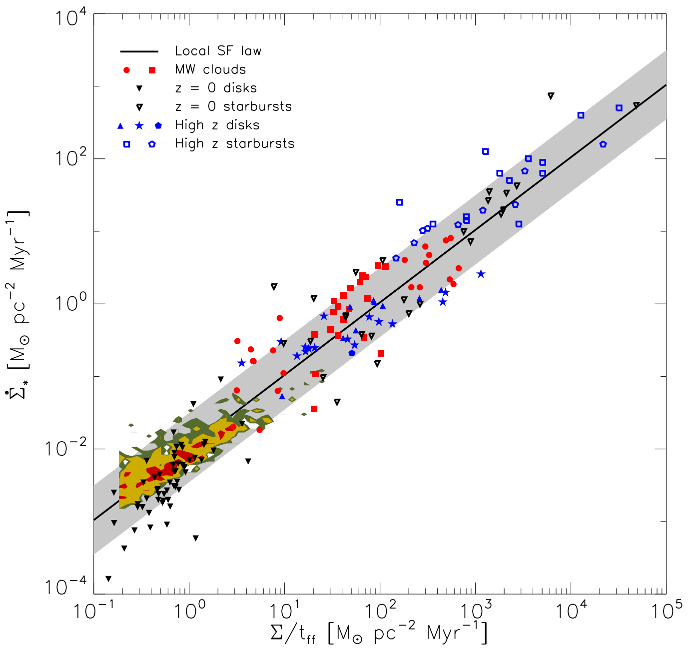

Fig. 2 Schmidt-Kennicutt laws on nearby (including Local Group galaxies as *shaded regions*) and distant galaxies, as well as Milky Way Giant Molecular Clouds (Krumholz et al., 2012). The solid line is similar to equation (1).

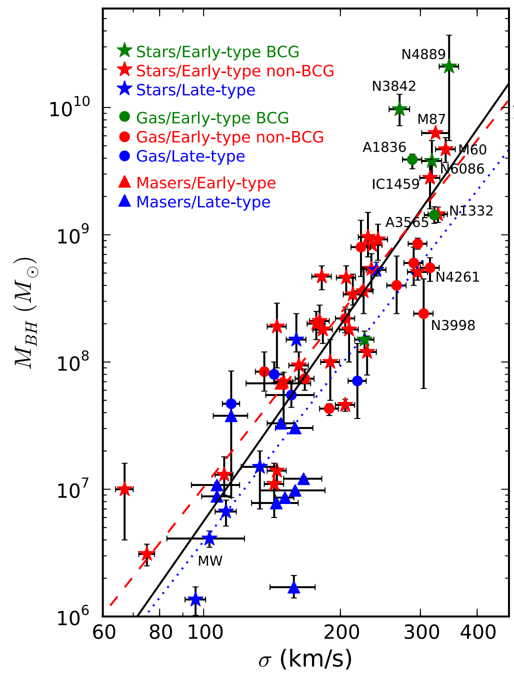

Fig. 8 Black hole mass versus spheroid velocity dispersion (luminosity-weighted within one effective radius), from McConnell et al. (2011)

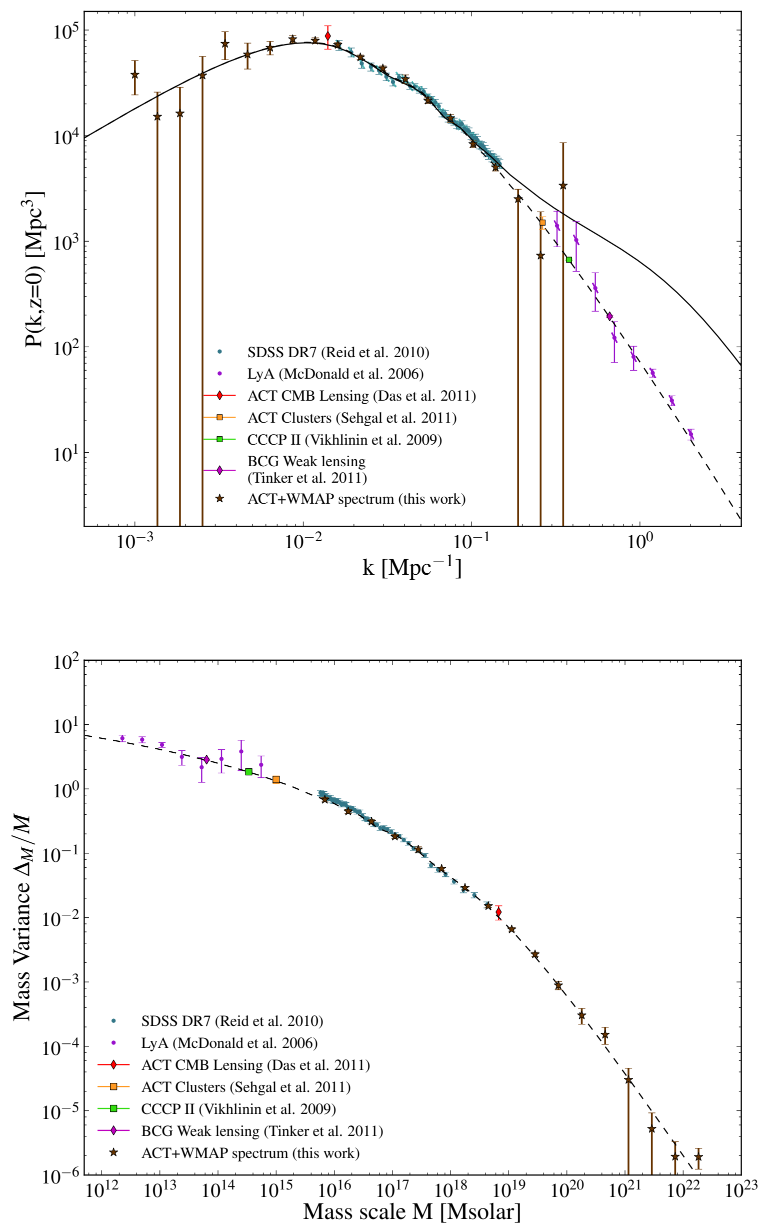

FIG. 5.— The reconstructed matter power spectrum: the stars show the power spectrum from combining ACT and WMAP data (top panel). The solid and dashed lines show the nonlinear and linear power spectra respectively from the best-fit ACT ΛCDM model with spectral index of $n_s = 0.96$ computed using CAMB and HALOFIT (Smith et al. 2003). The data points between $0.02 < k < 0.19$ Mpc^{-1} show the SDSS DR7 LRG sample, and have been deconvolved from their window functions, with a bias factor of 1.18 applied to the data. This has been rescaled from the Reid et al. (2010) value of 1.3, as we are explicitly using the Hubble constant measurement from Riess et al. (2011) to make a change of units from h^{-1}Mpc to Mpc. The constraints from CMB lensing (Das et al. 2011), from cluster measurements from ACT (Sehgal et al. 2011), CCCP (Vikhlinin et al. 2009) and BCG halos (Tinker et al. 2011), and the power spectrum constraints from measurements of the Lyman–α forest (McDonald et al. 2006) are indicated. The CCCP and BCG masses are converted to solar mass units by multiplying them by the best-fit value of the Hubble constant, $h = 0.738$ from Riess et al. (2011). The bottom panel shows the same data plotted on axes where we relate the power spectrum to a mass variance, Δ_M/M, and illustrates how the range in wavenumber k (measured in Mpc^{-1}) corresponds to range in mass scale of over 10 orders of magnitude. Note that large masses correspond to large scales and hence small values of k. This highlights the consistency of power spectrum measurements by an array of cosmological probes over a large range of scales.

Neutrinos

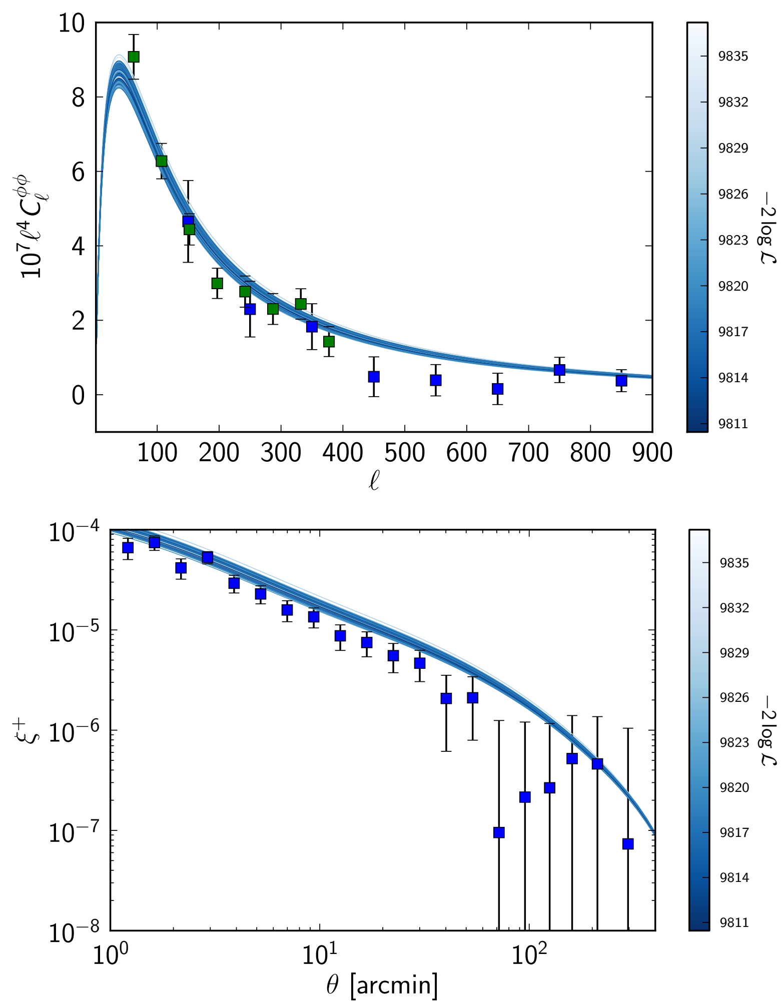

FIG. 1: The CMB lensing power spectrum (top) data points from *Planck* (green squares) and SPT (blue squares) and the shear correlation function ξ^+ from CFHTLenS (bottom), compared to predictions for parameters from samples of the *Planck* CMB+WP+BAO MCMC chains with non-linear corrections [18, 19]. In both cases, the data is systematically lower than theory, although the significance is somewhat lower than the eye would suggest in the case of CFHTLenS due to correlations between data points.

Battye and Moss 1308.5870

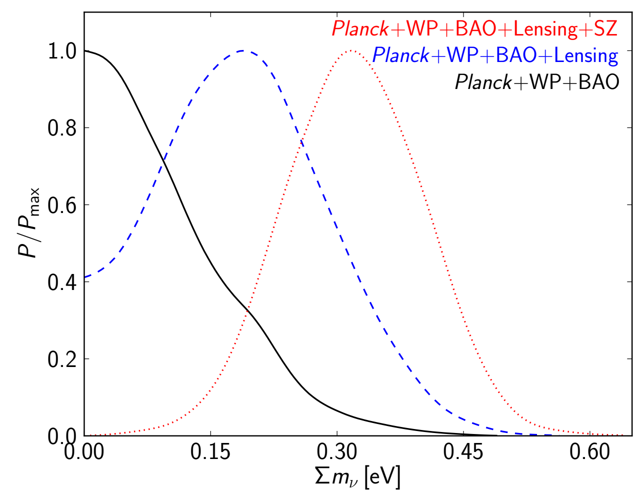

FIG. 2: Marginalized likelihoods for $\sum m_\nu$. The datasets are colour coded in the legend, but the solid line is for (I), the dashed line is for (II) and the dotted line is for (III). It is clear that inclusion of lensing leads to a preference for $\sum m_\nu > 0$ which is compatible with that coming from the SZ cluster counts and that there is a strong preference ($\approx 4\sigma$) in the case of dataset (III).